NATIONAL ADVISORY COMMITTEE FOR AERONAUTICS

TECHNICAL NOTE 3113

ANALYSIS OF STRAIGHT MULTICELL WINGS ON CAL-TECH ANALOG COMPUTER

By Stanley U. Benscoter and Richard H. MacNeal

California Institute of Technology

Washington
January 1954

NATIONAL ADVISORY COMMITTEE FOR AERONAUT.

TECHNICAL NOTE 3113

ANALYSIS OF STRAIGHT MULTICELL WINGS ON CAL-TECH ANALOG COMPUTER

By Stanley U. Benscoter and Richard H. MacNeal

SUMMARY

Using the Cal-Tech analog computer, structural analyses have been made for four straight multicell wings. Wings with aspect ratios of 2 and 4 with rectangular and biconvex cross sections have been considered. The wings are supported rigidly along two lines at the faces of the fuselage. Concentrated loads are applied at the intersection points of the ribs and spars. The effects of shearing strains in the ribs and spars are included. Deflections and all internal force quantities have been recorded as well as vibration modes and frequencies.

INTRODUCTION

The structural analysis of a thin multicell wing of low aspect ratio presents a rather difficult problem if one wishes to obtain better accuracy than can be obtained from elementary beam theory. Four such wings have been analyzed on the Cal-Tech analog computer for various static loads and in vibrational motion. Wings with rectangular and biconvex cross sections with aspect ratios of 2 and 4 have been analyzed. The wings are assumed to extend through the fuselage and to be supported rigidly along two lines at the faces of the fuselage.

When cross sections of a thin wing have a horizontal axis of symmetry, the wing deforms under load in the manner of a plate. Analogous circuits for elastic plates were given in reference 1. The structural theory and analogous circuits for multicell wings are given in reference 2. The present paper is devoted to a presentation of the results of computations based upon the method of reference 2. Comparisons with elementary beam theory are given wherever possible. In the case of bending loads the variation from beam theory becomes appreciable only at very low aspect ratios. In the case of torsional loads the variation from beam theory is more pronounced because of the occurrence of normal stresses due to warping restraint. The graphical illustrations represent only a small portion of the data which were obtained from the computer. The complete results of the computing work have been omitted for publication but are given in the tables in the manuscript copy of this report.

This copy is available for loan or reference in the Division of Research Information, National Advisory Committee for Aeronautics, Washington, D. C. The present investigation was conducted at the California Institute of Technology under the sponsorship and with the financial assistance of the National Advisory Committee for Aeronautics.

SYMBOLS

A	area of a cell
A'	transformed area used in shear-flow calculations
A_{in}	area of shear web of ith rib in nth bay
A_{jm}	area of shear web of jth spar in mth bay
c	chord of wing
d	transformation or carry-over factor
D_{ij}	bending stiffness of ith rib at jth spar
D_{ji}	bending stiffness of jth spar at ith rib
D_{mn}	twisting stiffness of a panel
E	Young's modulus
f	frequency
G	shearing modulus of elasticity
h_j	depth of jth spar
I	moment of inertia of skin per unit of width
I_j	moment of inertia of jth spar
I_T	total moment of inertia of cross section
J	torsion constant
L	distance from support line to wing tip

M	bending moment
M_{ij}	bending moment in ith rib at jth spar
M_{ji}	bending moment in jth spar at ith rib
P	concentrated load
P_{ij}	load at ith rib and jth spar
q	shear flow
q_j	shear flow in web of jth spar
$(q_j)_s$	statically determinate part of q_j
$(q_j)_i$	indeterminate part of q_j
q_n	cellular shear flow in nth cell
R_x	flexibility of spar
R_y	flexibility of rib
R_{xy}	interaction flexibility, $\lambda_j\mu_{ij}/D_{ji}(1 - \mu_{ij}\mu_{ji})$
R_{yx}	interaction flexibility, $\lambda_i\mu_{ji}/D_{ij}(1 - \mu_{ij}\mu_{ji})$
T	twisting moment
T_b	twisting moment computed from beam theory
t_1, t_2, t_3, t_4	transformer numbers
V	shear
V_{in}	shear in ith rib at nth bay
V_j	shear in jth spar
V_{jm}	shear in jth spar at mth bay

$(V_j)_s$	statically determinate part of V_j
w	deflection
w_b	deflection from beam theory
w_{ij}	deflection at ith rib and jth spar
w_V	deflection due to shearing strains only
w^*	deflection of a beam from difference equations
α	ratio of length to width of a wall segment
α_j	ratio of depth to width of web of jth spar
β_{in}	rotation of normal in ith rib in nth bay
β_{jm}	rotation of normal in jth spar in mth bay
Δ_i	jump in a function across ith rib
Δ_j	jump in a function across jth spar
λ_i	width of structure associated with ith rib
λ_j	width of structure associated with jth spar
λ_m	width of mth bay between ribs
λ_n	width of nth bay between spars
μ	Poisson's ratio
μ_{ij}	equivalent chordwise Poisson's ratio defined by equation (1)
μ_{ji}	equivalent spanwise Poisson's ratio defined by equation (1)
σ	normal stress
σ_x	spanwise normal stress
σ_b	normal stress computed from beam theory

Σ_n	summation about nth cell
τ	shearing stress
τ_b	shearing stress computed from beam theory

DESCRIPTION OF STRUCTURES

In order to arrive at a reasonable set of dimensions for the structures to be analyzed a few design computations were made by using elementary beam theory. The complete missile was assumed to weigh 20 kips and to be designed for an ultimate load factor of 4. The allowable normal stress in the skin was assumed to be 20 ksi and the allowable shearing stress in the spar webs was assumed to be 12 ksi. The loading was assumed to be uniformly distributed. The thickness of the rib webs was arbitrarily assumed to be one-half of the value determined for the spar webs. The resulting structure for an aspect ratio of 2 with a rectangular cross section is shown in figure 1.

In order that the skin might carry a normal stress of 20 ksi without buckling it would be necessary to reduce the spacing of the spars to approximately one-half of that shown in figure 1. This would provide 13 spars rather than 7 spars. The limitation to seven spars was dictated by the amount of electrical equipment which was available. Each spar which is shown in figure 1 should be considered as being equivalent to two spars in the structure as it would be built. Connection angles and shear web flanges have been omitted for convenience.

Details of the wing with a rectangular cross section and an aspect ratio of 4 are shown in figure 2. The structural chord of 72 inches has been retained for all of the wings. Also the fuselage bay has been assumed to be one-third of the total structural span for all wings. The allowable shearing stress in the spar webs was reduced to one-half of the previous value or 6 ksi. In order to develop this strength in the deeper web some form of stiffening against shear buckling would be required.

The dimensions of the wings with biconvex sections have been chosen more or less arbitrarily to give about the same strength as that provided by the rectangular cross sections. The dimensions of the wing of aspect ratio 2 are shown in figure 3. For the wing having an aspect ratio of 4 and a biconvex section the dimensions are shown in figure 4.

In order to record the computed results in tabular form a numbering system for points on the plan form has been adopted as shown in figure 5. A number has been assigned to each point at which some quantity is measured.

In presenting the results of the analyses it is only necessary to give the results for one quadrant of the plan form since the layout of the structure has double symmetry in its plan. The points at which concentrated loads are applied are shown in figure 6. The deflections and bending moments are also measured at these points. The points at which shears are determined are shown in figure 7. In figure 8 the points are shown at which twisting moments are determined. These twisting moments may be considered as average values over the panels.

A few sample calculations of structural constants are included to show in detail how these quantities are determined. The calculation of stiffness constants is made according to the formulas contained in reference 2. The wing is assumed to be constructed of an aluminum alloy having the material properties shown in table 1. Calculations for the spanwise and chordwise bending stiffnesses at an interior point of the wing with rectangular cross section and aspect ratio 2 are given below.

For the spar:

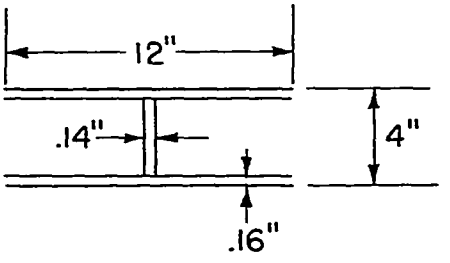

$$D_{ji} = 12 \times 0.16 \times \frac{(3.84)^2}{2} \times \frac{10.4 \times 10^6}{0.91} + \frac{1}{12} \times 0.14 \times (3.68)^3 \times 10.4 \times 10^6$$

$$= (161.8 + 6.0) \times 10^6$$

$$= 167.8 \times 10^6 \text{ lb-in.}^2$$

$$\mu_{ji} = \left(\frac{161.8}{167.8}\right) \times 0.3 = 0.289$$

For the rib:

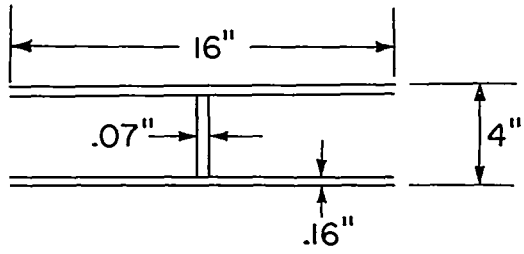

$$D_{ij} = 16 \times 0.16 \times \frac{(3.84)^2}{2} \times \frac{10.4 \times 10^6}{0.91} + \frac{1}{12} \times 0.07 \times (3.68)^3 \times 10.4 \times 10^6$$

$$= (216 + 3) \times 10^6$$

$$= 219 \times 10^6 \text{ lb-in.}^2$$

$$\mu_{ij} = \left(\frac{216}{219}\right) \times 0.3 = 0.296$$

It is convenient in the computation of structural constants to introduce spanwise and chordwise Poisson ratios according to the following definition:

$$\frac{\mu_{ji} D_{ji}}{\lambda_j} = \frac{\mu_{ij} D_{ij}}{\lambda_i} = \frac{\mu EI}{1 - \mu^2} \tag{1}$$

The relation between bending moments and curvatures may be expressed in the following form:

$$D_{ji} \frac{\Delta_i \beta_{jm}}{\lambda_i} + \mu_{ji} D_{ji} \frac{\Delta_j \beta_{in}}{\lambda_j} = -M_{ji} \tag{2a}$$

$$\mu_{ij} D_{ij} \frac{\Delta_i \beta_{jm}}{\lambda_i} + D_{ij} \frac{\Delta_j \beta_{in}}{\lambda_j} = -M_{ij} \tag{2b}$$

In order to design the analogous circuits, equations (2) must be inverted to obtain formulas for the curvatures in terms of the bending moments. The coefficients of such equations may be referred to as flexibilities. Formulas for the flexibilities become:

$$R_x = \frac{\lambda_i}{D_{ji}\left(1 - \mu_{ij}\mu_{ji}\right)}$$

$$R_y = \frac{\lambda_j}{D_{ij}\left(1 - \mu_{ij}\mu_{ji}\right)}$$

$$R_{xy} = \frac{\lambda_j\mu_{ij}}{D_{ji}\left(1 - \mu_{ij}\mu_{ji}\right)}$$

$$R_{yx} = \frac{\lambda_i\mu_{ji}}{D_{ij}\left(1 - \mu_{ij}\mu_{ji}\right)}$$

A sample calculation of the numerical values for the flexibilities at an interior point of a rectangular section with aspect ratio 2 are:

$$1 - \mu_{ij}\mu_{ji} = 1 - (0.289)(0.296) = 0.914$$

$$R_x = \frac{16}{167.8 \times 10^6 \times 0.914} = 0.1043 \times (10)^{-6}$$

$$R_y = \frac{12}{219 \times 10^6 \times 0.914} = 0.0600 \times (10)^{-6}$$

$$R_{xy} = \frac{12 \times 0.296}{167.8 \times 10^6 \times 0.914} = 0.0231 \times (10)^{-6}$$

$$R_{yx} = \frac{16 \times 0.289}{219 \times 10^6 \times 0.914} = 0.0231 \times (10)^{-6}$$

A sample calculation of the shearing constant of an interior spar is:

$$\frac{1}{\lambda_m GA_{jm}} = \frac{1}{16 \times 4 \times 10^6 \times 0.14 \times 3.68} = 0.0303 \times (10)^{-6}$$

A calculation of the shearing constant of an interior rib is:

$$\frac{1}{\lambda_n GA_{in}} = \frac{1}{12 \times 4 \times 10^6 \times 0.07 \times 3.68} = 0.0809 \times (10)^{-6}$$

A sample calculation of the twisting constant for the skin is as follows:

$$GI = 4 \times 10^6 \times 0.16 \times \frac{(3.84)^2}{2} = 4.72 \times 10^6$$

$$\frac{\lambda_n}{D_{mn}} = \left(\frac{\lambda_n}{\lambda_m}\right)\frac{1}{GI} = \frac{12}{16 \times 4.72 \times 10^6} = 0.1589 \times (10)^{-6}$$

LOADING CONDITIONS

Since the plan form of each wing has two axes of symmetry the loading may be divided into four types according to the symmetry conditions. Loads which are symmetrical about the midchord line are referred to as bending loads and loads which are antisymmetrical about the midchord line provide the torsional loading. Since the loads may be symmetric or antisymmetric about the plane of symmetry of the aircraft the following four types of loading may be considered: Symmetric bending, symmetric torsion, antisymmetric bending, and antisymmetric torsion.

For the static loading conditions the loads are assumed to be applied as concentrated forces at the points of intersection of the ribs and spars. The loads are applied as a group of four forces, one in each quadrant of the plan form, to form a doubly symmetrical arrangement. In designing the analogous circuit and in recording the results of the analysis it is only necessary to consider one quadrant of the structure. A circuit was designed to correspond to the first quadrant of the plan form. Each point of this quadrant was loaded independently. The four types of loading were obtained by using the appropriate boundary conditions for the quadrant along the lines of symmetry of the plan form.

Four wings, each to be loaded with loads having four types of symmetry, provide 16 cases. In each case there are 16 loadings. Such a complete program of computation would be too extensive to be justifiable. Hence it was decided to load all points in 4 cases and to load only the tip points in the remaining 12 cases. The choice of loading points for the various cases is shown in table 2. In order to make a further saving in the calculation work for those cases wherein all points were loaded, the internal force quantities were not recorded when the four points in the fuselage bay were loaded. Deflections were, however, recorded in all cases.

BOUNDARY CONDITIONS

Along the leading edge of the wing the chordwise shear, chordwise bending moment, and chordwise twisting moment must vanish. Along the wing tip the spanwise shear, spanwise bending moment, and spanwise twisting moment must vanish. Along the line of support the vertical deflection must be zero. It has also been assumed that the wing is clamped along the support in such a manner as to prevent chordwise rotation of the normals to the elastic axis of the rib which lies over the support. This clamping, however, does not prevent the rib from warping

out of its own plane. This assumption that the normals in the rib do not rotate provides a relation between spanwise and chordwise bending moments over the support. Since β_{in} is zero at all points along the support the quantity $\Delta_j\beta_{in}$ may be set equal to zero in equations (2). This gives the following formula for the chordwise bending moments in terms of the spanwise bending moments:

$$M_{ij} = \mu_{ij} \frac{D_{ij}}{D_{ji}} M_{ji} \tag{3}$$

The center lines of the plan form are boundary lines for the quadrant of the wing. Along these lines the boundary conditions are symmetry conditions and are determined from the known symmetry of the applied load. It can be shown and it is obvious from physical intuition that the symmetry of the deflection surface is the same as the symmetry of the applied load. From the known symmetry of the deflection surface the symmetry conditions of the various derivatives can be determined. From this information the symmetry conditions for the internal forces may be determined. This determination of the symmetry conditions for the internal forces follows the arguments which are customary in elastic plate analysis.

ANALOGOUS ELECTRICAL CIRCUITS

Since all of the four wings to be analyzed have the same general arrangement of ribs and spars, the same arrangement of circuit elements may be used for all of the wings. The complete circuit consists of three planar circuits which are shown in figures 9 to 11. These circuits are similar to those given in reference 1 except that they include the effect of shearing strains in the ribs and spars. The design of the circuits is in exact agreement with the methods of reference 2.

For each type of loading, changes along the planes of symmetry are required to satisfy the conditions of symmetry. These changes are indicated on the drawings of the circuits. Along the leading edge and wing tip the natural boundary conditions are automatically satisfied by the circuit. Along the support the deflections and chordwise rotations of normals are made to vanish by grounding the proper nodal points in figures 9 and 11.

ANALYSIS OF WINGS BY BEAM THEORY

In presenting the results of the analysis it is of particular interest to compare results obtained from the analog computer with solutions obtained by applying elementary beam theory to the wing. In torsion the expression "elementary beam theory" is used to indicate that stresses and displacements at a cross section are computed from the section torque by using formulas from the solution of St. Venant. In bending action "elementary beam theory" is based on the assumption that plane sections remain plane and in addition that cross sections are preserved by ribs which are rigid in their own plane. This differs from the bending theory of St. Venant which predicts a chordwise camber. All comparisons in this paper will be made with elementary beam theory.

The shear flows in torsion were computed by using the numerical procedure of reference 3. An example of this procedure is given in table 3 for the biconvex section of the wing of aspect ratio 2. The solution is obtained by a process of successive corrections and checked by a cycle of iteration. Because of the symmetry of the cross section about a vertical axis it is only necessary to write the computation for one-half of the section. At each step in the calculations it must be remembered that the shear flows in torsion are symmetrical about the center line. The torsion constant is also computed in table 3. The torsion constants for all of the wings are given in table 1.

The shear flows in bending may be divided into a statically determinate part and an indeterminate part. This division may be indicated for the shear web of the jth spar as

$$q_j = (q_j)_s + (q_j)_i \tag{4}$$

It is convenient to define the statically determinate shear flows in the top and bottom skin as being zero. The statically determinate shear flows in the spar webs are computed from shears which are proportional to the moments of inertia of the spars as follows:

$$(q_j)_s h_j = (V_j)_s = V\left(\frac{I_j}{I_T}\right) \tag{5}$$

The statically determinate shear flows are in equilibrium with the normal stresses and are also in equilibrium with the external loads. The

indeterminate shear flows are completely self-equilibrating and are determined by the condition of continuity of warping displacements. The indeterminate shear flows consist of cellular shear flows which are antisymmetric about the vertical axis of symmetry of the cross section. The indeterminate shear flow in a spar web may be expressed as the difference between the cellular shear flows in the two adjacent cells as follows:

$$\left(q_j\right)_i = -q_n + q_{n-1} \tag{6}$$

In writing equation (6) it is assumed that the jth spar lies between cell number n and cell number n - 1.

The condition of continuity of warping displacements leads to a difference equation governing the cellular shear flows as follows:

$$-\alpha_{j+1}q_{n+1} + \left(\Sigma_n\alpha\right)q_n - \alpha_j q_{n-1} = -\alpha_{j+1}\left(q_{j+1}\right)_s + \alpha_j\left(q_j\right)_s \tag{7}$$

Equation (7) is written for the nth cell. The coefficients are computed as ratios of length to width of the wall segments. The system of equations corresponding to equation (7) has a matrix of coefficients which is the same as for the torsion case. Consequently the numerical procedure of reference 3 may again be employed. An example of the calculation of shear flows in bending is given in table 4. Moments of inertia of the cross sections and of the individual spars are given in table 1.

SOURCES OF ERROR

Errors in the computed results due to inadequacy of the structural theory cannot be estimated. However, other sources of error have been estimated roughly as follows:

Error in computer, percent	±1.0
Error in meter, percent	±1.0
Error in reading meter, percent	±0.5
Error in computing stiffness constants, percent	±1.0
Error from using difference equations	(see figs. 10 and 11)

An inspection of the data obtained from the computer showed that the total bending moments and shears on various cross sections violated statics

by amounts ranging from 1 percent to 3 percent. A factor to correct for this error was introduced at the same time that the electrical quantities were converted to structural quantities. The error in the computer which is shown in the above table is an estimation of that error which remains after the correction for statics has been introduced. The error in the computer is due to parasitic effects in the components of the circuit.

Some error is contained in the meter which is used for measuring the voltages or currents. Some additional human error is also involved in reading the meter. The errors for the computer and the meter, as given above, are applicable to the largest numbers which are given in the tables of data. For the smaller quantities the percentage errors may be much larger, even though the absolute size of the errors will be less.

In the case of the rectangular cross sections there are no errors in the stiffness constants. However, in the case of the biconvex sections there is a small error. A more significant error arises from the use of difference equations in expressing the structural theory. No specific value has been given for this error since there is a large difference between the symmetric and antisymmetric cases. (See figs. 12 and 13.) In order to obtain an estimate of the error in deflections a uniform beam was analyzed by solving difference equations and by solving differential equations. The central span and external spans were each divided into three parts in forming the difference equations. The beam was assumed to be loaded with a concentrated force at each tip.

For the case of symmetric loads the ratio of deflections from difference equations to deflections from differential equations is shown in figure 12(b). Here the error is seen to vary between 2 and 3 percent. The antisymmetric case is illustrated in figure 13(b). In this case the error is more than five times as great as in the symmetric case. It is obvious that an accurate treatment of deflections in the antisymmetric case requires more stations along the span in forming the difference equations or a more accurate formulation of the structural theory in terms of difference equations. The effect of the use of difference equations on the distribution of internal forces in the multicell wings is not known. However, it can be shown that all relations of statics between the internal forces and applied loads are satisfied.

It is also of interest to estimate the error which would be made if the deflections due to shearing strains were neglected. This requires the use of specific cross sections. Such an estimate was computed for the wings with rectangular cross sections by using elementary beam theory. The ratio of deflections due only to shearing strains to the total deflections, using differential equations, was computed and plotted. For symmetric loading the ratio is shown in figure 12(c) where it is seen that the error varies from 2 to 6 percent.. For the antisymmetric case, which is shown in figure 13(c), the ratio is approximately five times as large.

TREATMENT OF DATA FROM COMPUTING MACHINE

A simple check which can be made on the results from the computer consists of comparing the total shear, bending moment, or torque on a cross section with the value given by statics from the external loads. When this check was made errors were found which ranged from approximately 1 to 3 percent. These errors were due to parasitic effects in the computer and not to the use of difference equations for the structural theory. The error did not show large variations over a given planar circuit and hence it was decided that the voltages and currents in each planar circuit should be corrected by a single scalar factor.

The correction factors were determined by applying statics to the sections shown in figure 14. For bending loads the correction factor for both of the bending-moment circuits was determined to satisfy statics for the bending moment over the support. The shear circuit was corrected to satisfy statics in the first bay outboard from the support. With torsional loads the bending-moment circuits were corrected to give the correct section torque in the first bay outboard from the support. The shear circuit was corrected to give the correct total shear on section D-D as shown in figure 14(b). Since the shears in the spars contribute to the section torque it is necessary to correct the shears first and the twisting moments subsequently.

DEFLECTIONS DUE TO BENDING LOADS

The results of the computations on the analog computer are given in the tables available on loan from NACA. From these tables a small portion of the data has been taken to prepare illustrations of cases which seemed to be most interesting. For all of the bending cases which are illustrated the loading consists either of two corner loads at the tip or a single load on the central spar at the tip.

The chordwise distribution of deflections at the tip is shown in figure 15 for the wing of aspect ratio 2 with rectangular cross section. Both types of bending loads are applied symmetrically. For the central load the effect of shearing strains in the rib is clearly evident. A comparison is made with elementary beam theory using both differential equations and difference equations. The solution for a plate of infinite width with a uniform line load at the tip is also shown. This solution is obtained from the solution for a beam by multiplying by $1 - \mu^2$. It may be seen that the average deflection of the wing structure is somewhere between the values predicted by the two beam theories.

The chordwise distributions of deflections for the wing of aspect ratio 2 and biconvex section are shown in figure 16. In this figure a central load is applied at the tip and a comparison is made between the symmetric and antisymmetric cases. Both cases show fairly good agreement with beam theory.

Chordwise distributions of deflections along each of the ribs are shown in figure 17 for both wings of biconvex section. The graphs are plotted as a ratio of computed deflection to the deflection from beam theory.

The spanwise distributions of deflections for the leading-edge spar and the central spar are shown in figure 18 for the wing of aspect ratio 2 with rectangular cross section. A comparison is given between the symmetric and antisymmetric cases.

SHEARS IN SPARS DUE TO BENDING LOADS

The chordwise distributions of shears in the spars at each outboard bay are shown in figure 19 for both wings of rectangular section. The ratio of shear from the computer to shear obtained from beam theory is plotted. This ratio may also be regarded as a ratio of shearing stresses.

For the wing of aspect ratio 2 with biconvex section the shears in the spars are illustrated in figure 20. A comparison is made of the distribution for a central load and for corner loads.

The spanwise distribution of shears in the leading-edge spar and the central spar are shown in figure 21 for a wing of aspect ratio 2 with rectangular cross section. Values obtained from beam theory are also shown.

SHEARS IN RIBS DUE TO BENDING LOADS

A single illustration of shears in the ribs is given in figure 22 for the wing of aspect ratio 2 with rectangular section. The chordwise distribution of shear in all of the ribs is shown. These distributions are given for symmetrical cases of a central load and for corner loads.

BENDING MOMENTS IN SPARS DUE TO BENDING LOADS

From the spanwise bending moments one may compute the spanwise normal stresses. The ratio of spanwise normal stress from the computer to

the same stress from beam theory was computed for all four wings for symmetric bending loads. The stresses were computed for points over the support and are shown in figure 23 for a central tip load and in figure 24 for corner loads. It is of interest to note that the maximum variation from beam theory for the wing of aspect ratio 4 is only 3 percent while the variation for the wing of aspect ratio 2 is 15 percent.

For each of the wings of aspect ratio 2 the normal stresses over the remaining ribs are shown in figure 25 for a central load. In regions of smaller stress it is seen that the percentage variation from beam theory becomes larger.

The spanwise variations of bending moment in the leading-edge spar and central spar are shown in figure 26 for the beam of aspect ratio 2 with rectangular section. The effects of both corner loads and a central load are compared with beam theory for the symmetric case. The corresponding antisymmetric case is shown in figure 27.

BENDING MOMENTS IN RIBS DUE TO BENDING LOADS

An illustration of chordwise bending moments in all of the ribs is shown in figure 28 for a wing of aspect ratio 2 with rectangular section. The effects of a central load and of corner loads are compared for symmetric cases.

TWISTING MOMENTS DUE TO BENDING LOADS

The chordwise distributions of twisting moments in the various bays are shown in figure 29 for the wing of aspect ratio 2 with rectangular section. A comparison is made between the effects of a central load and corner loads. It may be seen that the twisting moments act in opposite directions for the two types of loads in all bays which are outboard from the fuselage.

DEFLECTIONS DUE TO TORSIONAL LOAD

In preparing the illustrations for torsional loading the only loading which has been considered is that of a pair of equal and opposite forces at the corners. The chordwise distribution of deflections at the tip is shown in figure 30 for the wing of aspect ratio 2 with rectangular section. The symmetric and antisymmetric cases show very close agreement. The maximum variation from beam theory is about 10 percent.

The chordwise distribution of deflections for symmetric loads is shown in figure 31 for the wing of aspect ratio 2 with a biconvex section. The curvature of the rib in this case is more noticeable than in the previous figure.

For the wing of aspect ratio 4 with biconvex section the chordwise distributions of deflections for symmetric loading are shown in figure 32.. A comparison with beam theory is given. The curvature of the tip rib is noticeable.

Spanwise deflections of the leading-edge spar, and also the adjacent spar, are shown in figure 33 for the wing of aspect ratio 2 with a rectangular section. Symmetric and antisymmetric cases are compared with beam theory. The same quantities are illustrated for the biconvex section in figure 34.

SHEARS IN SPARS DUE TO TORSIONAL LOAD

The chordwise distributions of shears in the spars are shown in figure 35 for both wings of aspect ratio 2. Ratios of shearing stress as computed to shearing stress from beam theory are shown. In almost all positions of the plan form the ratio is larger than unity. This is due to the torsion-bending action in which normal stresses arise because of torsional loading.

The spanwise distribution of shear in the spars is shown in figure 36 for the wing of aspect ratio 2 with biconvex section. Large variations from beam theory are evident.

SHEARS IN RIBS DUE TO TORSIONAL LOADS

The chordwise distributions of shears in the ribs are shown in figure 37 for the two wings with rectangular section. A comparison is shown for the two aspect-ratio cases for symmetric loads.

BENDING MOMENTS IN SPARS DUE TO TORSIONAL LOAD

For purposes of illustration the bending moments in the spars have been converted to normal stresses. The chordwise distributions of spanwise normal stress over the support are shown in figure 38 for the four wings with symmetric loads. This illustration shows that the normal

stresses due to torsion are more than twice as large in the wings of lower aspect ratio. Similar results are given for the antisymmetric case in figure 39.

The variation of spanwise normal stress along the leading-edge spar is shown in figure 40 for the wings of aspect ratio 2. Results are shown for both types of cross sections with symmetric and antisymmetric loading. Corresponding stresses for the wings of aspect ratio 4 are shown in figure 41.

BENDING MOMENTS IN RIBS DUE TO TORSIONAL LOADS

The bending moments in the ribs have again been converted to normal stress. The distribution of chordwise normal stress in the various ribs is shown in figure 42 for the wing of aspect ratio 2 with rectangular section. Symmetric loading is considered.

TWISTING MOMENTS DUE TO TORSIONAL LOADS

The chordwise distributions of twisting moments for various bays are shown in figure 43 for the wings of aspect ratio 2. The quantity which is plotted is the ratio of computed twisting moment to the value of twisting moment given by beam theory. In most of the bays the ratio is less than unity. This is due to the torsion-bending action of the structure.

EFFECT OF SHEARING STRAINS IN RIBS AND SPARS

Throughout all of the analyses on the analog computer the effect of shearing strains was taken into account. These shearing strains affect not only the deflections but also the distribution of internal forces. A few calculations were made on the assumption of an infinite shearing stiffness for the ribs and spars. The effect of shearing strains upon the distribution of shears in the spars is shown in figure 44 for the wing of aspect ratio 4 with rectangular section. The change in shear due to the existence of finite shearing strains is generally small and is less than 10 percent in almost all cases.

The effect of shearing strains upon the spanwise normal stress over the support is shown in figure 45 for the wing of aspect ratio 4 with rectangular section. Symmetric bending and torsional loads are considered. The effect of shearing strains upon the normal stress distribution is somewhat less than the effect upon shear distribution.

ANALYSIS OF A GRIDWORK OF RIBS AND SPARS

In the analysis of a multicell beam the calculation work consists of two parts. In the first part the normal stresses are computed from the flexure formula and a statically determinate set of shear flows are computed. In the second part of the analysis the indeterminate cellular shear flows are computed. Consideration was given to the possibility of developing a similar method of analysis for a multicell plate. In such a method it would be assumed that the skin is cut to prevent it from carrying any twisting moment. Shears and bending moments would be calculated for the gridwork of ribs and spars. A subsequent calculation would be made to determine cellular shear flows required to restore continuity of the skin.

The above method of solution is based on the assumption that the distribution of bending moments in the gridwork will be approximately the same as the distribution in the multicell shell. In order to check this assumption an analysis was made on the analog computer of the wing of aspect ratio 2 as a gridwork. The results are compared with the analysis of the complete wing in figure 46 for spanwise normal stress over the support. From this figure it can be seen that with bending loads the distribution from gridwork theory agrees fairly well with the correct distribution for the wing. However, under torsional loading the discrepancy is very large. Further research study would be required to develop this method of analysis.

VIBRATION MODES

In order to determine vibration modes and frequencies on the analog computer it is necessary to replace the resistors by inductors. It is assumed that the inertia forces are provided by an equivalent set of concentrated masses. Each mass is represented in the analogous circuit by a condenser which is connected to ground. An illustration with detailed explanation of the vibration circuit for a beam is given in reference 4. In references 1, 2, and 4 the analogous circuits have been designed by connecting the condensers to the circuit at the deflection points. In the present calculation work this technique has been modified in order to obtain better accuracy.

It can be shown in certain beam analyses based upon the use of difference equations that better accuracy can be obtained if the equivalent concentrated masses are located at points midway between the deflection points than if the masses are located at the deflection points. This improvement in accuracy can also be shown to be true for a rectangular simply supported plate. Consequently the wing modes have been computed

by considering concentrated masses to act at points on the ribs and spars midway between the intersection points of the ribs and spars. This divides the total mass into approximately twice as many small concentrated masses as would be obtained by assigning the masses to the deflection points. This greater subdivision of the total mass should also tend to improve the accuracy.

Symmetric modes for the wing of aspect ratio 2 with rectangular cross section are illustrated in figure 47 by means of contour drawings. The first bending mode in figure 47(a) shows very little camber. The mode shape is the same as would be obtained from beam theory. The second bending mode, as shown in figure 47(b), consists almost entirely of chordwise bending. This camber mode cannot be predicted by beam theory.

In the bending theory of Saint Venant the chordwise camber is obtained by multiplying the spanwise curvature by Poisson's ratio. If this relationship should tend to hold approximately true under various loading conditions it would provide a very convenient way of determining elastic camber effects in aeroelastic analyses. A consideration of the first two bending modes as shown in figure 47 shows clearly that no relationship between spanwise and chordwise curvatures can be assumed to hold under various loading conditions.

The first torsion mode is shown in figure 47(c). The frequency for this mode lies between the two values for the first two bending modes. The third bending mode is shown in figure 47(d).

The measured frequencies of the lowest modes in bending and torsion were compared, for all four wings, with frequencies computed from beam theory without shearing strains. For the bending cases the variation from beam theory was less than 1 percent. The omission of shearing strains in the beam analysis compensated for the Poisson ratio effect in the wing. In the torsion cases the discrepancy was somewhat greater for the wing of aspect ratio 2. The wing of aspect ratio 4 showed a variation of 1 percent while the wing of aspect ratio 2 showed a frequency 8 percent higher than beam theory.

For the wing of aspect ratio 4 with rectangular section two symmetric modes are shown in figure 48. The first torsion mode is shown in figure 48(a). The first three bending modes for this wing showed very little evidence of camber. A small amount of camber is seen in the third bending mode which is illustrated in figure 48(b).

The torsion modes can be illustrated more clearly by drawing deflection diagrams for the various ribs and spars. The deflections of the spars in the first symmetric torsion mode are shown in figure 49 for the wing of aspect ratio 2 with rectangular section. The curves do not show the curvature that would be obtained from beam theory. For the same mode

the deflections of the ribs are shown in figure 50. The curves show an appreciable amount of camber which is not predicted by beam theory.

The deflections of spars in the first symmetric torsion mode are shown in figure 51 for the wing of aspect ratio 4 with rectangular section. For the same mode the deflections of the ribs are illustrated in figure 52. For the wing of aspect ratio 4 the deflections are more nearly like those which would be obtained from beam theory.

CONCLUSIONS

In preparing the illustrations for this paper it has only been possible to consider a very small portion of the data which were computed. The reader will find that the data in the tables available on loan will permit him to make a more thorough study of any particular case in which he may be interested than could be given in the limited space herein available. However, a few general statements can be made.

Under bending loads all of the wings show fairly good agreement with beam theory. The wings of aspect ratio 2 show poorer agreement than the wings of aspect ratio 4 but still agree, in general, more closely than one would be inclined to expect. The spanwise normal stresses show about the same percentage variation from beam theory as the deflections. The shearing stresses in the skin and spars, however, show much poorer agreement than the normal stresses.

Under torsional loading the wings show poorer agreement with beam theory than under bending loads. This is apparently due to the fact that torsional beam theory contains no effect of warping restraint (torsion-bending effect). The warping restraint which actually exists causes normal stresses in the spars and brings about a redistribution of the internal shear flows. It is clear that there is need for a practical theory of torsion bending for multicell beams.

For the wing of aspect ratio 2 the second symmetric bending-vibration mode consists almost entirely of chordwise camber. For the wing of aspect ratio 4 the first three symmetric bending modes contained only a small amount of chordwise camber. From the results of these analyses it is not unreasonable to believe that for wings of very low aspect ratio the effects of chordwise elastic camber should be included in aeroelastic analyses. In the torsional modes of vibration, due to the presence of warping restraint, the deflections of the spars showed appreciably less curvature near the tip than would be obtained from beam theory.

The data considered herein required the use of the analog computer for 4 weeks of normal working time. Consequently it may be concluded that the analysis of such complex structures as those herein considered is practicable with large automatic computers.

California Institute of Technology,
Pasadena, Calif., October 20, 1952.

REFERENCES

1. MacNeal, R. H.: The Solution of Elastic Plate Problems by Electrical Analogies. Jour. Appl. Mech., vol. 18, no. 1, Mar. 1951, pp. 59-67.

2. Benscoter, Stanley U., and MacNeal, Richard H.: Equivalent Plate Theory for a Straight Multicell Wing. NACA TN 2786, 1952.

3. Benscoter, S. U.: Numerical Transformation Procedures for Shear-Flow Calculation. Jour. Aero. Sci., vol. 13, no. 8, Aug. 1946, pp. 438-443.

4. Benscoter, Stanley U., and MacNeal, Richard H.: Introduction to Electrical-Circuit Analogies for Beam Analysis. NACA TN 2785, 1952.

TABLE 1

ELEMENTARY STRUCTURAL PROPERTIES

(a) Material properties

Quantity	Value
E, psi	10.4×10^6
G, psi	4.0×10^6
μ	0.3
Specific weight, lb/cu in.	0.107

(b) Properties of total cross section

Rectangular section			Biconvex section	
Aspect ratio	2	4	2	4
I_T, in.^{4}	88.4	386	73.4	318
J, in.^{4}	308	1,192	268	1,094

(c) Relative moments of inertia of spars

Section	Spar number			
	1	3	5	7
Rectangular	1/6	1/6	1/6	1/12
Biconvex	0.255	0.220	0.128	0.0245

TABLE 2

LOADED POINTS FOR VARIOUS CASES

	Rectangular section (a)		Biconvex section (a)	
Aspect ratio	2	4	2	4
Symmetric bending	A	T	A	T
Symmetric torsion	A	T	A	T
Antisymmetric bending	T	T	T	T
Antisymmetric torsion	T	T	T	T

[a] A, all points loaded; T, tip points loaded.

TABLE 3

SHEAR FLOWS IN TORSION FROM BEAM THEORY

[Biconvex section; aspect ratio, 2;
$J = 134.0 \times 2 = 268$ in.^{4}]

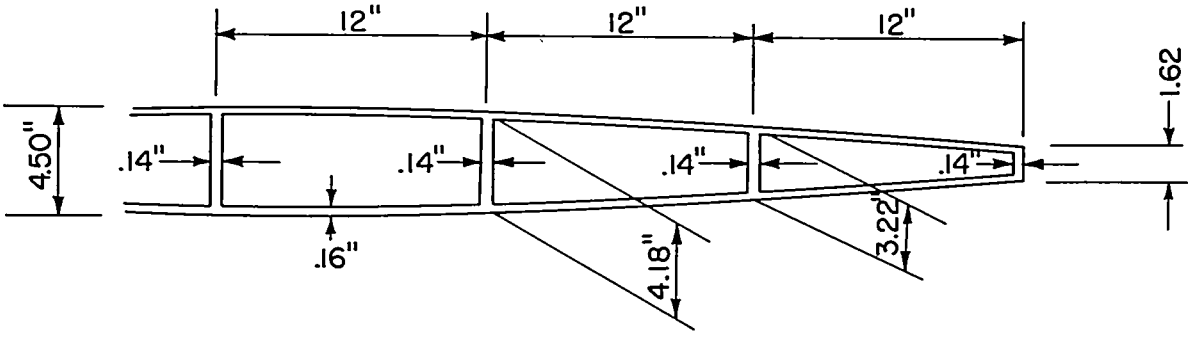

α (skin) . . .	75		75		74.6	
α (shear webs) . . .	31.0		28.7		21.9	10.4
A	50.80		42.48		26.96	
$\Sigma\alpha$	209.7		200.6		181.5	
d	(0.1478)	(0.1369)	(0.1431)	(0.1092)	(0.1207)	
A	50.8		42.5		27.0	
	7.5	6.1	7.0	3.3	4.6	
	2.0	1.5	1.9	0.6	1.1	
	0.5	0.4	0.5	0.1	0.3	
	0.1	0.1	0.1	0	0.1	
	69.0		56.0		33.1	
	10.2	8.0	9.4	4.1	6.1	
$\bar{A}$	69.0		56.0		33.1	
$q = \frac{2\bar{A}}{\Sigma\alpha}$ . . .	0.658		0.558		0.365	
2Aq	66.9		47.4		19.7	

TABLE 4

SHEAR FLOWS DUE TO VERTICAL SHEAR FROM BEAM THEORY

Biconvex section; aspect ratio, 2; total section shear, 2 lb

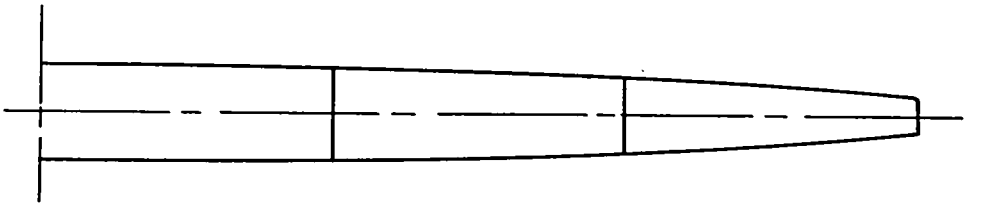

I_j	18.84	16.20	9.40	1.79
$(V_j)_s$	0.512	0.440	0.255	0.049
h_j	4.34	4.02	3.06	1.46
$(q_j)_s$	0.1180	0.1093	0.0834	0.0336
d	(0.1478)	(0.1369) (0.1431)	(0.1092) (0.1207)	(0.0573)
d $(q_j)_s$ . . .	0.0174	-0.0150 0.0156	-0.0091 0.0101	-0.0019
	(0.1478)	(0.1431) (0.1369)	(0.1207) (0.1092)	
	0.0024	0.0065	0.0082	
	-0.0004	0.0009 0.0003	0.0009 0.0008	
	-0.0001	0.0002 0.0001	0.0001 0.0001	
	0.0030	0.0079	0.0091	
	-0.0004	0.0011 0.0004	0.0010 0.0010	
q_n	0.0031	0.0079	0.0092	
$(q_j)_i$	-0.0062	-0.0048	-0.0013	0.0092
q_j	0.1118	0.1045	0.0821	0.0428
V_j	0.485	0.420	0.251	0.062

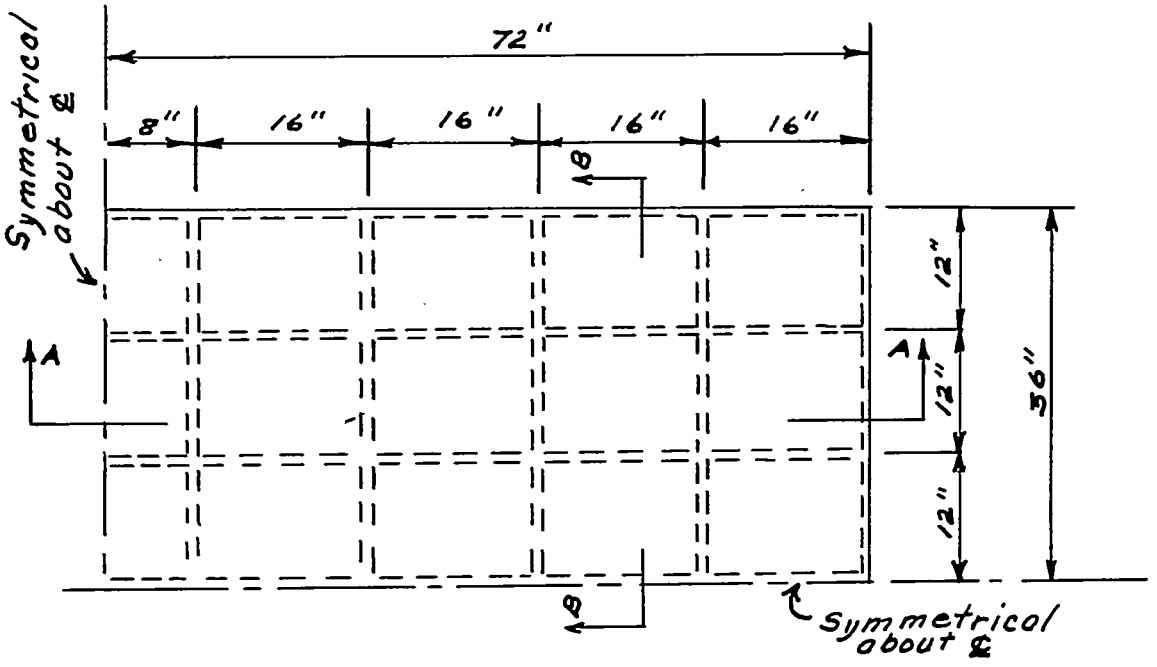

(a) Plan form.

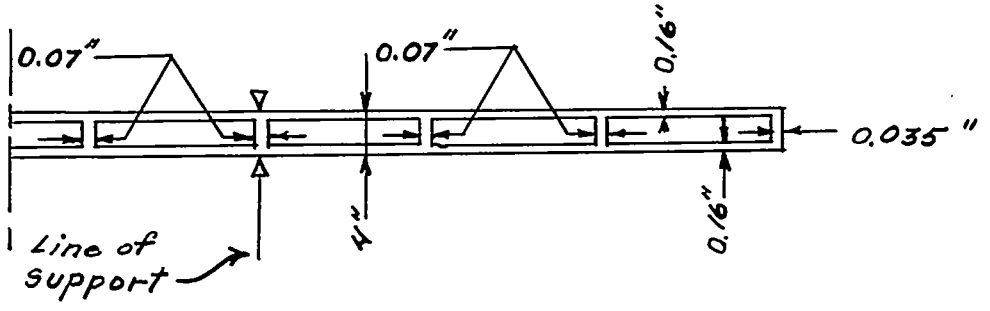

(b) Section A-A.

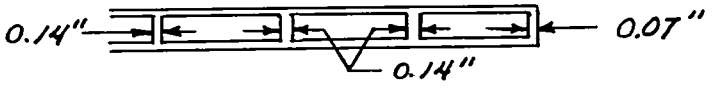

(c) Section B-B.

Figure 1.- Wing with rectangular cross section. Aspect ratio, 2.

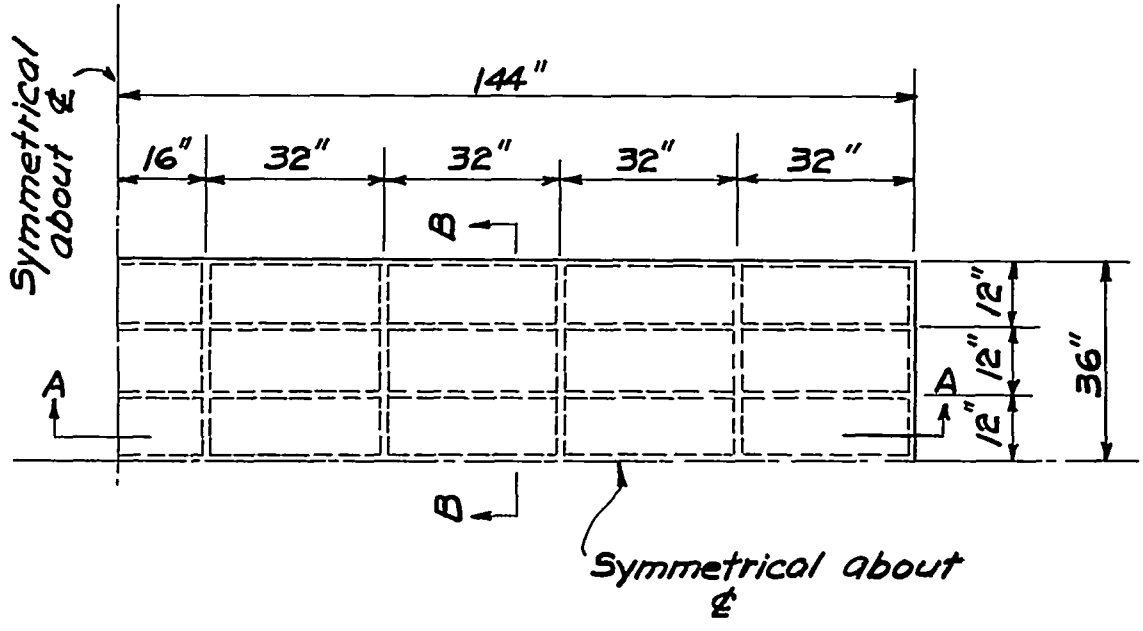

(a) Plan form.

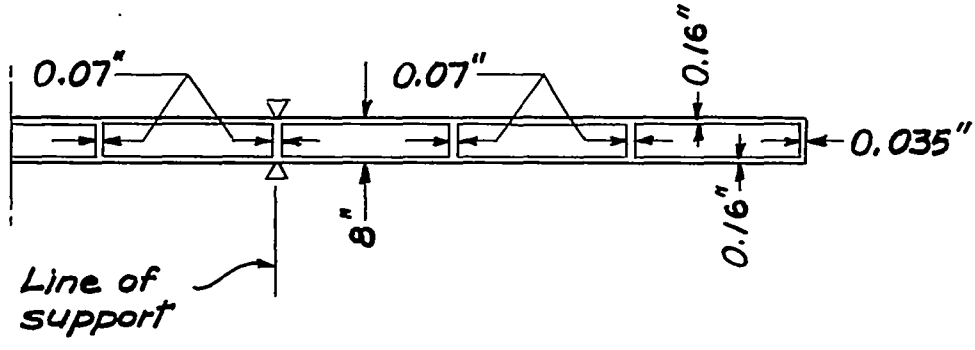

(b) Section A-A.

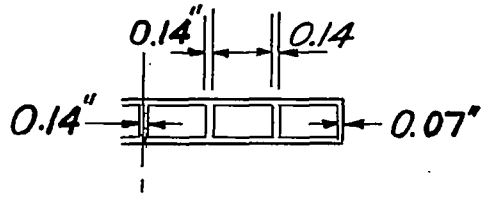

(c) Section B-B.

Figure 2.- Wing with rectangular cross section. Aspect ratio, 4.

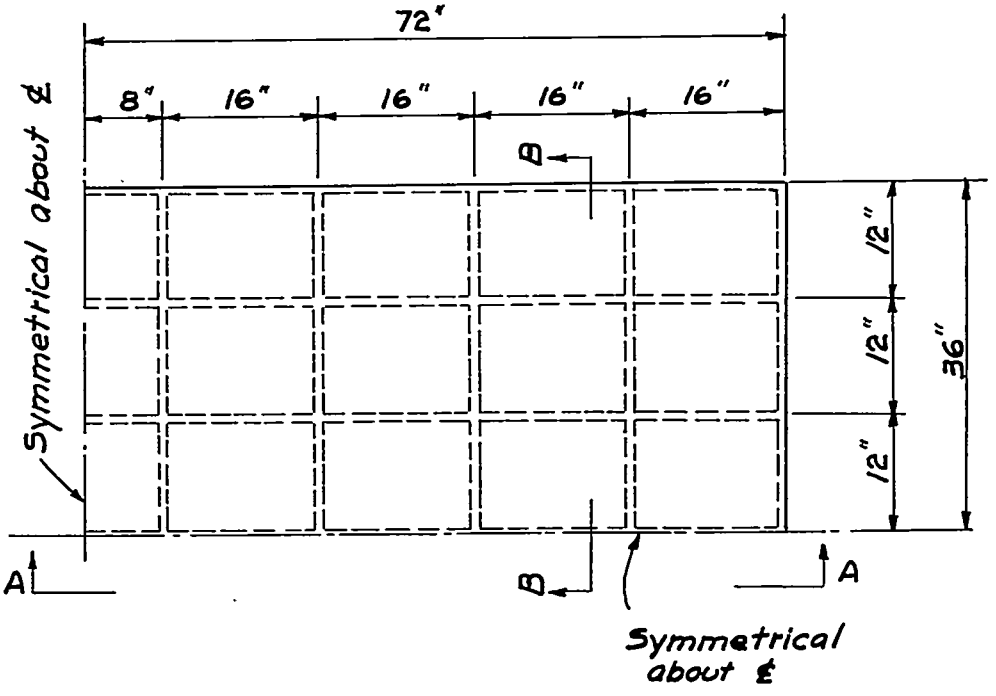

(a) Plan form.

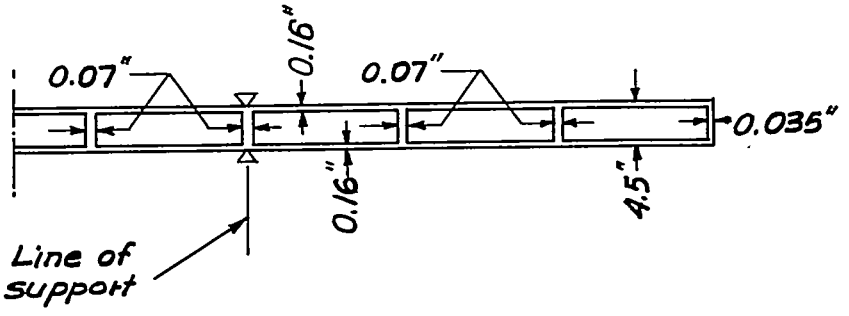

(b) View A-A.

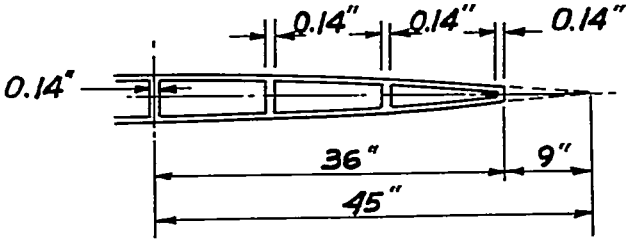

(c) Section B-B.

Figure 3.- Wing with biconvex cross section. Aspect ratio, 2.

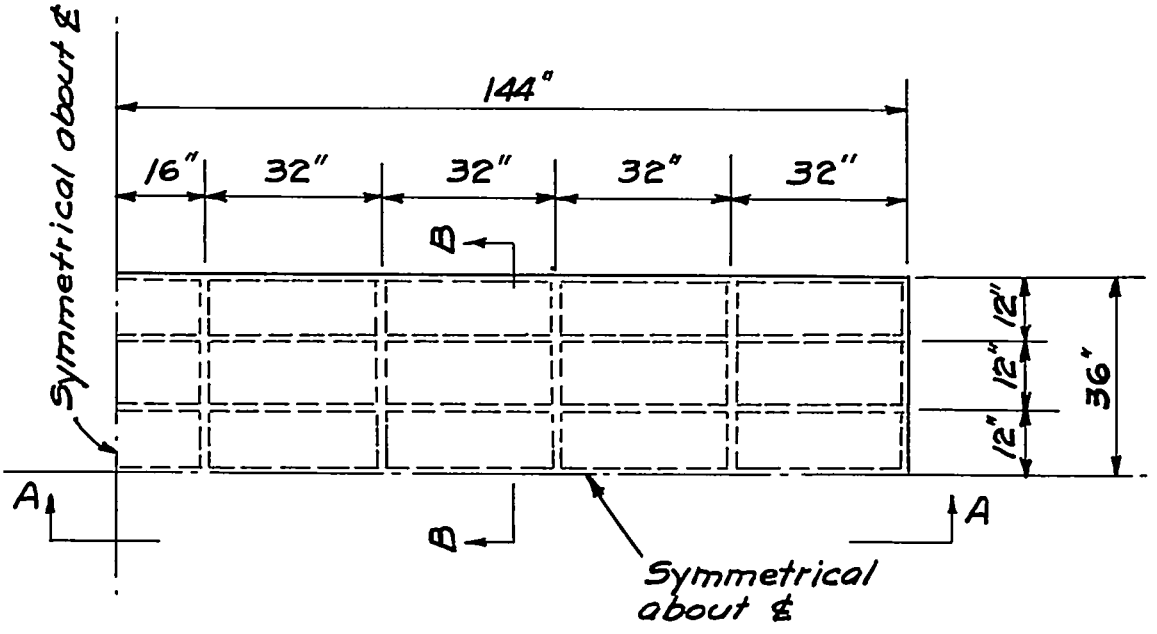

(a) Plan form.

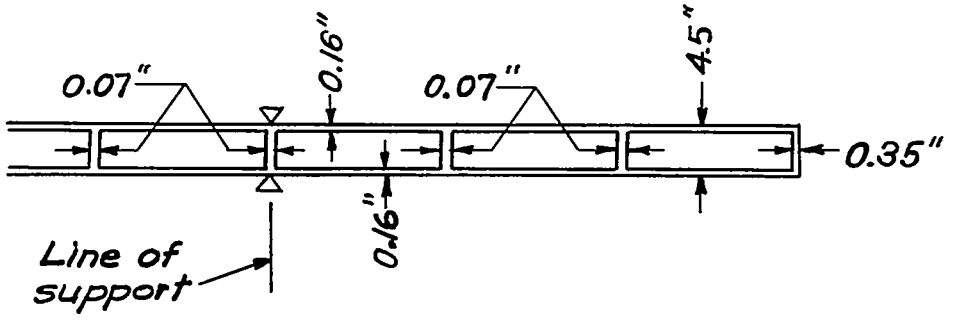

(b) View A-A.

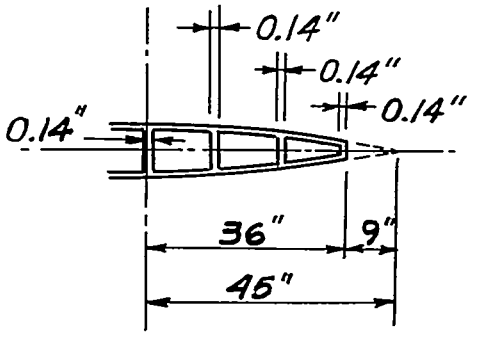

(c) Section B-B.

Figure 4.- Wing with biconvex cross section. Aspect ratio, 4.

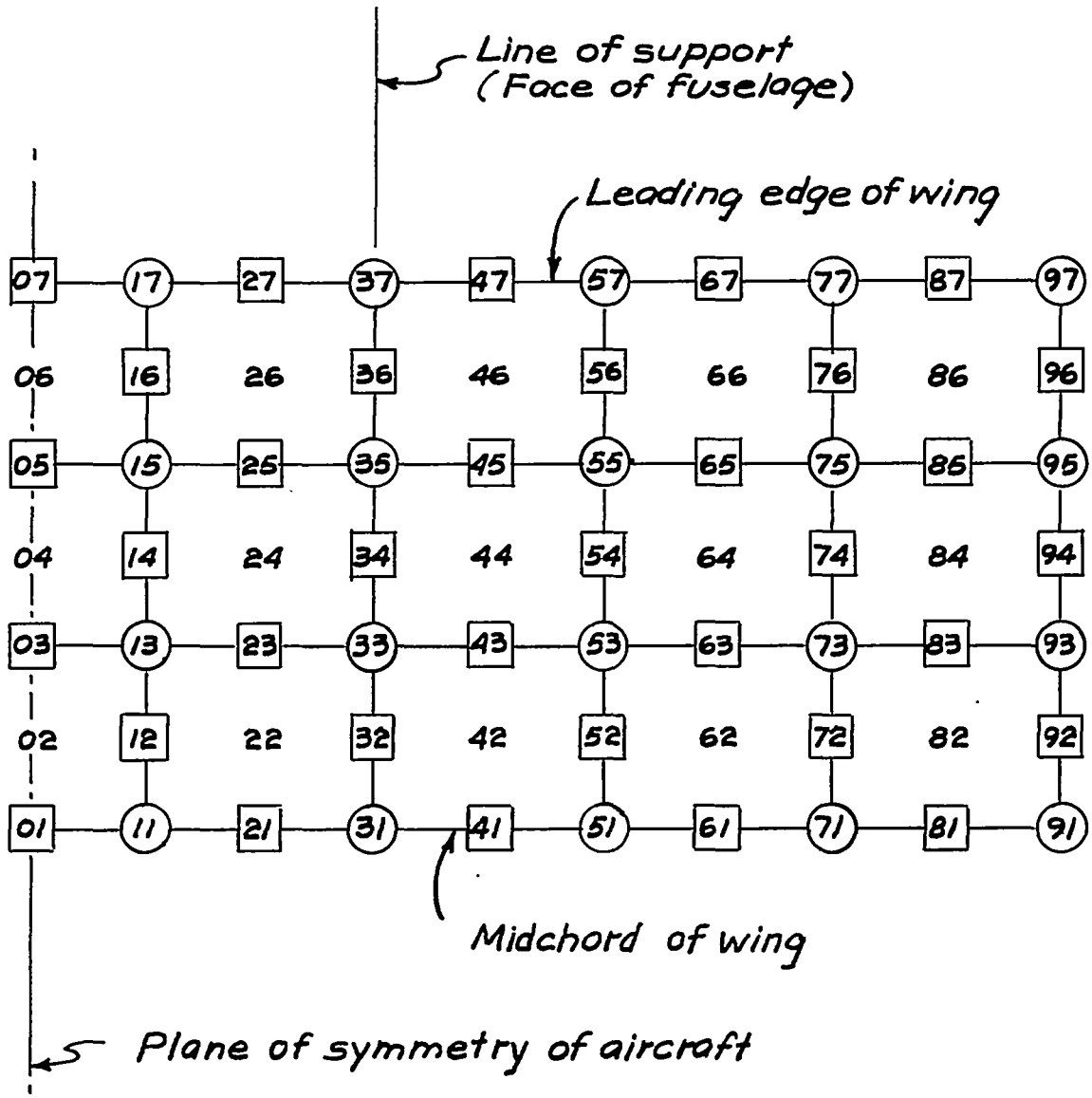

Figure 5.- Numbering of points at which quantities are measured.

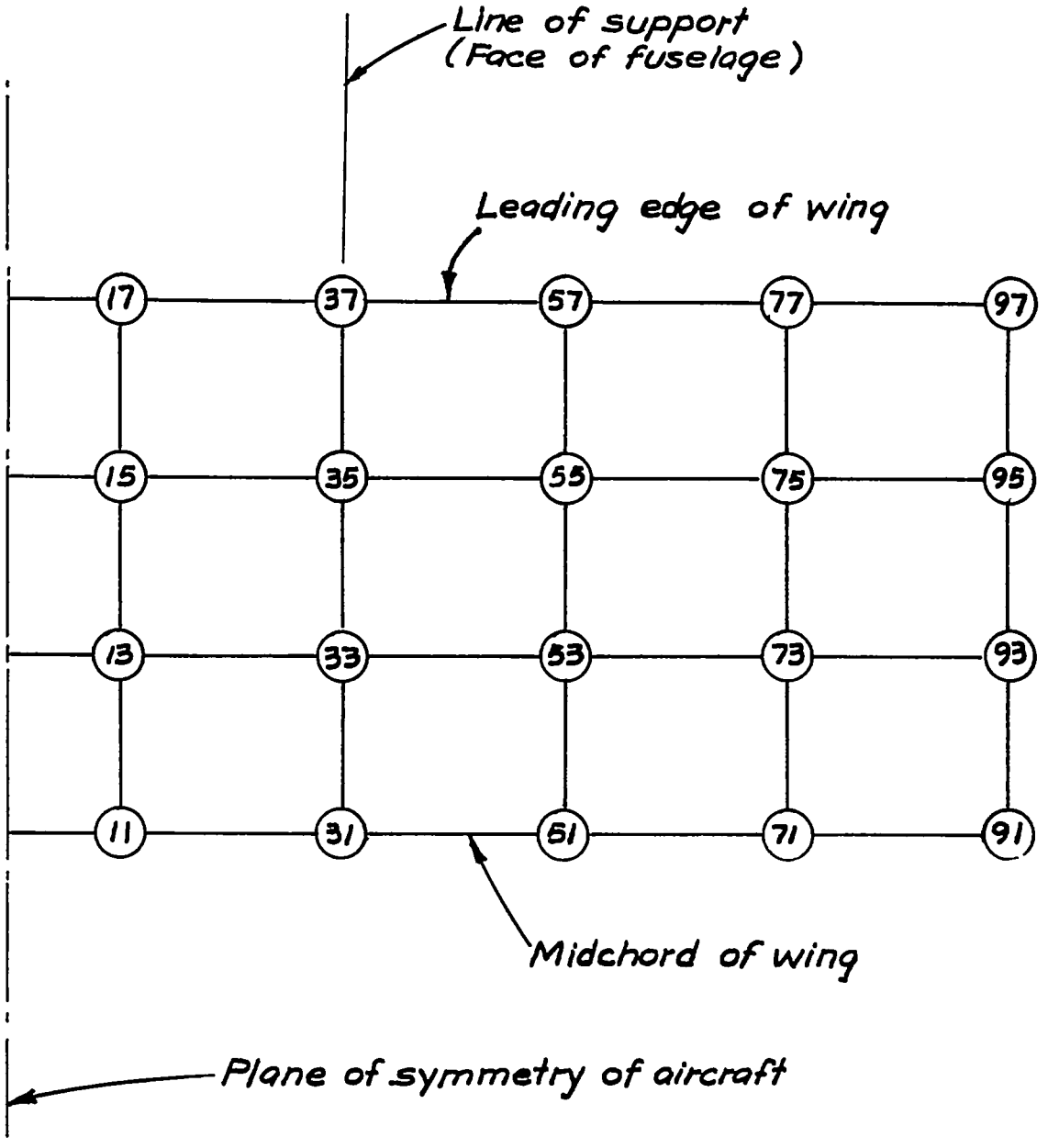

Figure 6.- Points at which concentrated loads are applied and deflections and bending moments are measured.

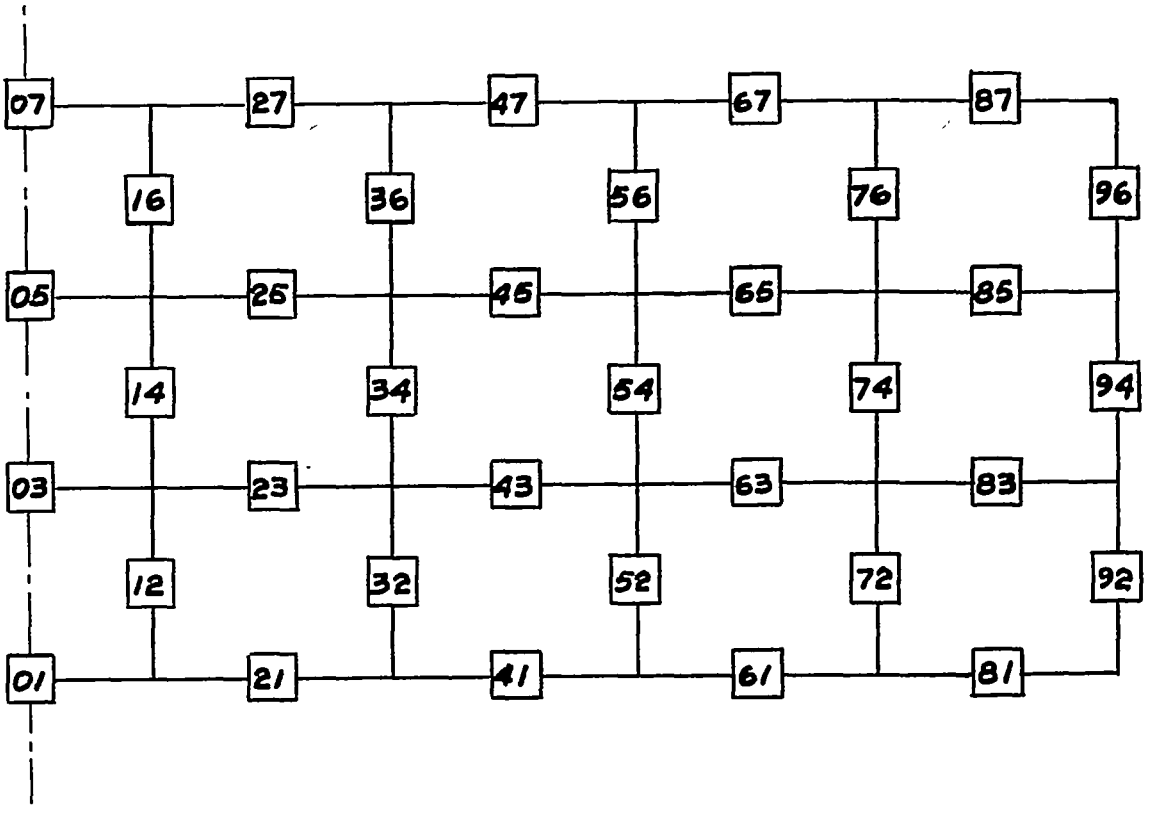

Figure 7.- Points at which spanwise and chordwise shears are determined.

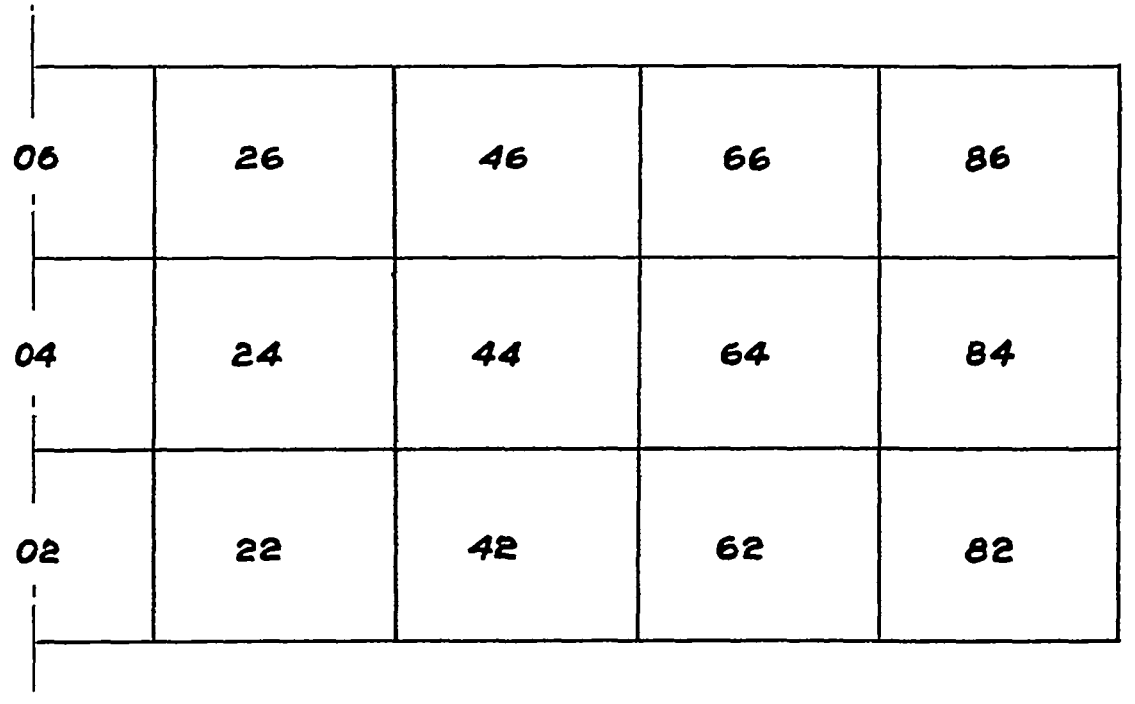

Figure 8.- Points at which twisting moments are determined.

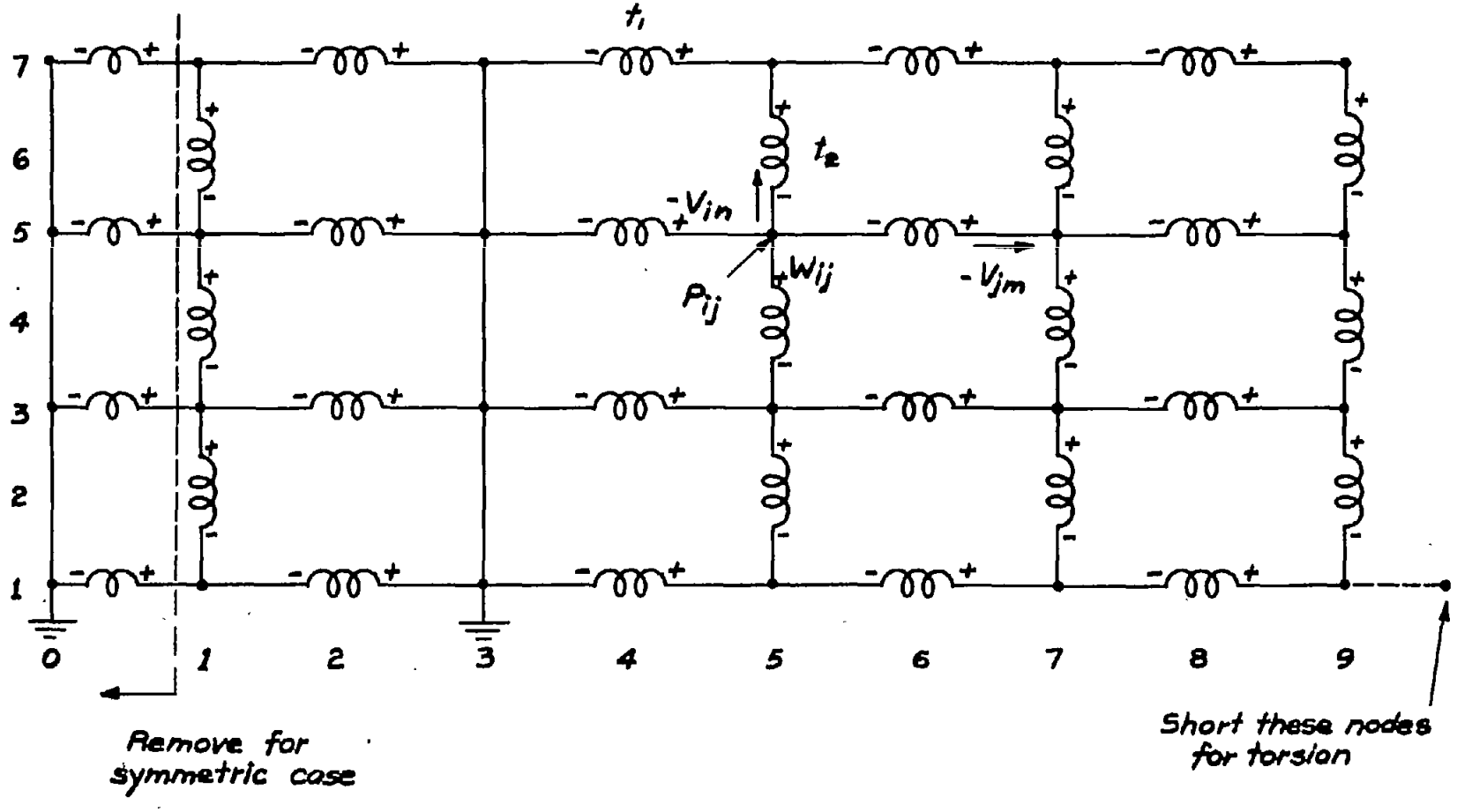

Figure 9.- Circuit for shears and deflections.

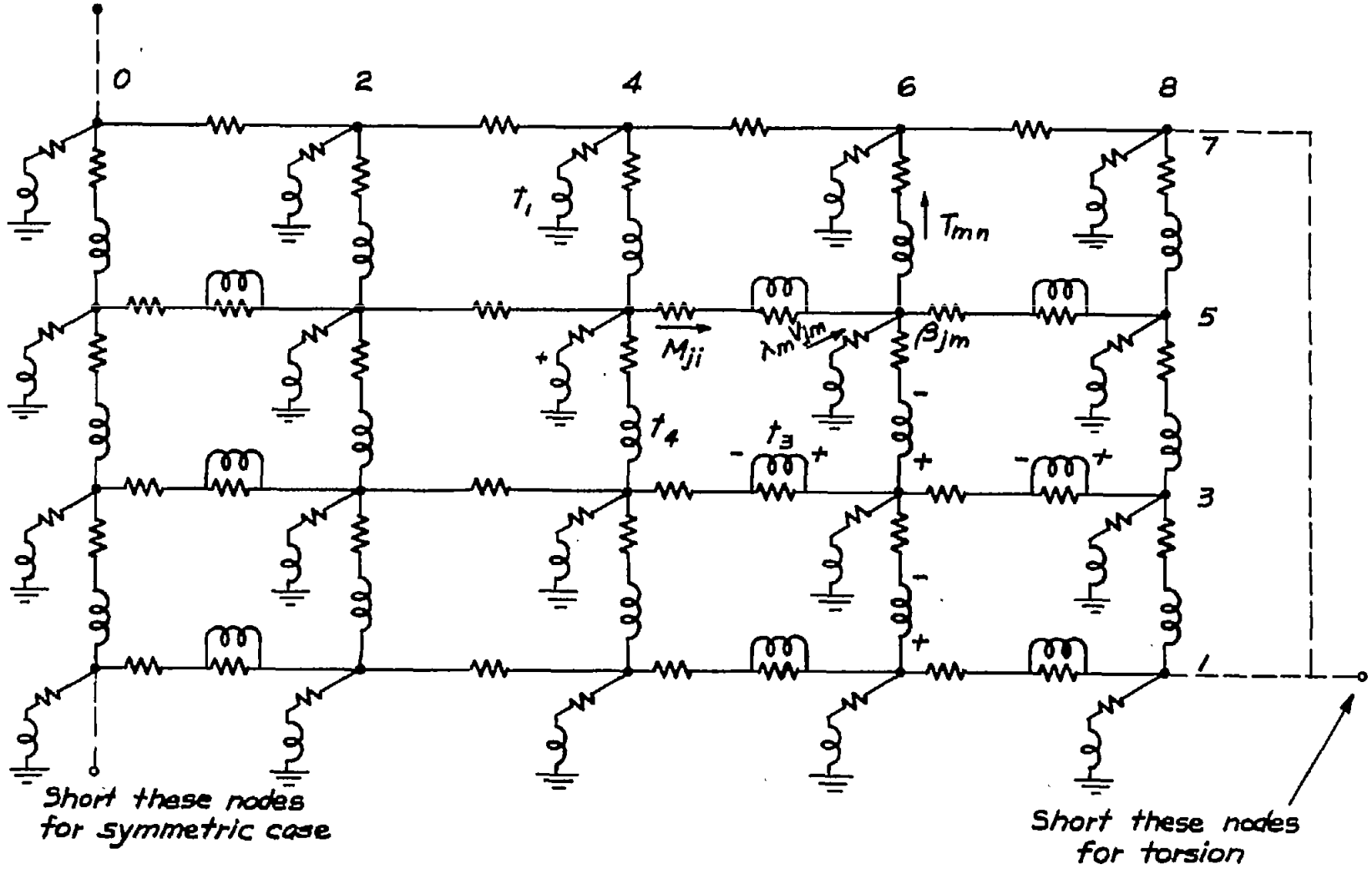

Figure 10.- Circuit for spanwise bending moments and chordwise twisting moments.

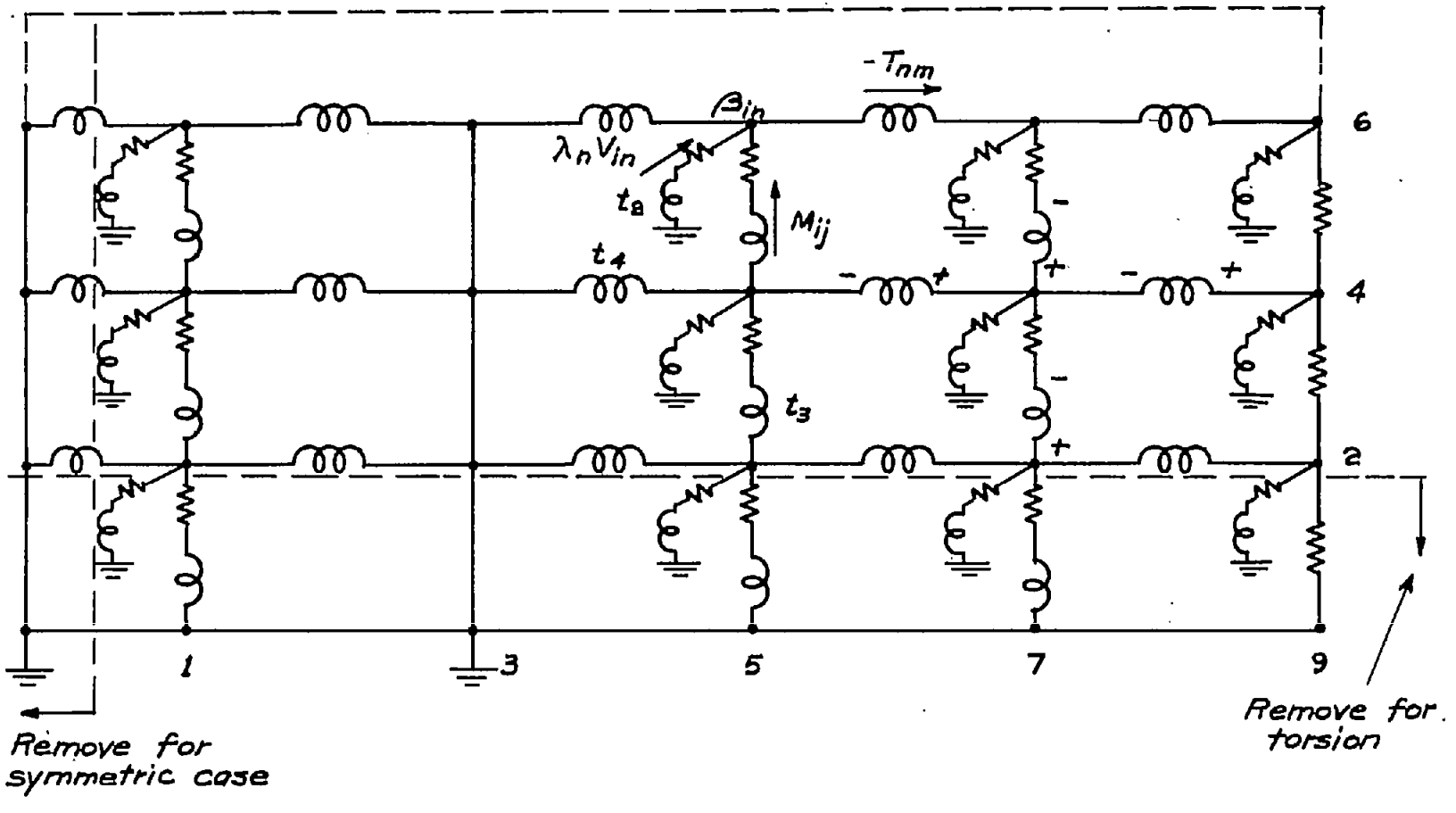

Figure 11.- Circuit for chordwise bending moments and spanwise twisting moments.

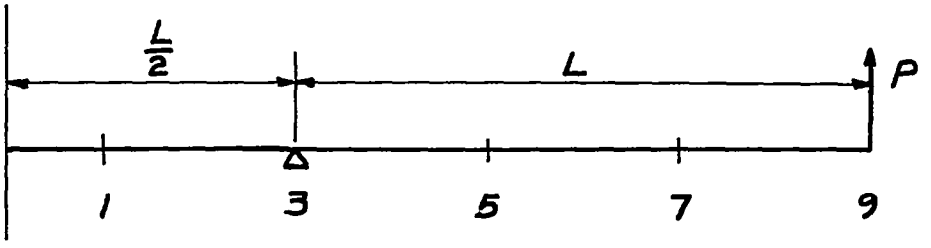

(a) Loaded beam.

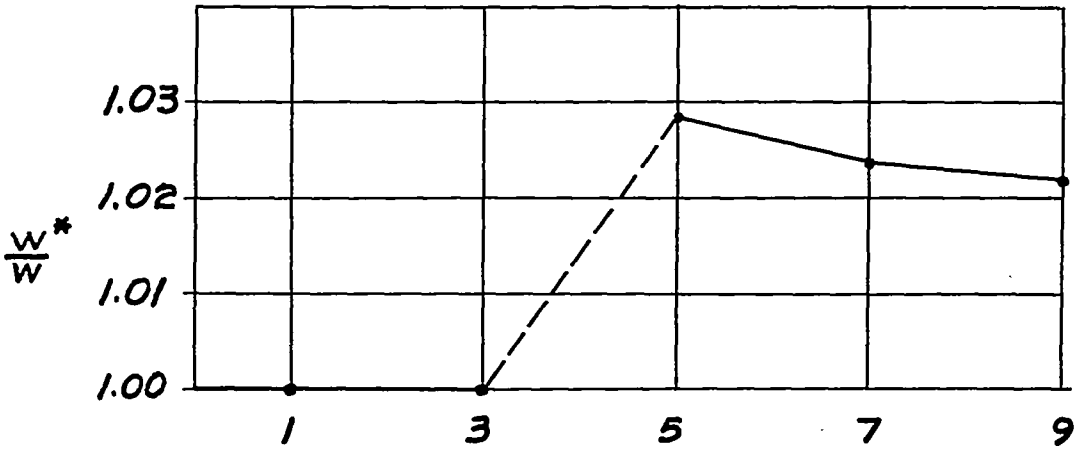

(b) Relative deflections from difference equations.

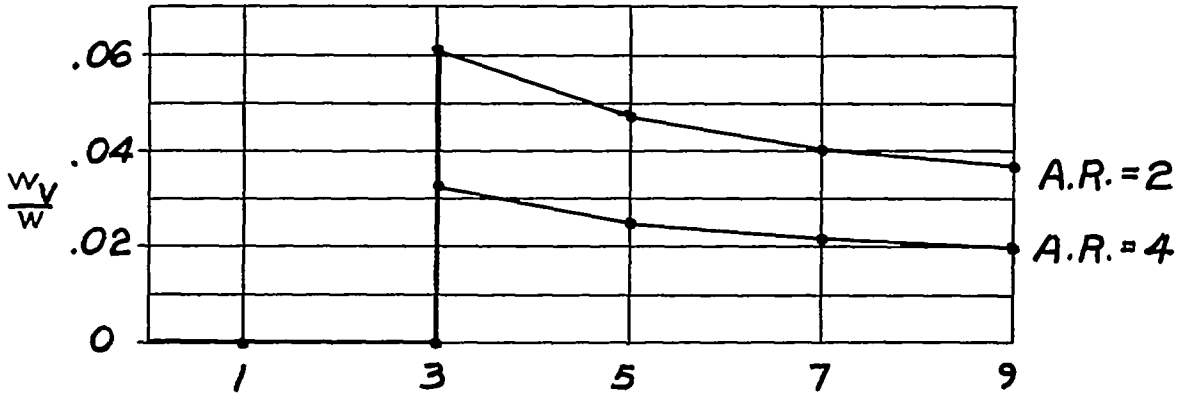

(c) Deflections due to shear for rectangular cross section.

Figure 12.- Deflections from beam theory for symmetrical loads.

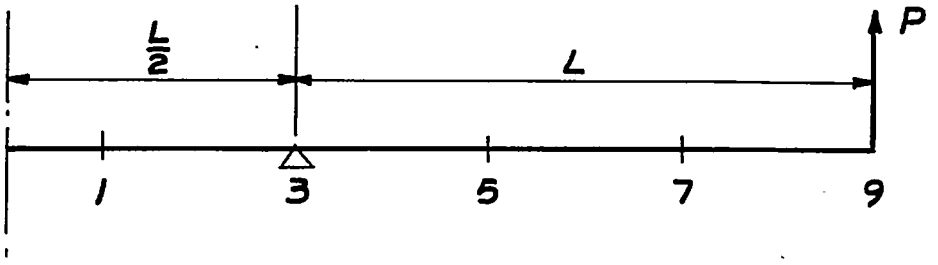

(a) Loaded beam.

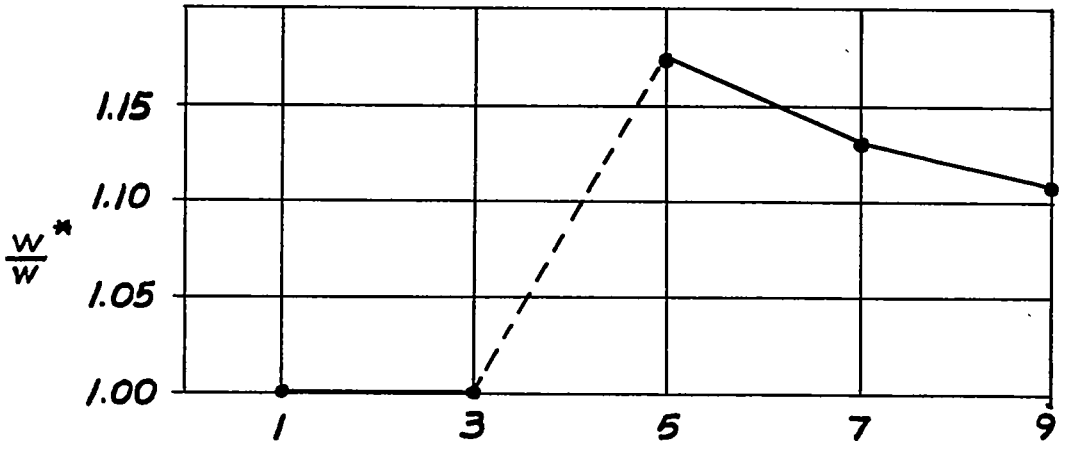

(b) Relative deflections from difference equations.

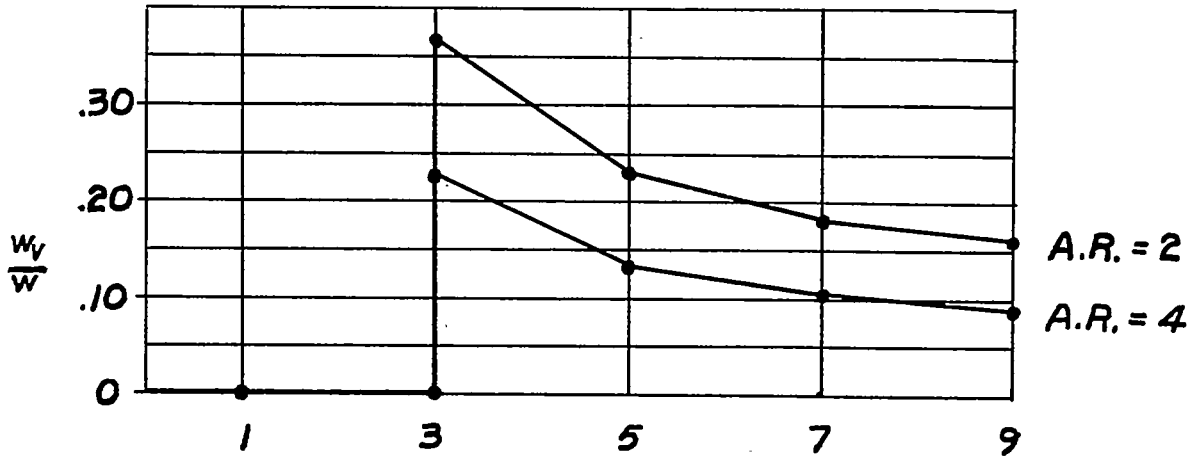

(c) Deflections due to shear for rectangular cross section.

Figure 13.- Deflections from beam theory for antisymmetrical loads.

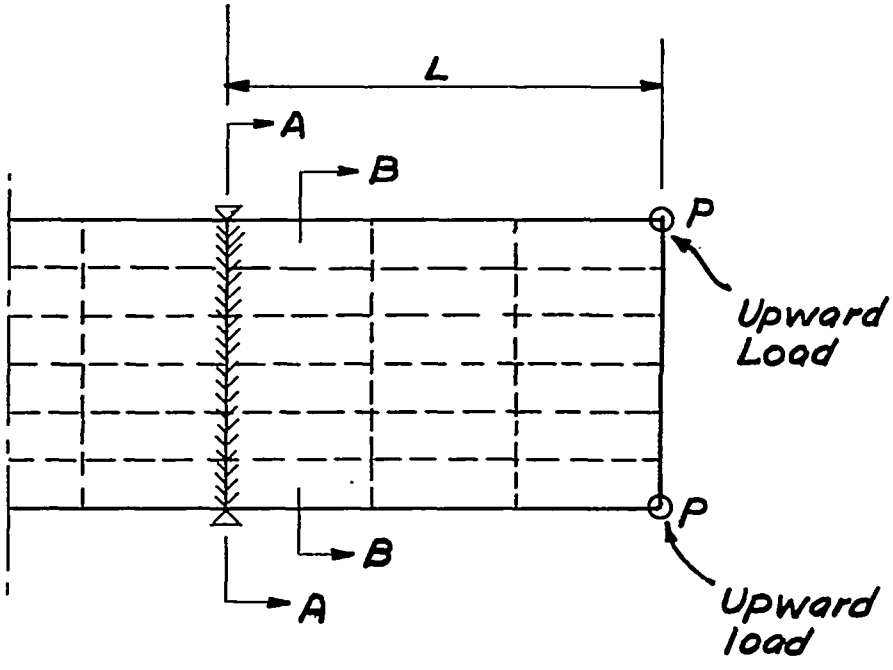

(a) Bending load. Bending moment on section A-A is 2PL. Shear on section B-B is 2P.

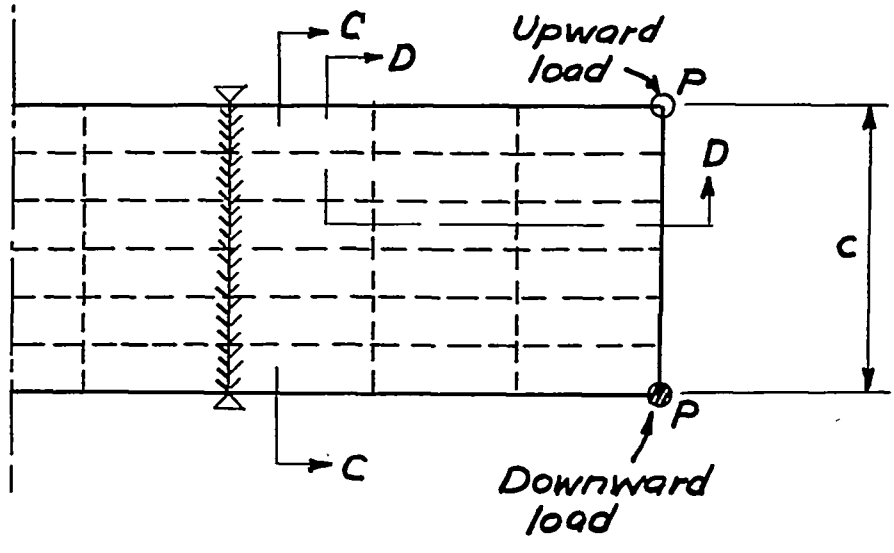

(b) Torsional load. Torque on section C-C is Pc. Shear on section D-D is P.

Figure 14.- Control sections for correcting electrical quantities to satisfy statics.

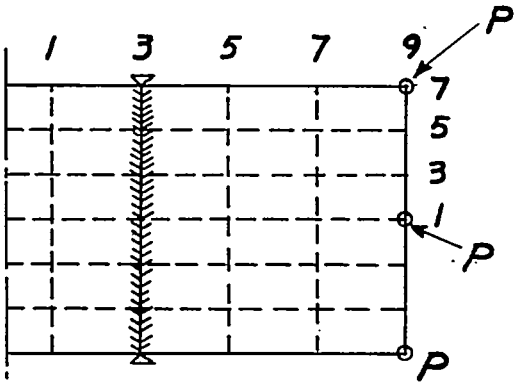

(a) Loading points. P = 1 kip.

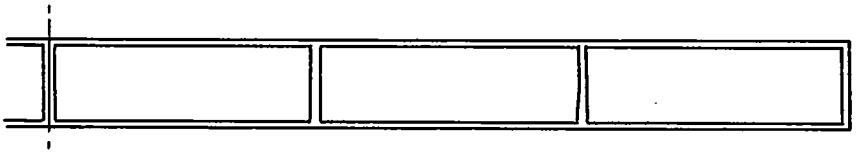

(b) Half cross section.

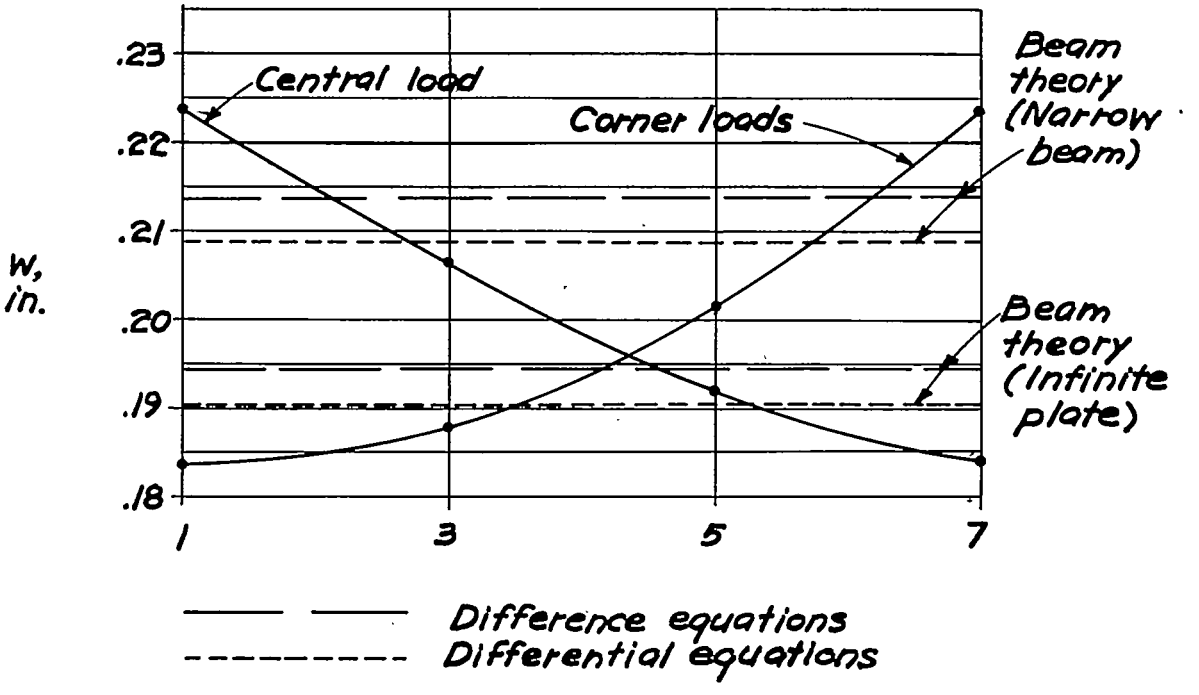

(c) Deflections.

Figure 15.- Chordwise deflections at tip. Aspect ratio, 2. Symmetric bending.

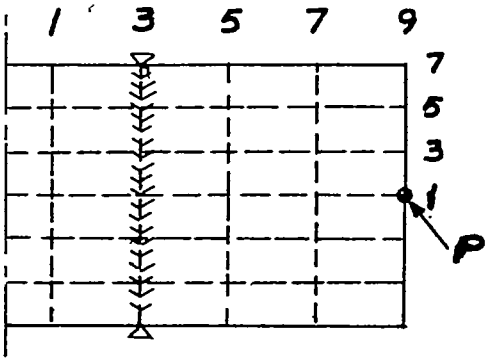

(a) Loading point. P = 2 kips.

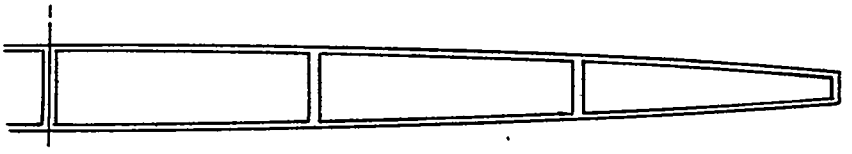

(b) Half cross section.

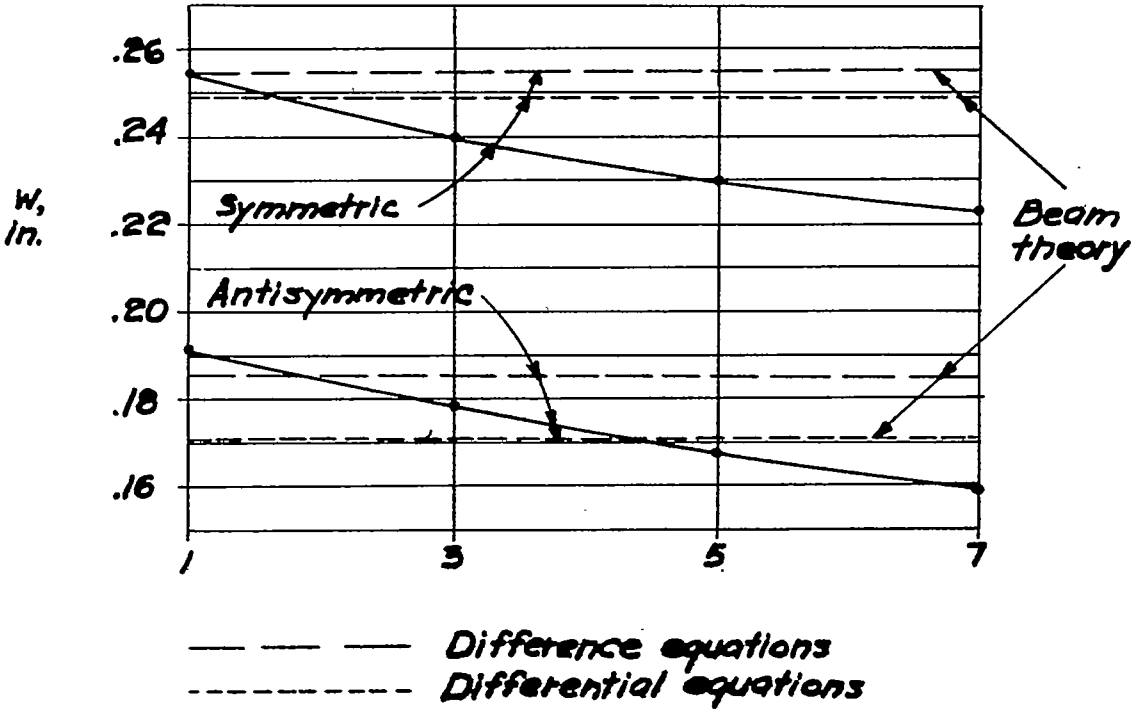

(c) Deflections.

Figure 16.- Chordwise deflections at tip. Aspect ratio, 2. Central load at tip.

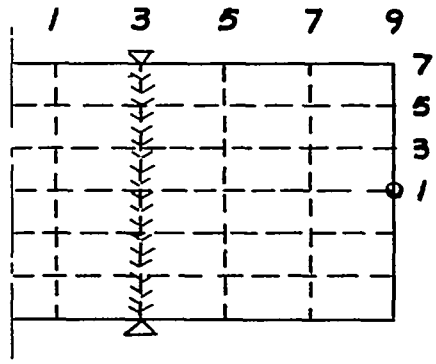

(a) Loading point.

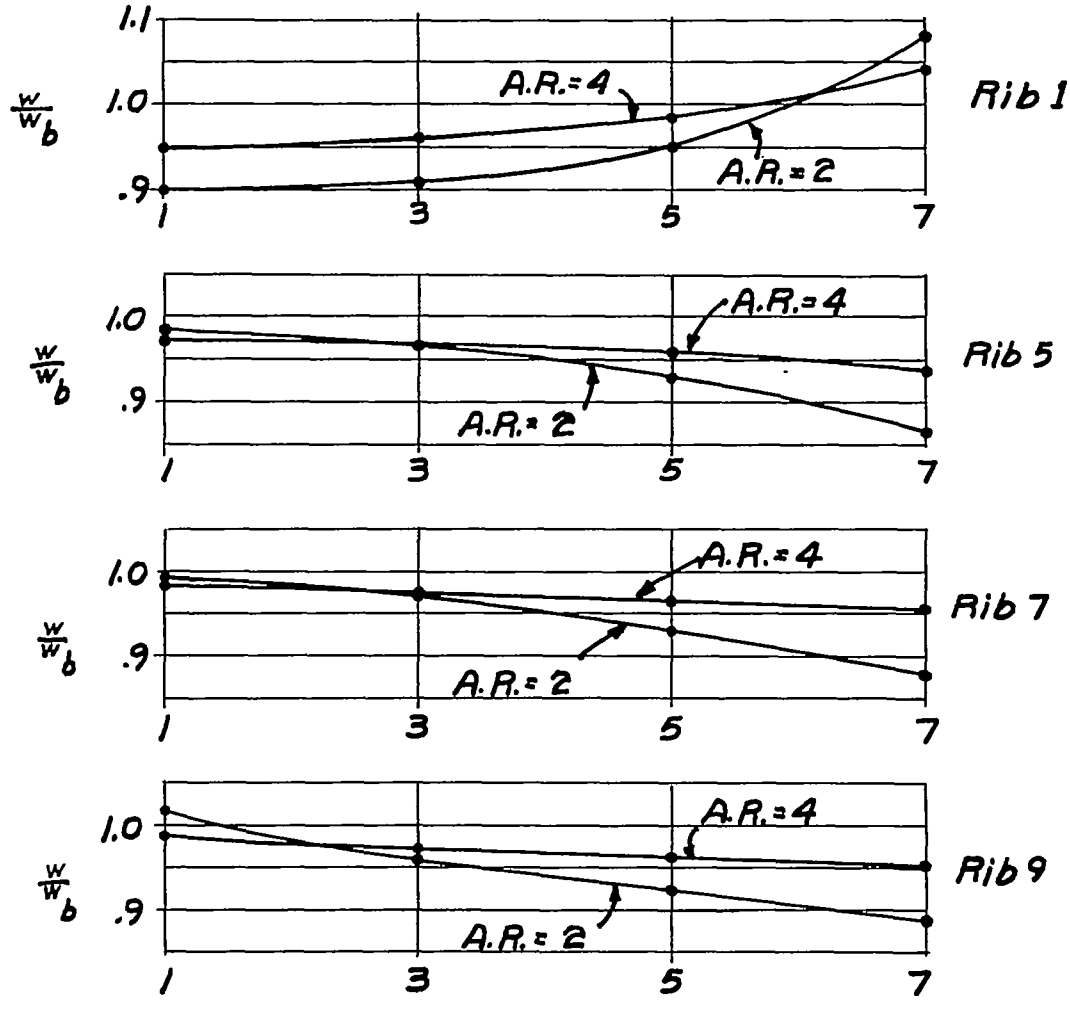

(b) Relative values of deflections.

Figure 17.- Chordwise deflections at ribs. Biconvex section. Symmetric bending.

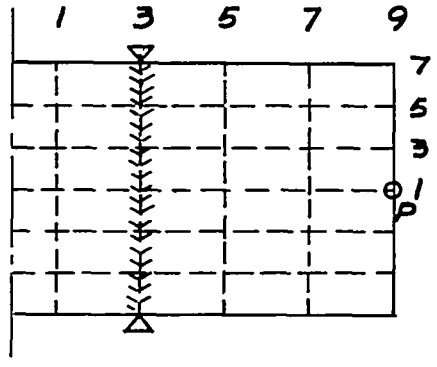

(a) Loading point. P = 2 kips.

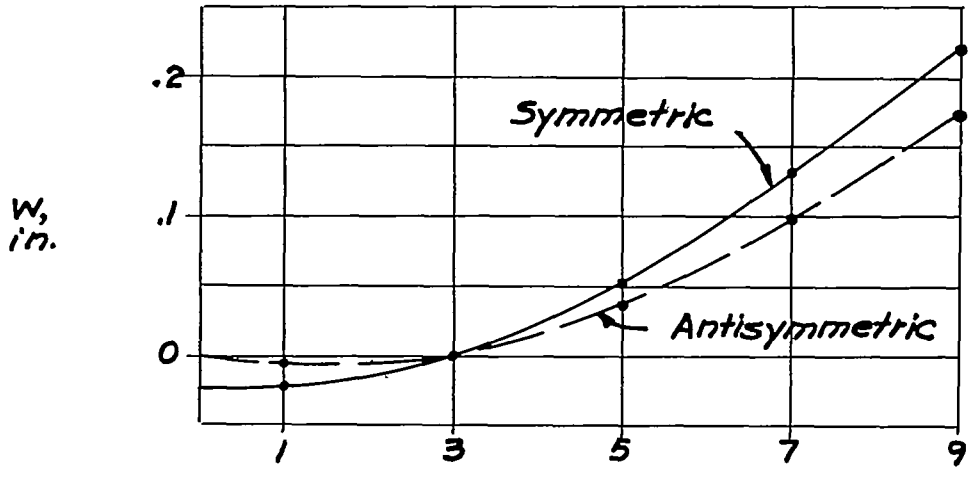

(b) Spar 1.

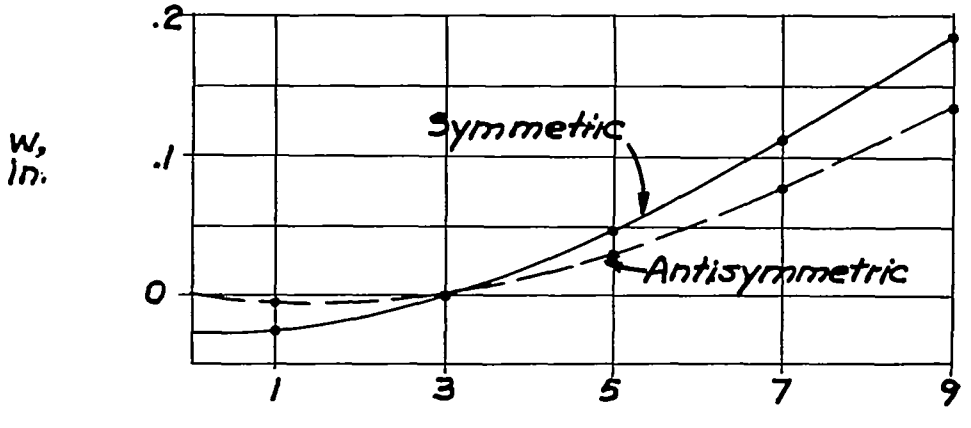

(c) Spar 7.

Figure 18.- Spanwise deflection of spars. Aspect ratio, 2. Rectangular section.

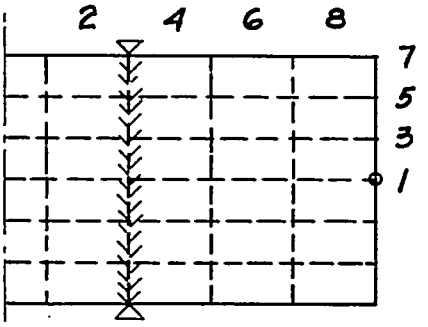

(a) Loading point.

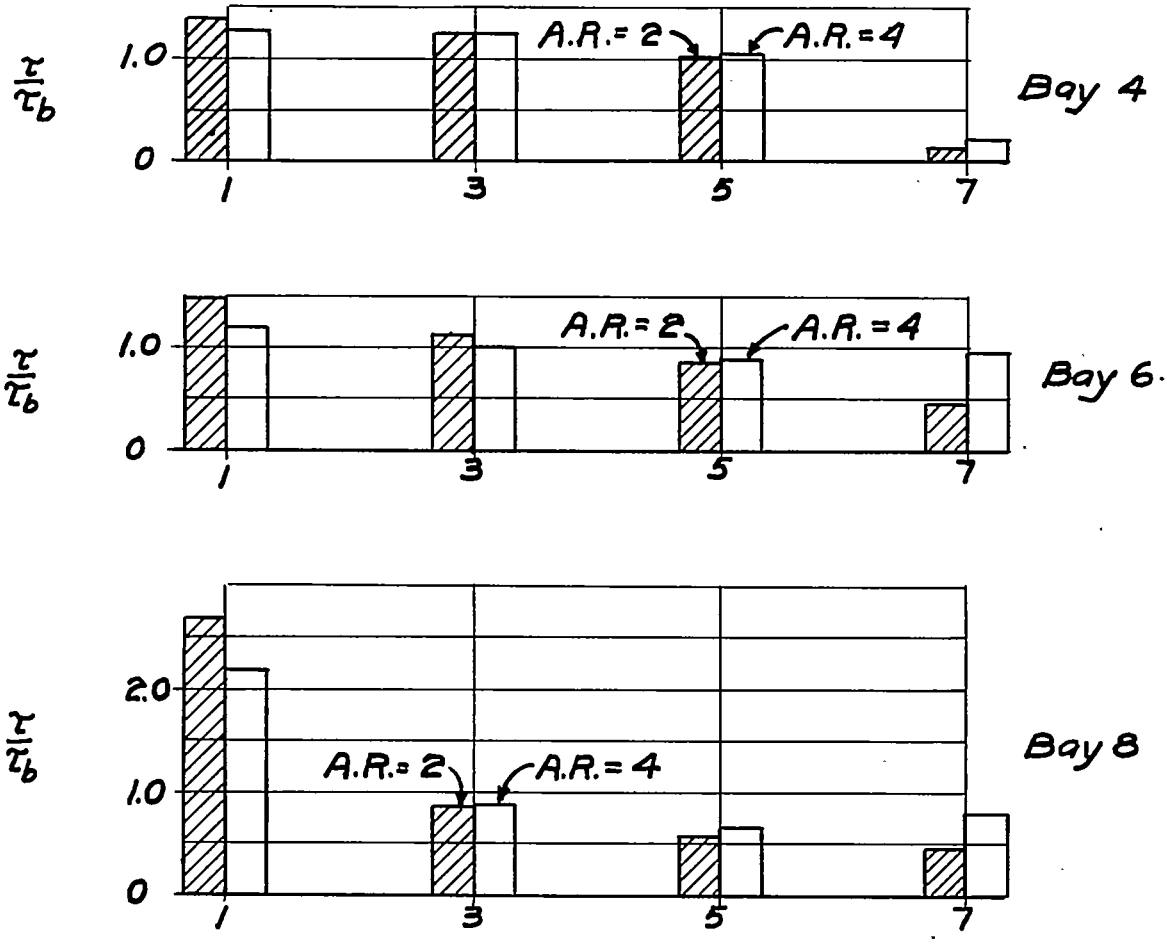

(b) Relative values of stress.

Figure 19.- Chordwise distribution of shears in spars. Symmetric bending. Rectangular section.

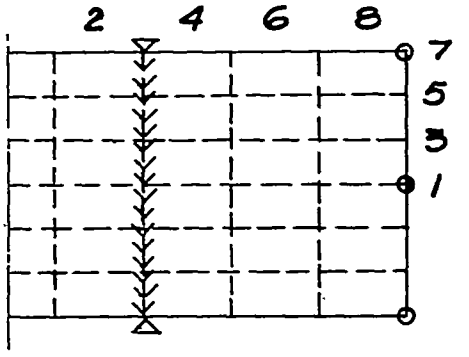

(a) Loading points.

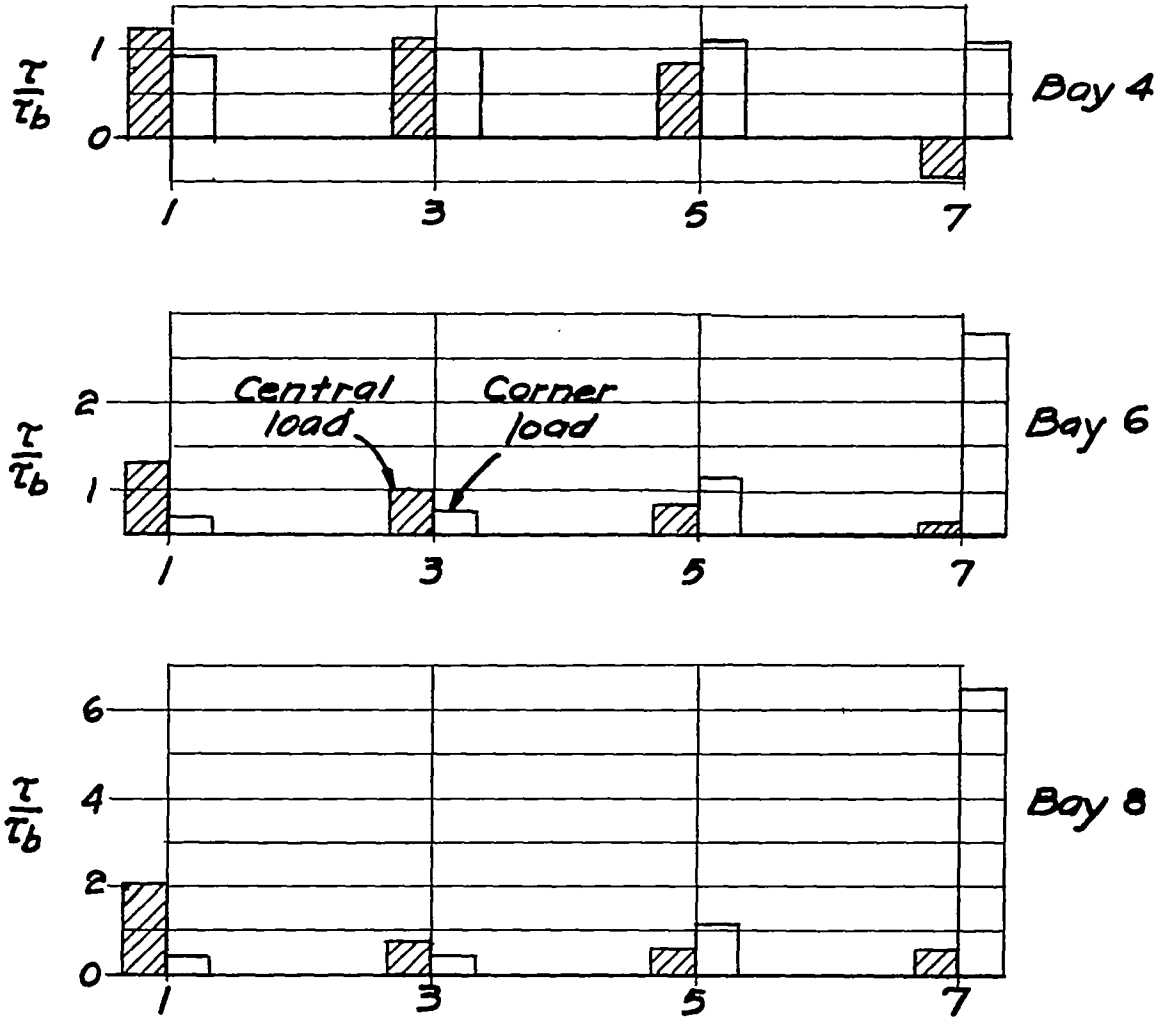

(b) Relative values of stress.

Figure 20.- Chordwise distribution of shears in spars. Aspect ratio, 2. Symmetric bending. Biconvex section.

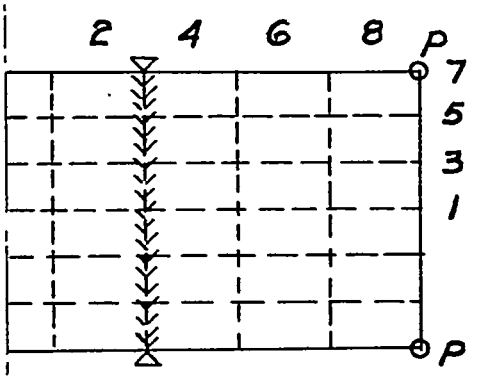

(a) Loading points. P = 1 pound.

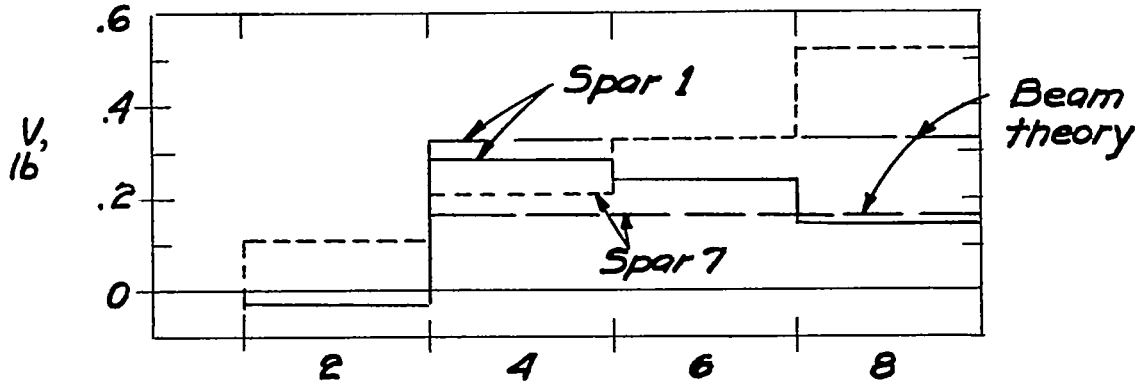

(b) Symmetric loads.

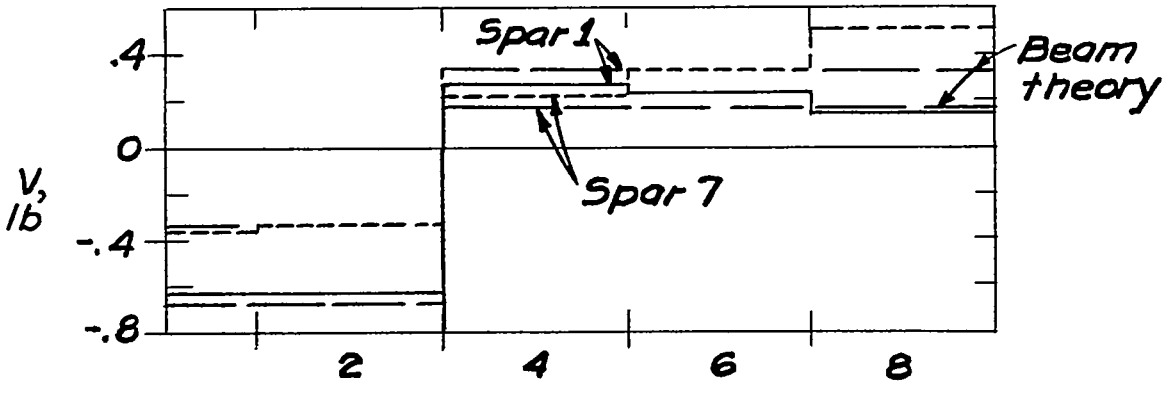

(c) Antisymmetric loads.

Figure 21.- Spanwise distribution of shears in spars. Aspect ratio, 2. Rectangular section.

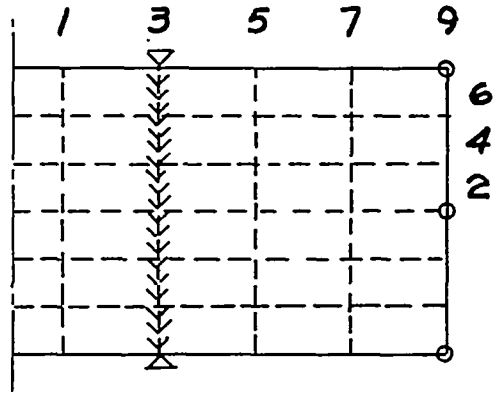

(a) Loading points.

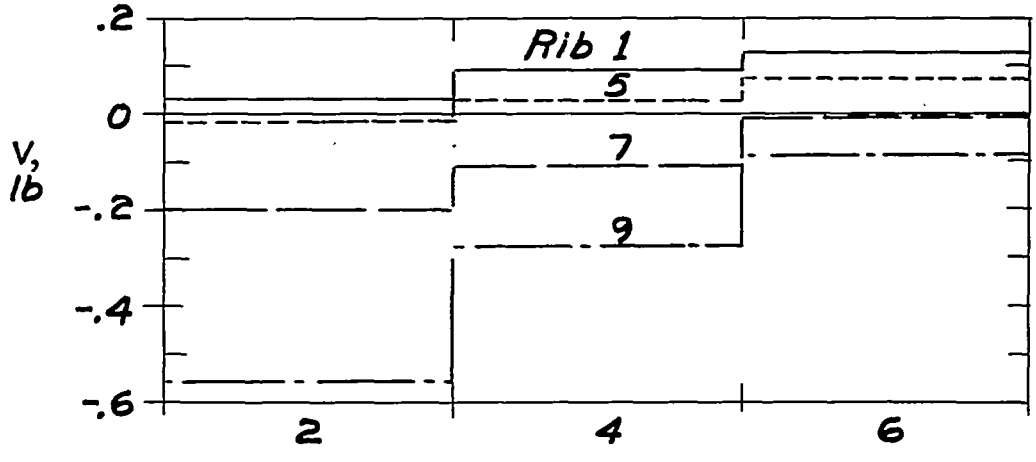

(b) Central load (2 pounds).

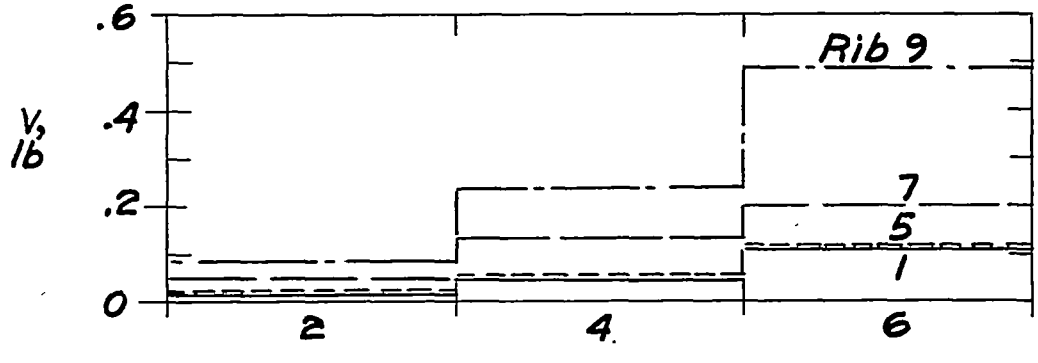

(c) Corner loads (1 pound each).

Figure 22.- Chordwise distribution of shears in ribs. Aspect ratio, 2. Symmetric bending. Rectangular section.

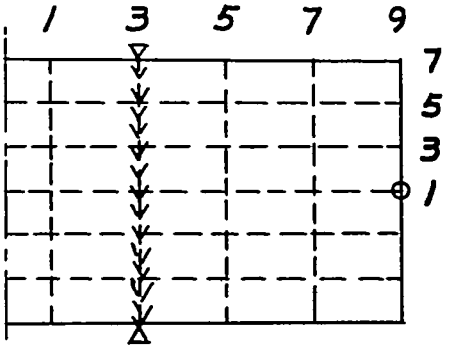

(a) Loading point.

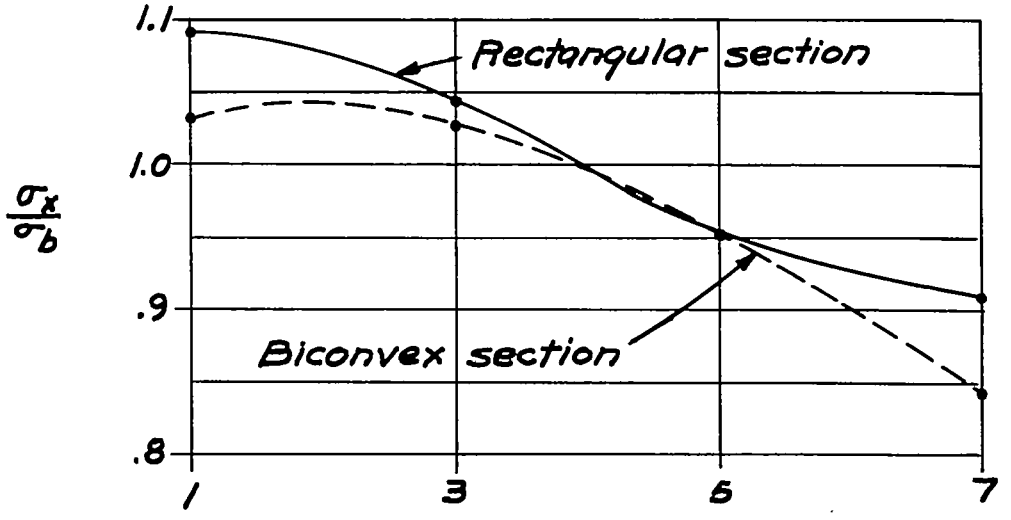

(b) Aspect ratio, 2.

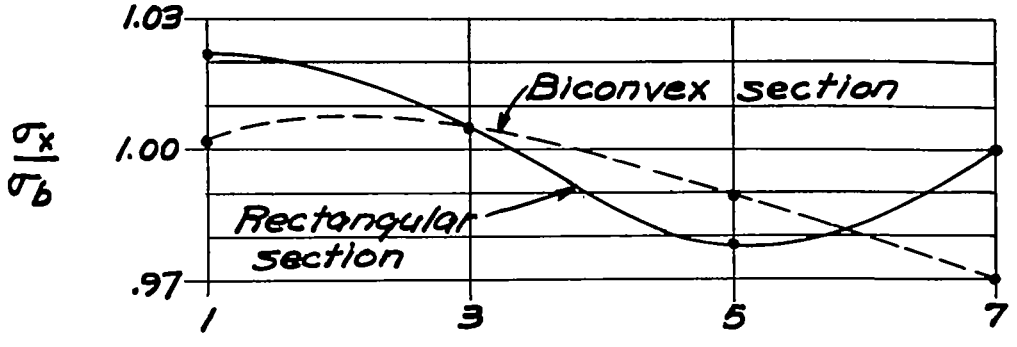

(c) Aspect ratio, 4.

Figure 23.- Spanwise normal stress over support. Symmetric bending. Central load.

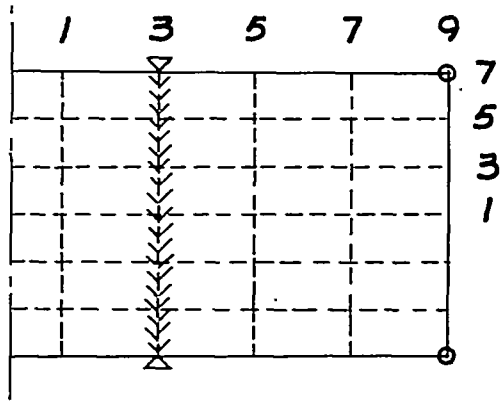

(a) Loading points.

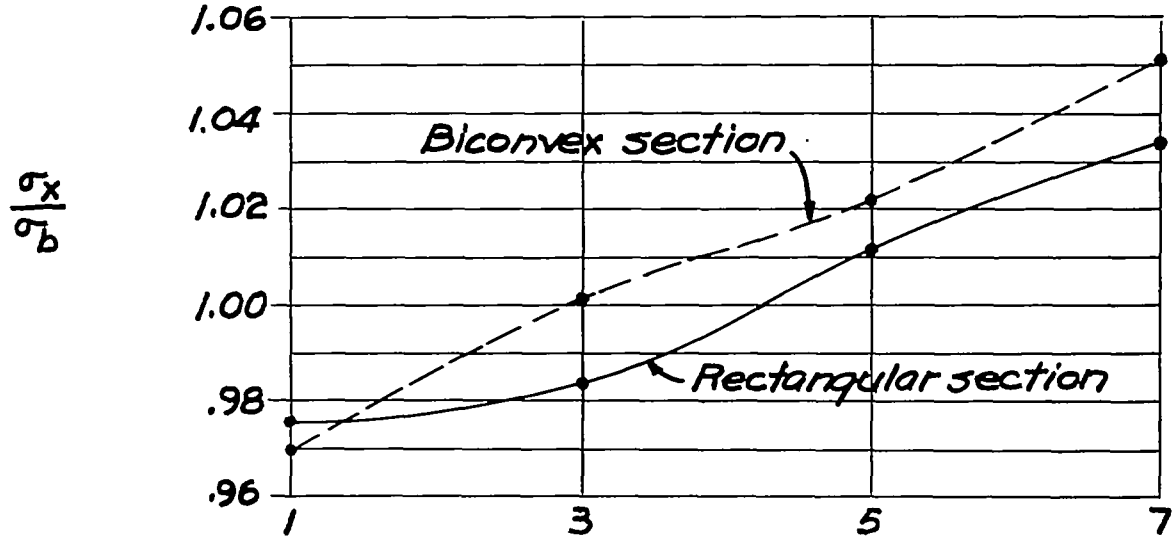

(b) Aspect ratio, 2.

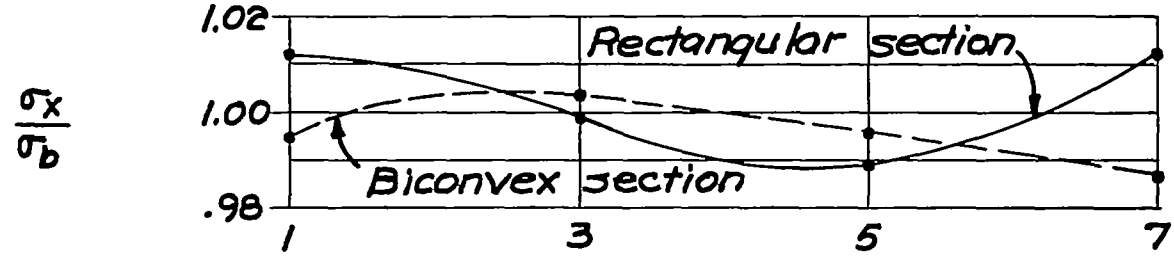

(c) Aspect ratio, 4.

Figure 24.- Spanwise normal stress over support. Symmetric bending. Corner loads.

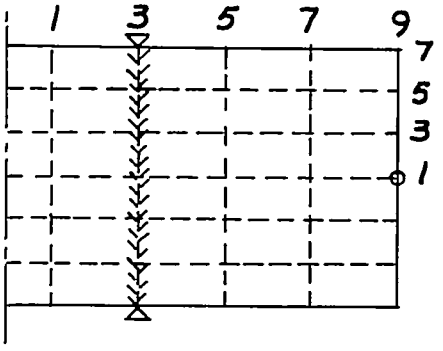

(a) Loading point.

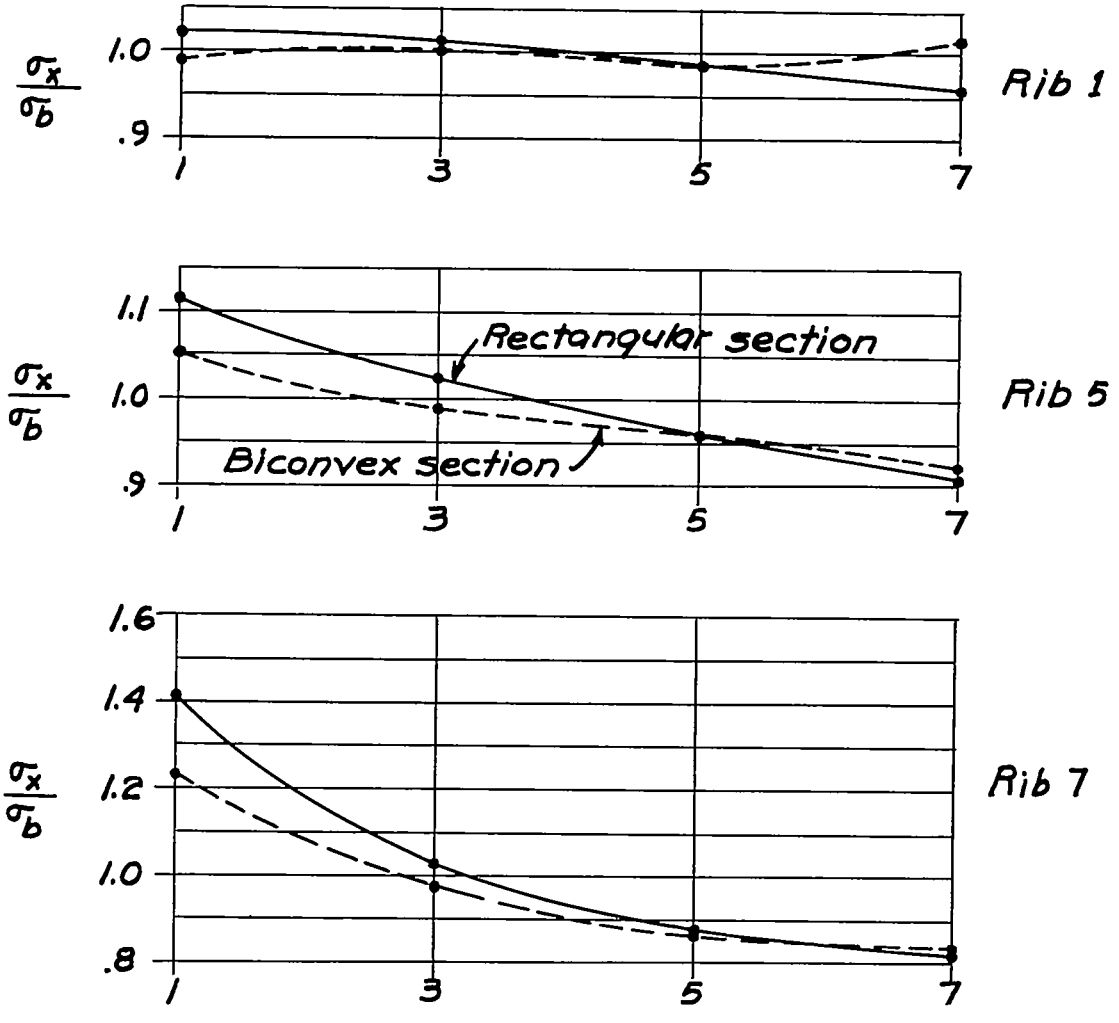

(b) Relative values of stress.

Figure 25.- Spanwise normal stress at various ribs. Aspect ratio, 2. Symmetric bending.

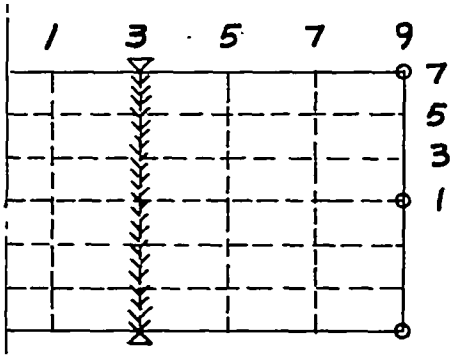

(a) Loading points.

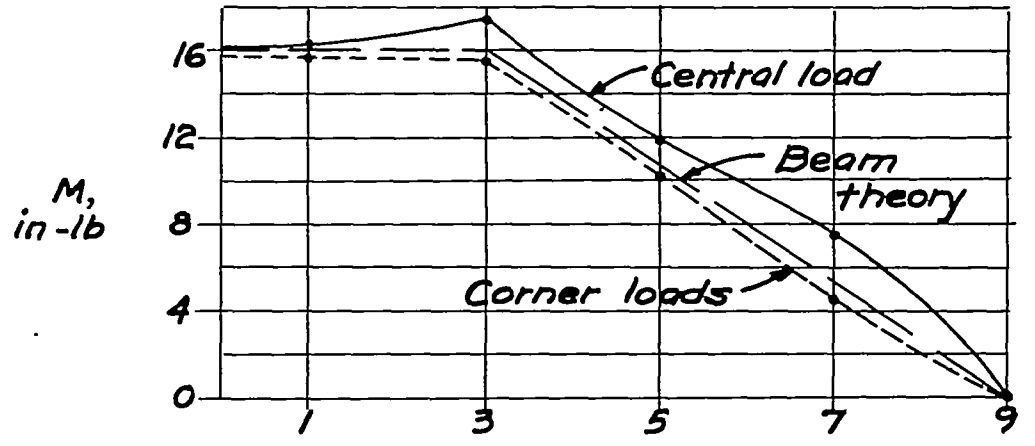

(b) Spar 1.

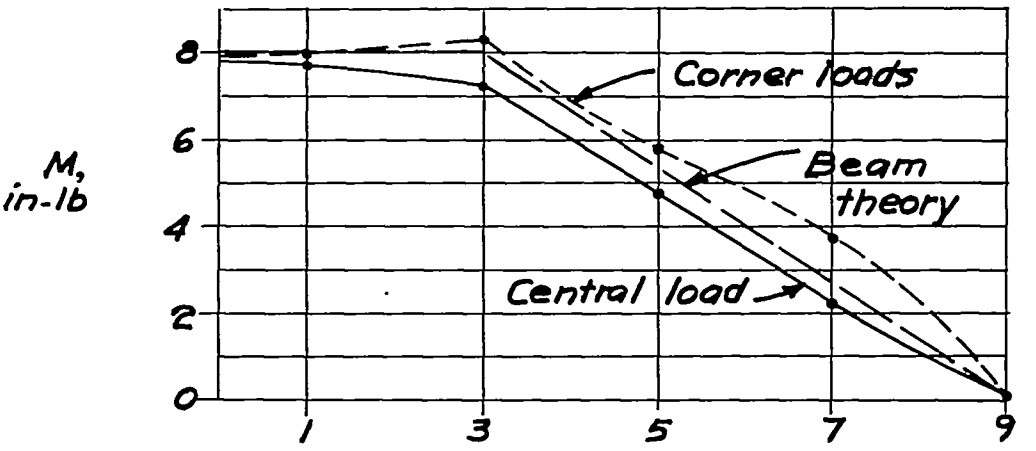

(c) Spar 7.

Figure 26.- Bending moments in spars. Aspect ratio, 2. Symmetric bending. Rectangular section.

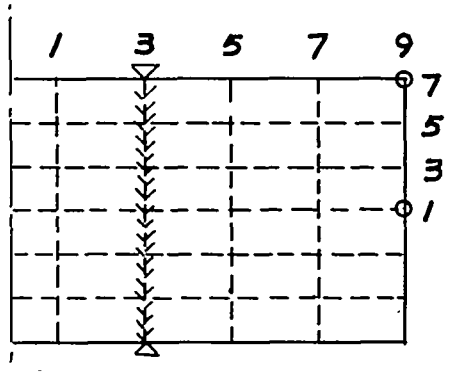

(a) Loading points.

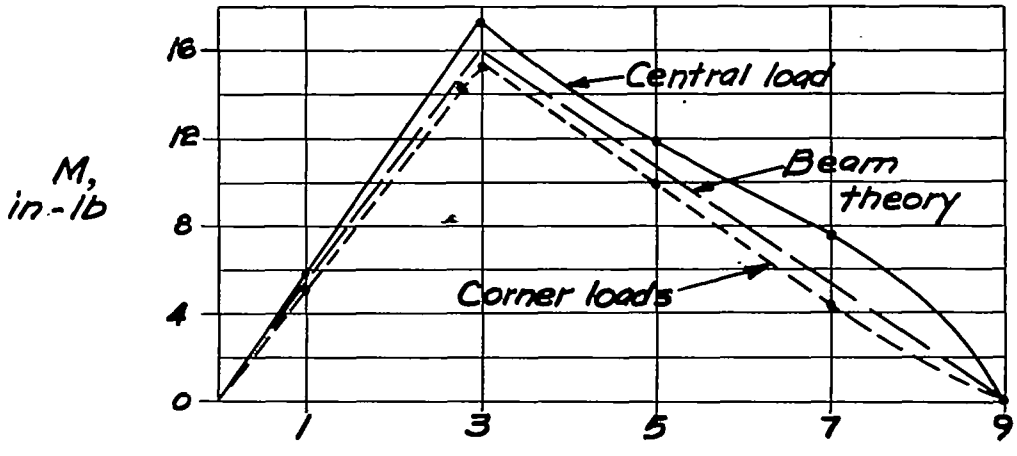

(b) Spar 1.

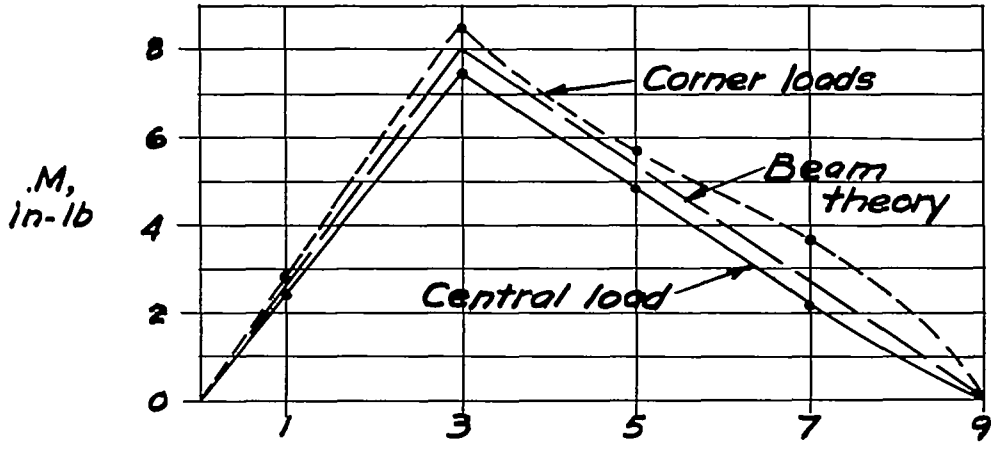

(c) Spar 7.

Figure 27.- Bending moments in spars. Aspect ratio, 2. Antisymmetric bending. Rectangular section.

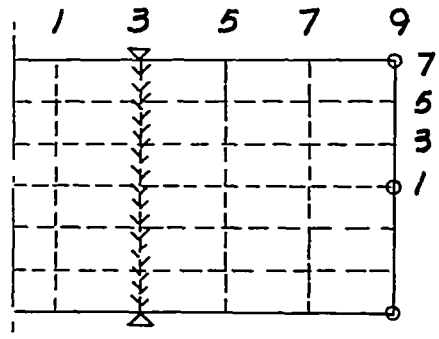

(a) Loading points.

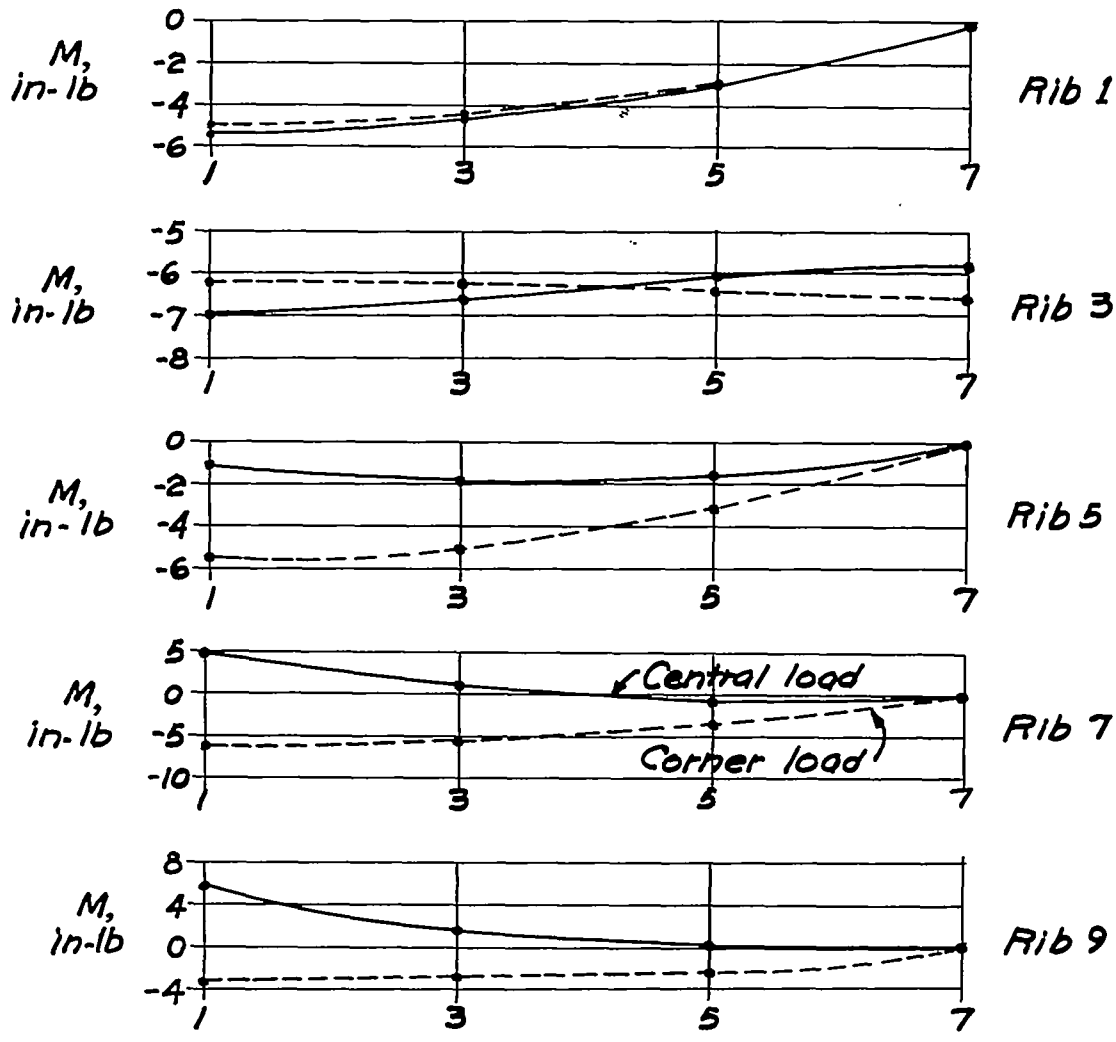

(b) Bending moments.

Figure 28.- Bending moments in ribs. Aspect ratio, 2. Symmetric bending. Rectangular section.

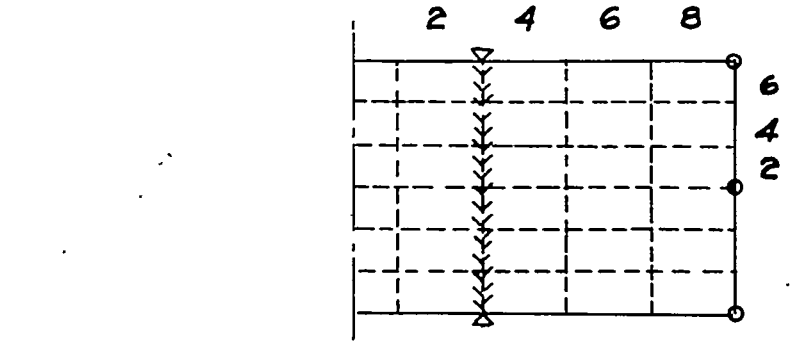

(a) Loading points.

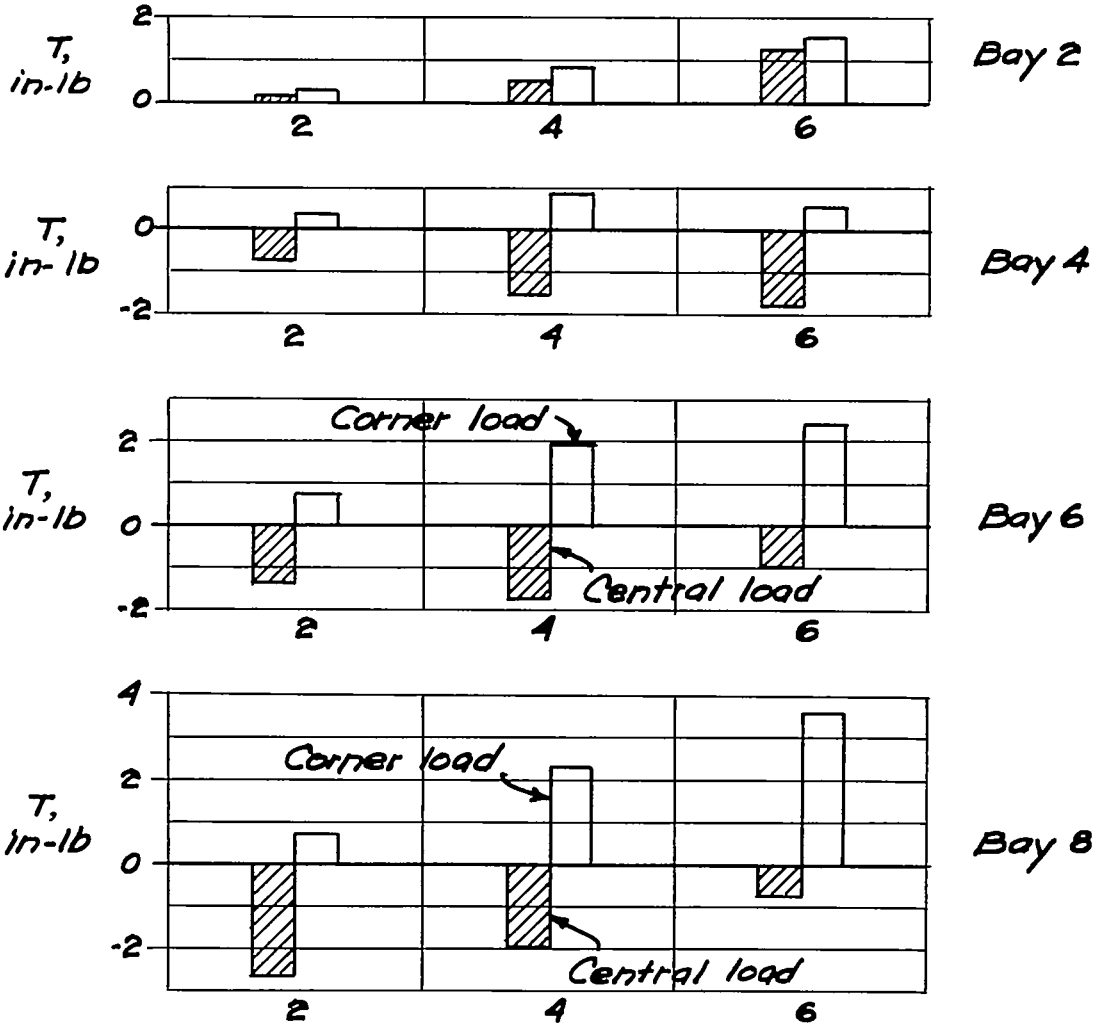

(b) Twisting moments.

Figure 29.- Twisting moments on chordwise cross sections. Aspect ratio, 2. Symmetric bending. Rectangular section.

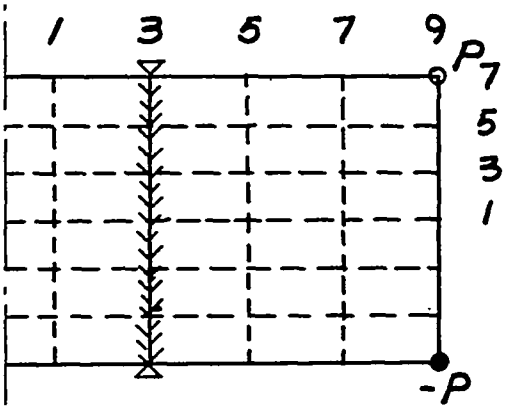

(a) Loading points. P = 1 kip.

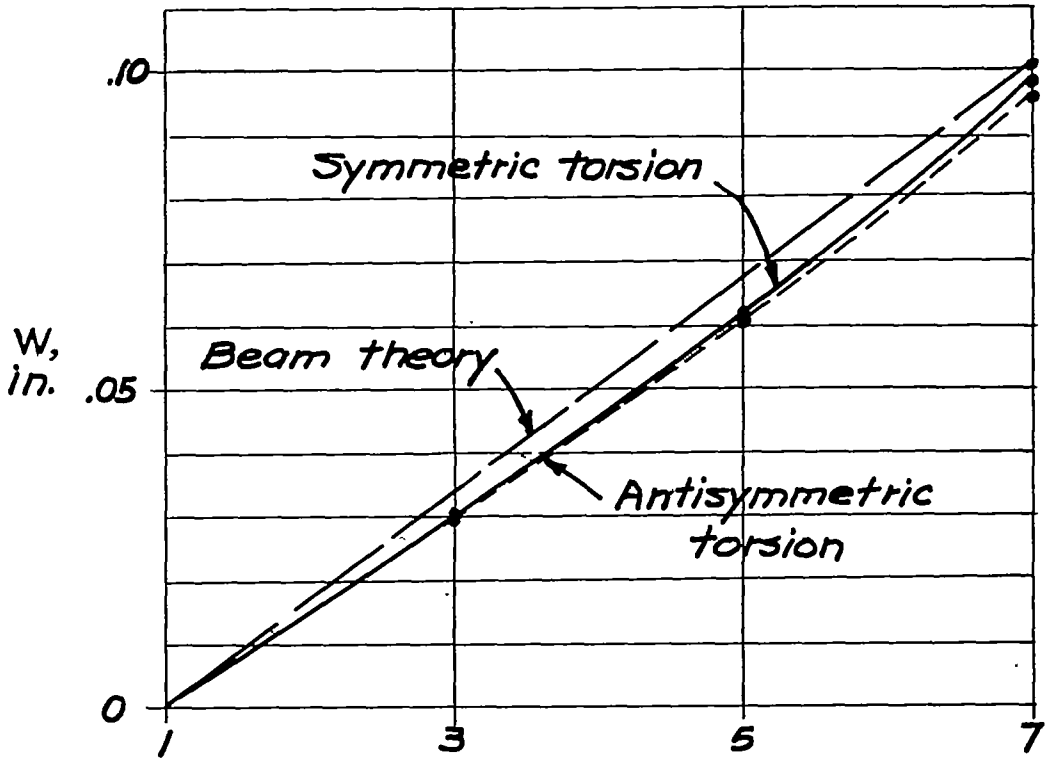

(b) Deflections.

Figure 30.- Chordwise deflections at tip. Aspect ratio, 2. Rectangular section.

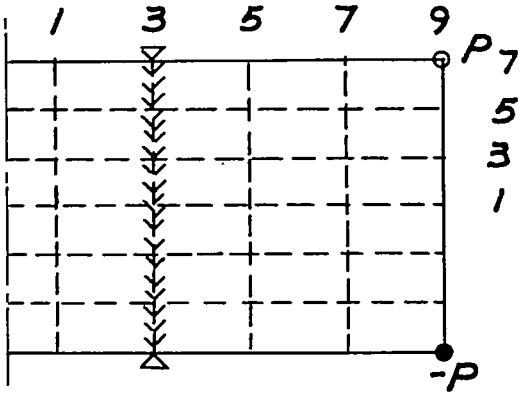

(a) Loading points. P = 1 kip.

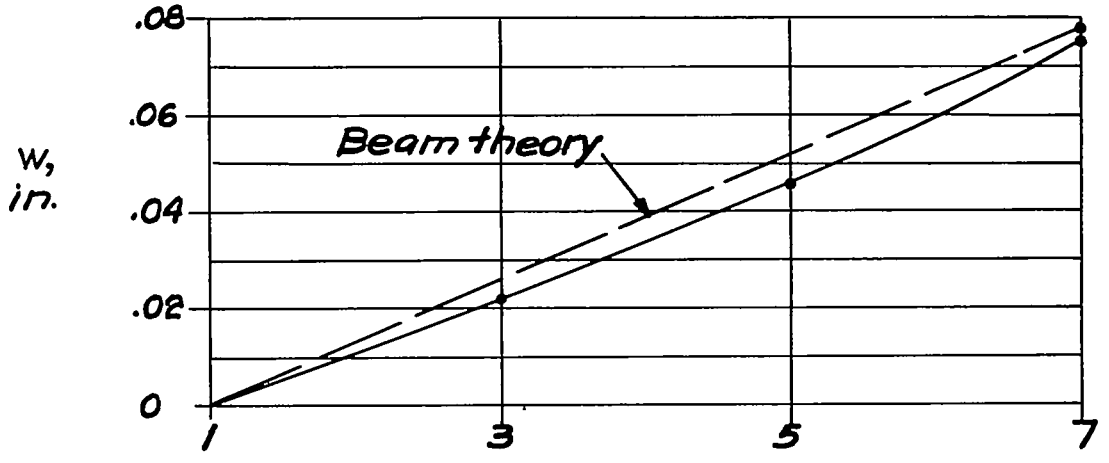

(b) Rib 7.

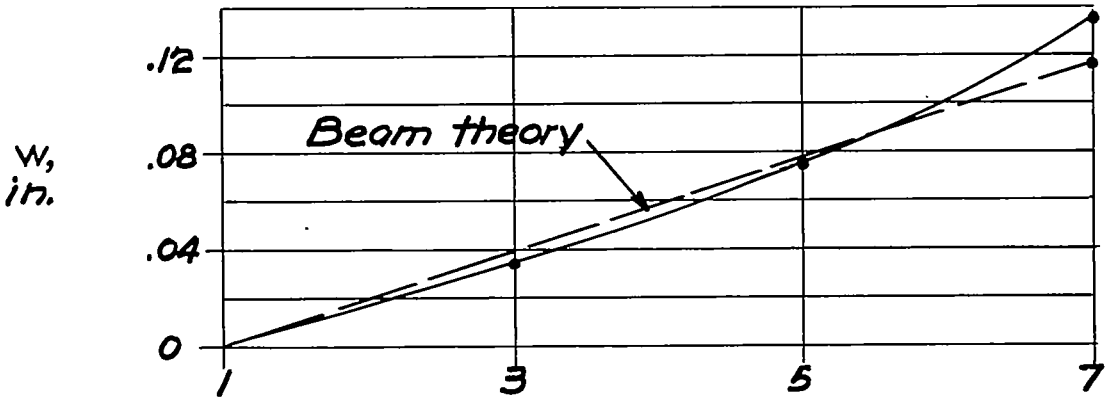

(c) Rib 9.

Figure 31.- Chordwise deflections. Aspect ratio, 2. Symmetric torsion. Biconvex section.

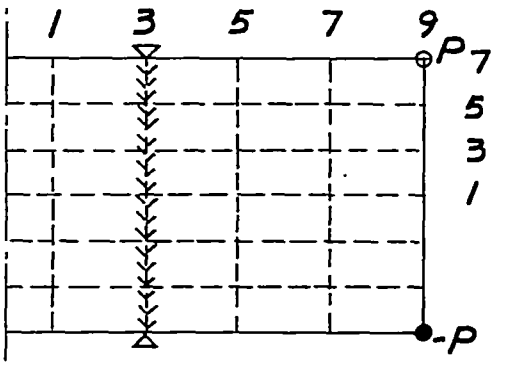

(a) Loading points. P = 1 kip.

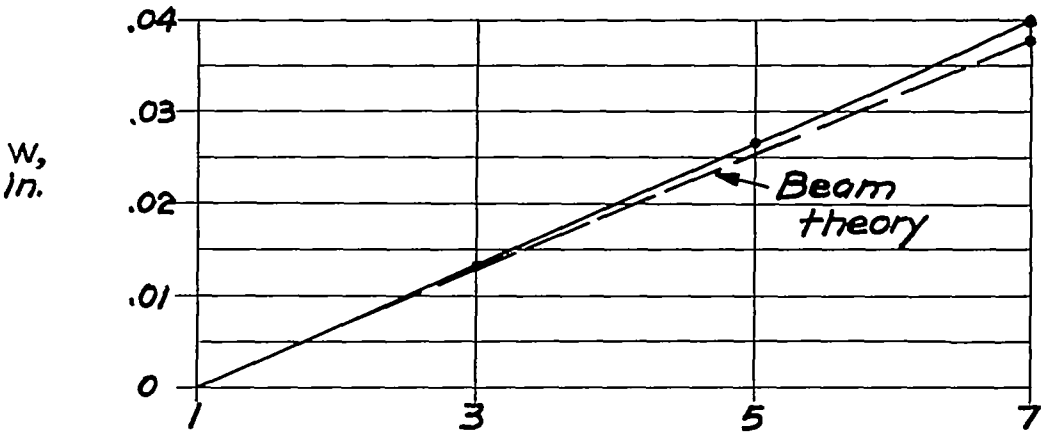

(b) Rib 7.

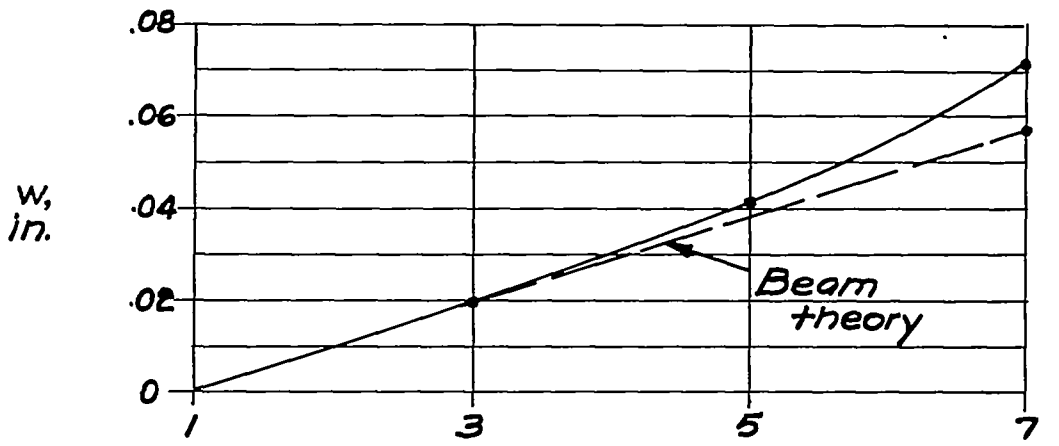

(c) Rib 9.

Figure 32.- Chordwise deflections. Aspect ratio, 4. Symmetric torsion. Biconvex section.

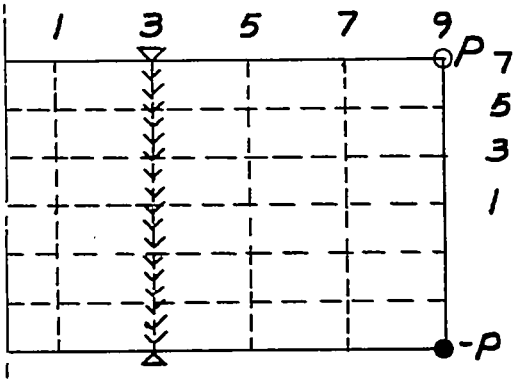

(a) Loading points. P = 1 kip.

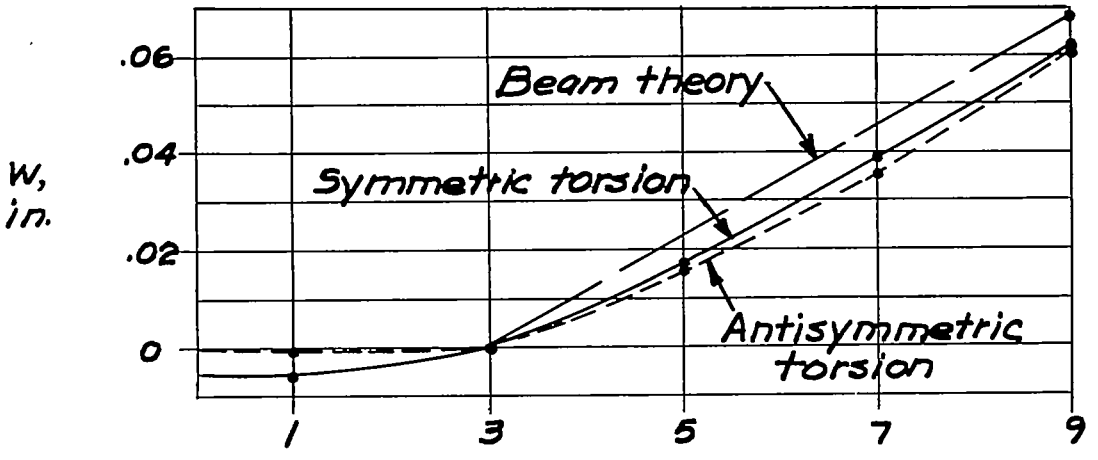

(b) Spar 5.

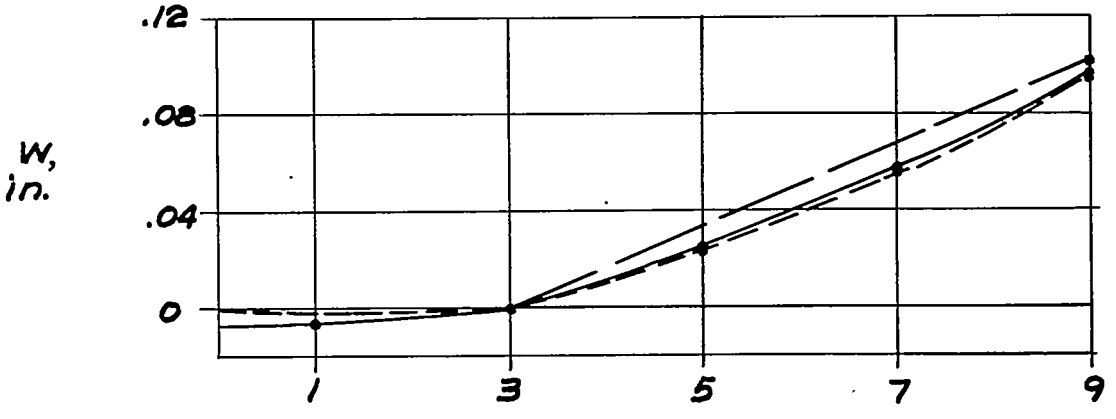

(c) Spar 7.

Figure 33.- Spanwise deflection of spars. Aspect ratio, 2. Rectangular section.

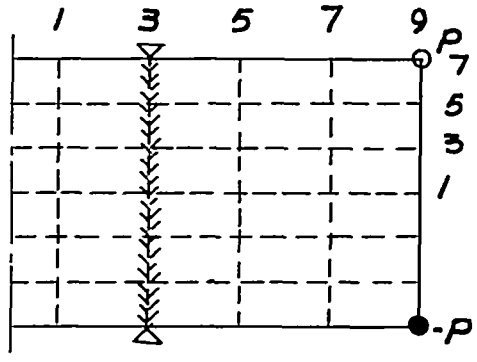

(a) Loading points. P = 1 kip.

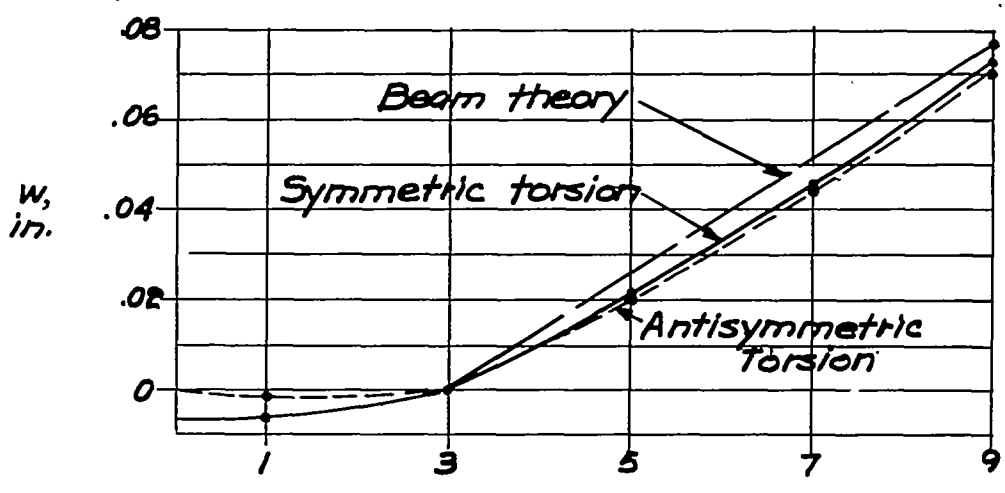

(b) Spar 5.

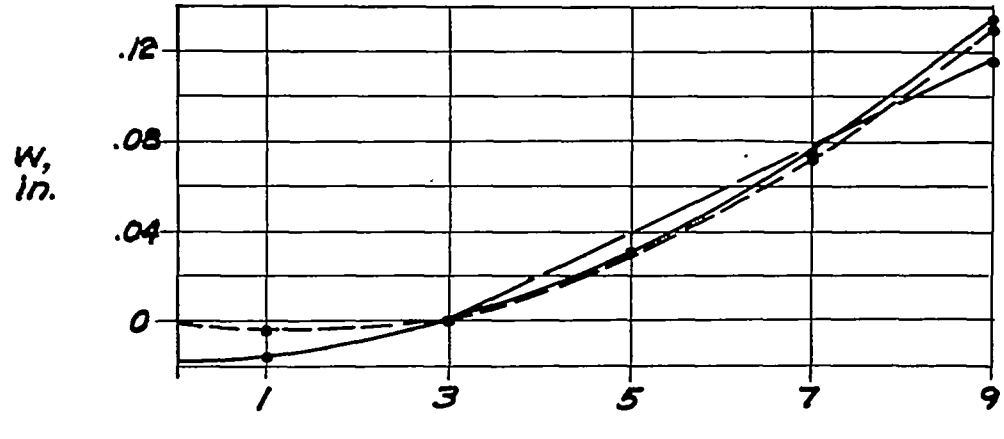

(c) Spar 7.

Figure 34.- Spanwise deflection of spars. Aspect ratio, 2. Biconvex section.

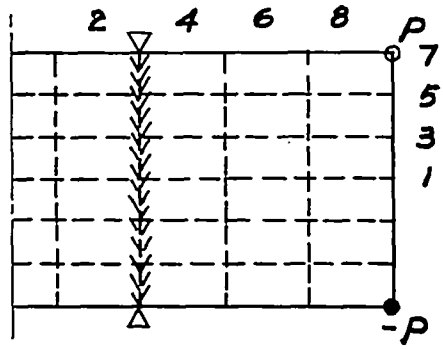

(a) Loading points. P = 1 pound.

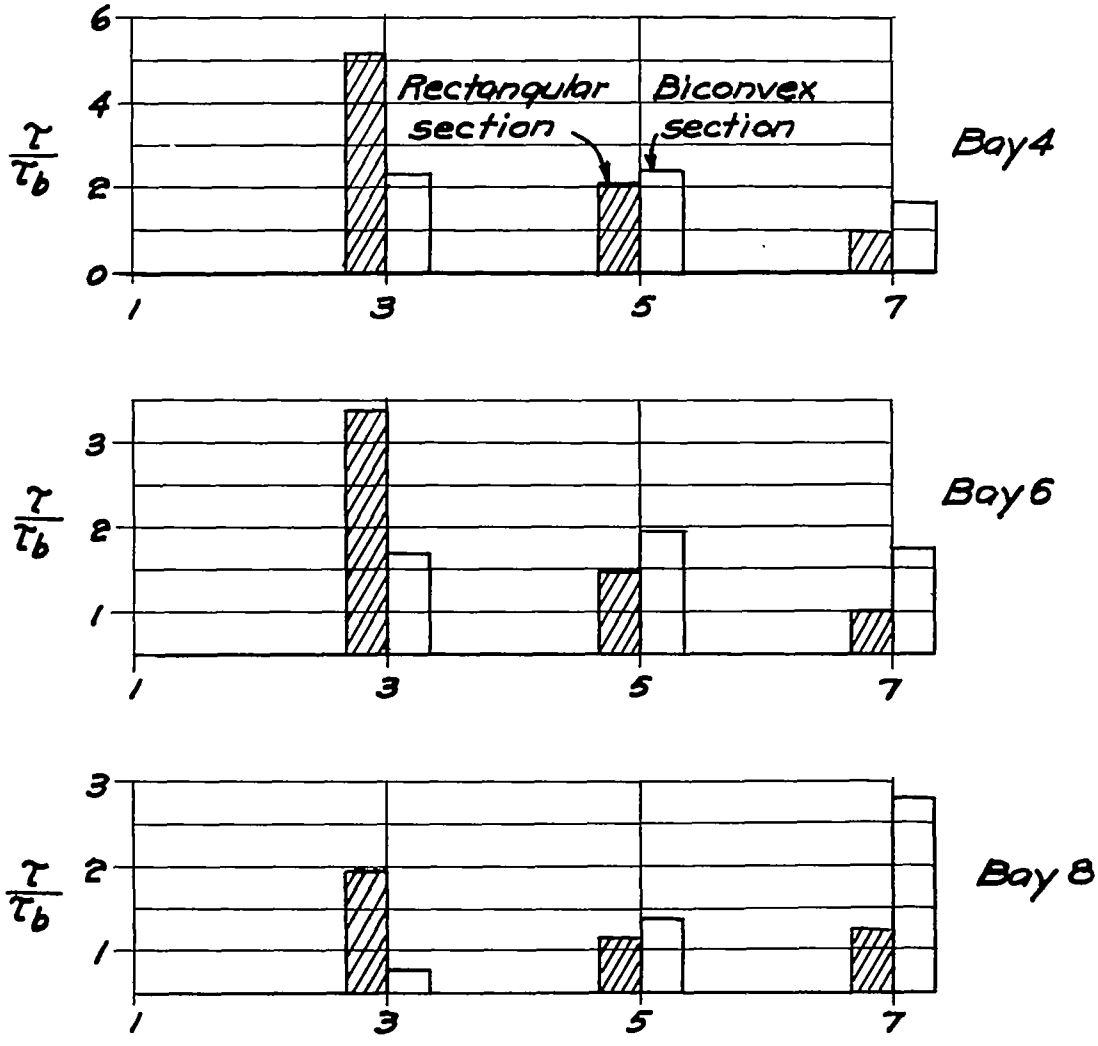

(b) Relative values of stress.

Figure 35.- Shearing stress in spars. Aspect ratio, 2. Symmetric torsion.

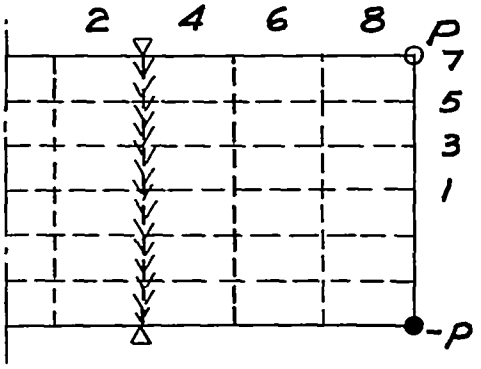

(a) Loading points. P = 1 pound.

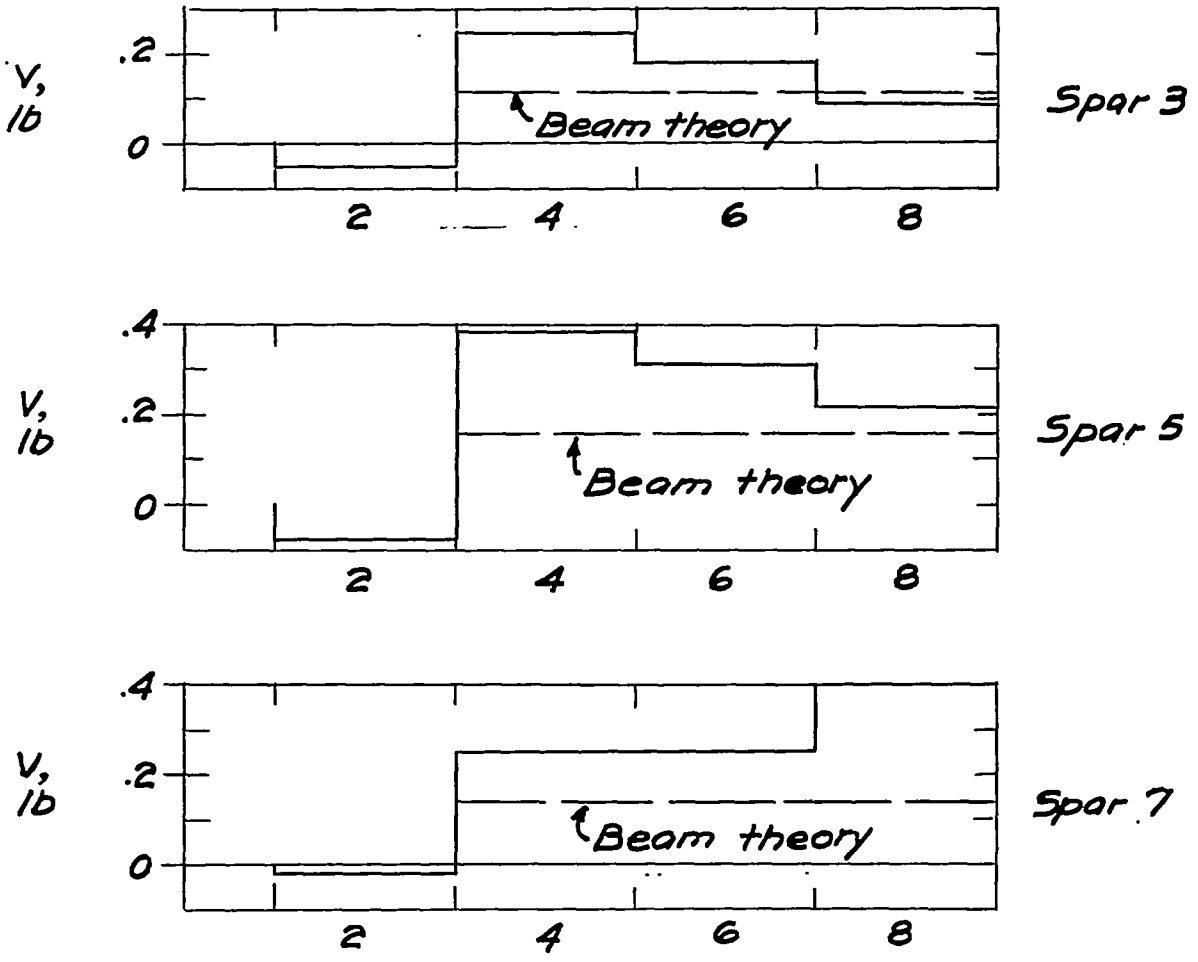

(b) Shear distributions.

Figure 36.- Spanwise distribution of shear in spars. Aspect ratio, 2. Symmetric torsion. Biconvex section.

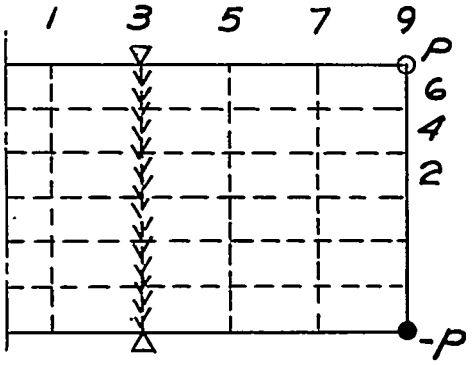

(a) Loading points. P = 1 pound.

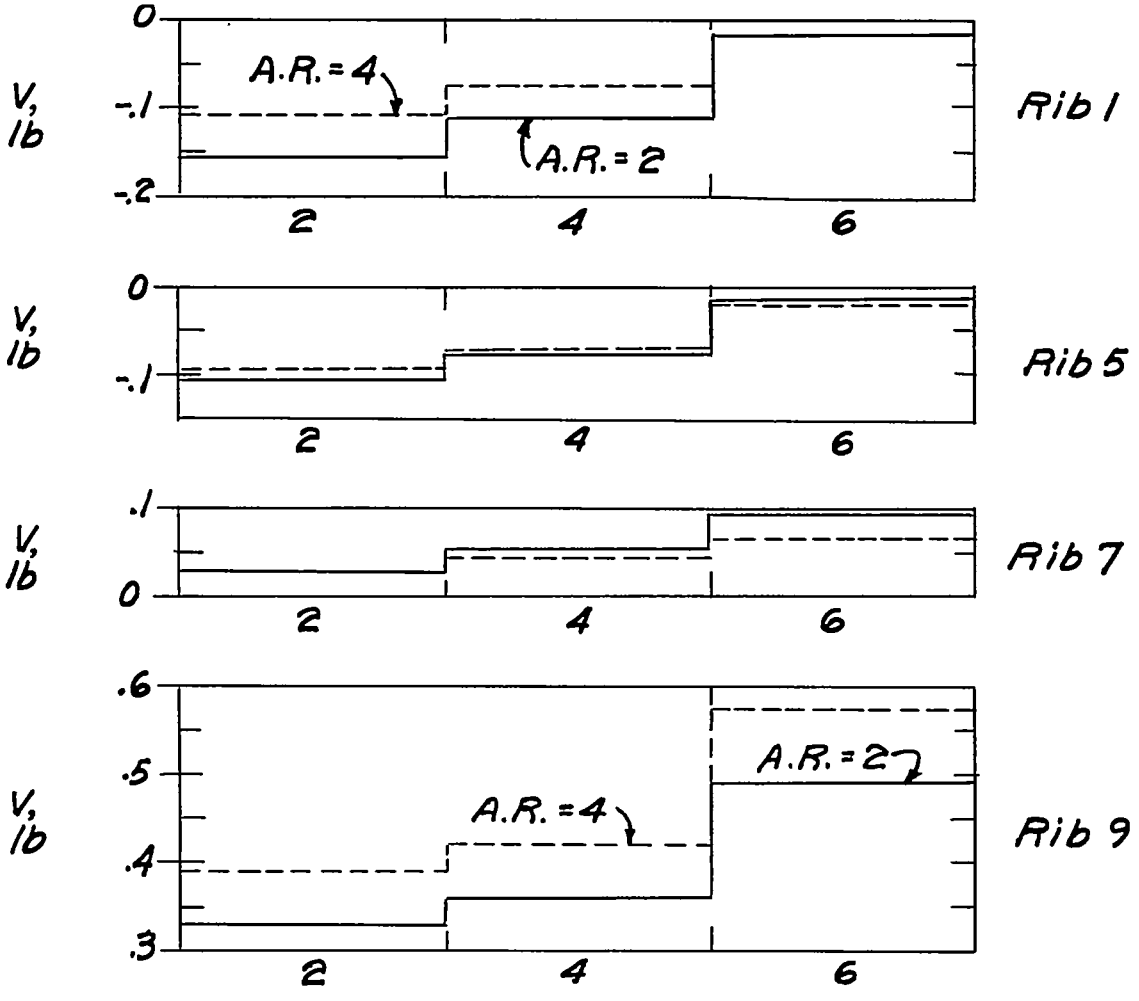

(b) Shear distributions.

Figure 37.- Chordwise distribution of shear in ribs. Symmetric torsion. Rectangular section.

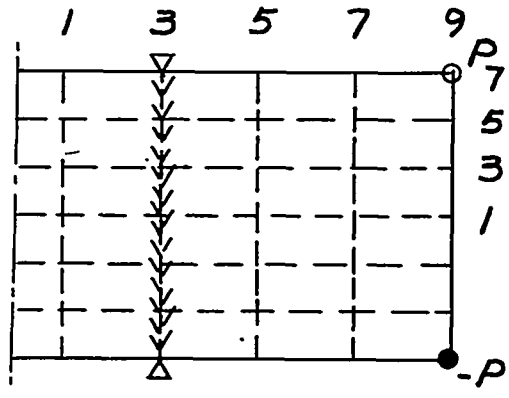

(a) Loading points. P = 1 pound.

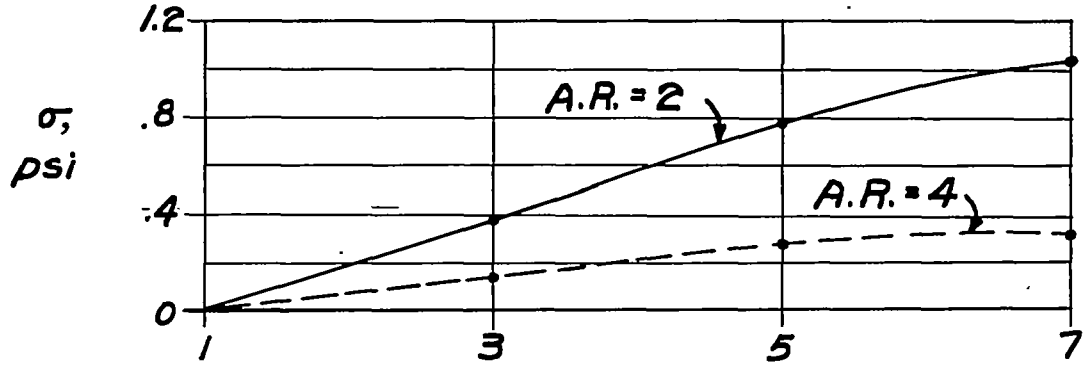

(b) Rectangular section.

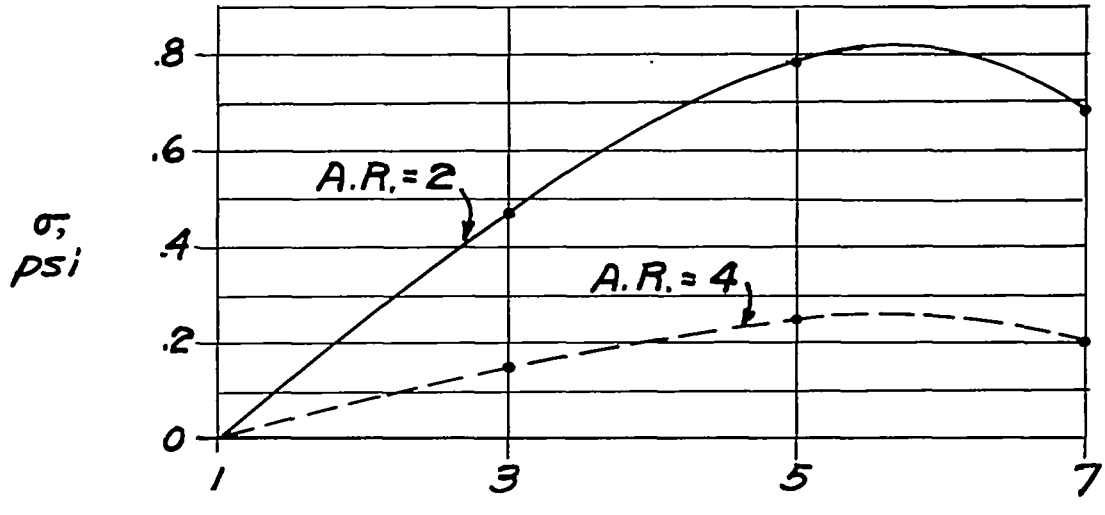

(c) Biconvex section.

Figure 38.- Spanwise normal stress over support. Symmetric torsion.

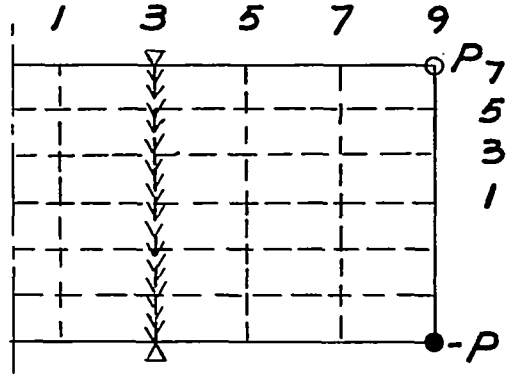

(a) Loading points. P = 1 pound.

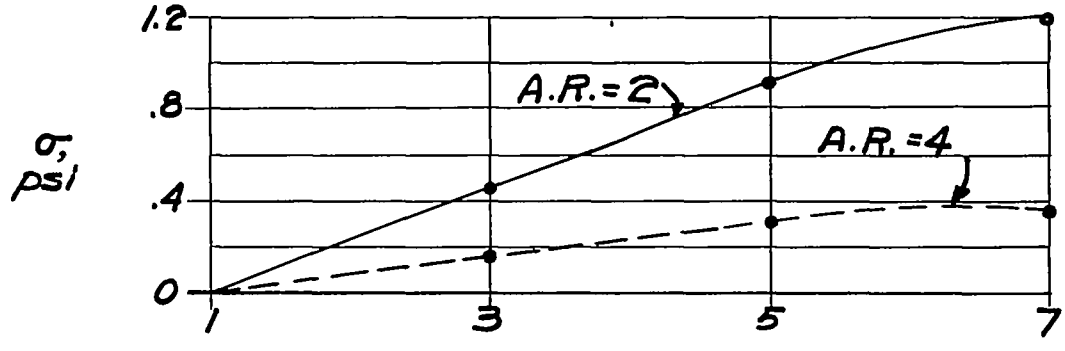

(b) Rectangular section.

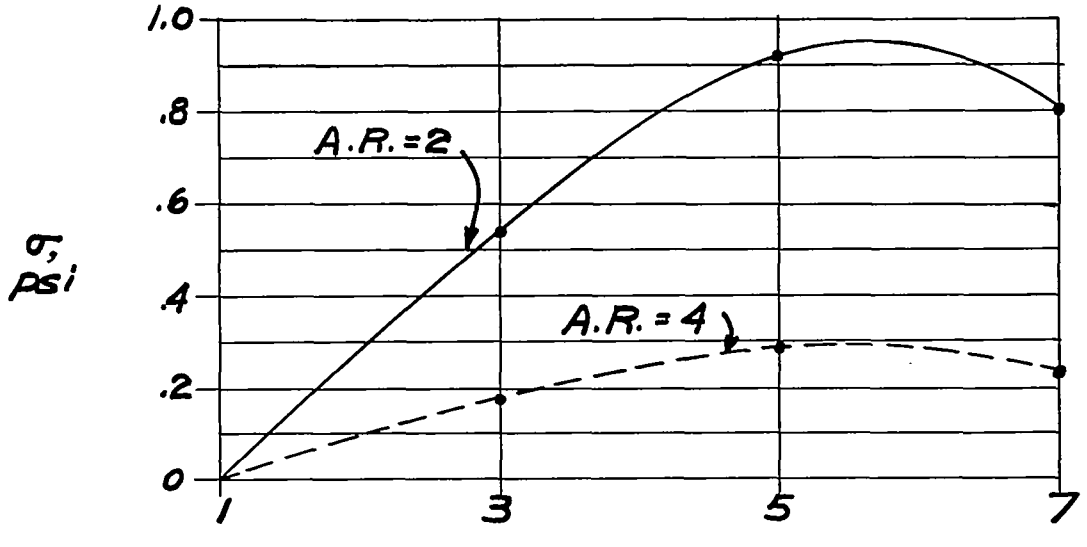

(c) Biconvex section.

Figure 39.- Spanwise normal stress over support. Antisymmetric torsion.

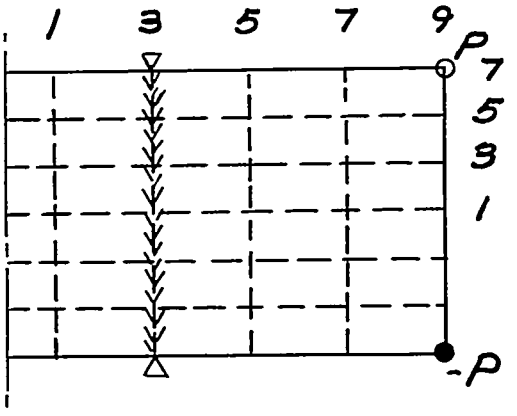

(a) Loading points. P = 1 pound.

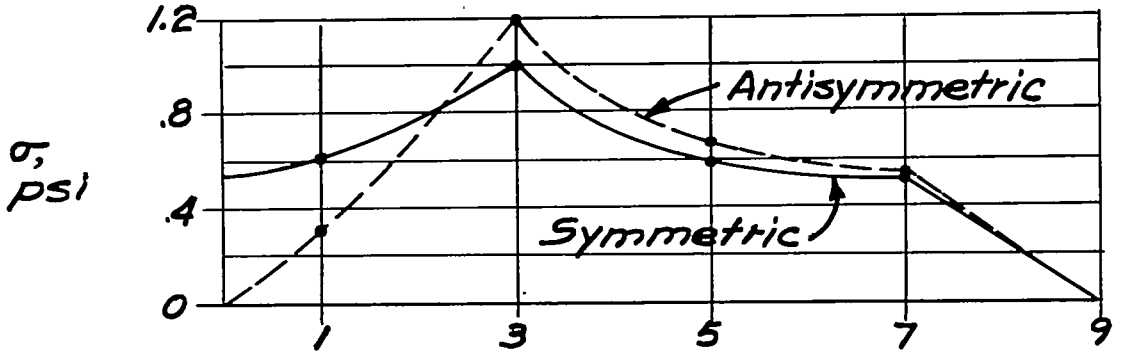

(b) Rectangular section.

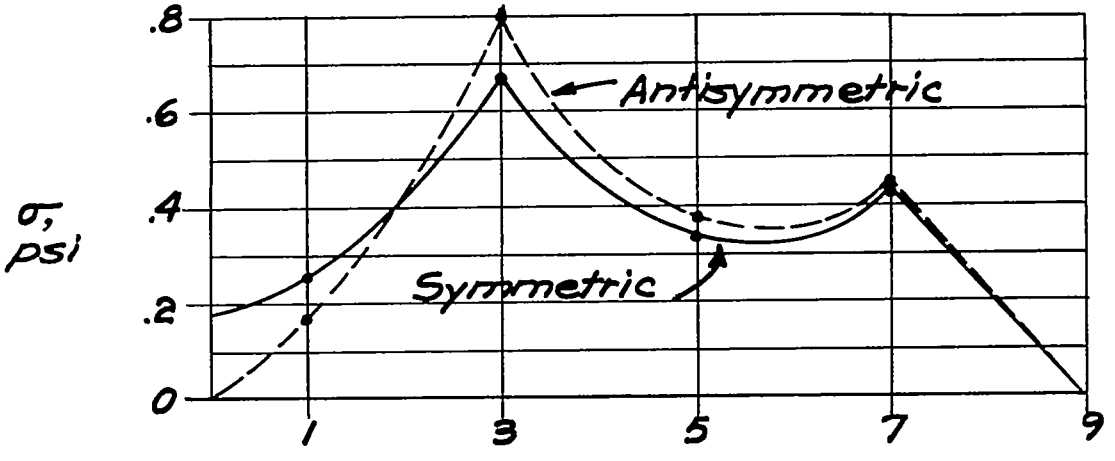

(c) Biconvex section.

Figure 40.- Spanwise normal stress along leading edge due to torsional load. Aspect ratio, 2.

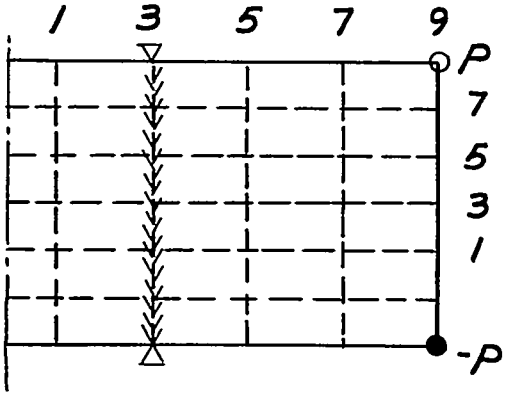

(a) Loading points. P = 1 pound.

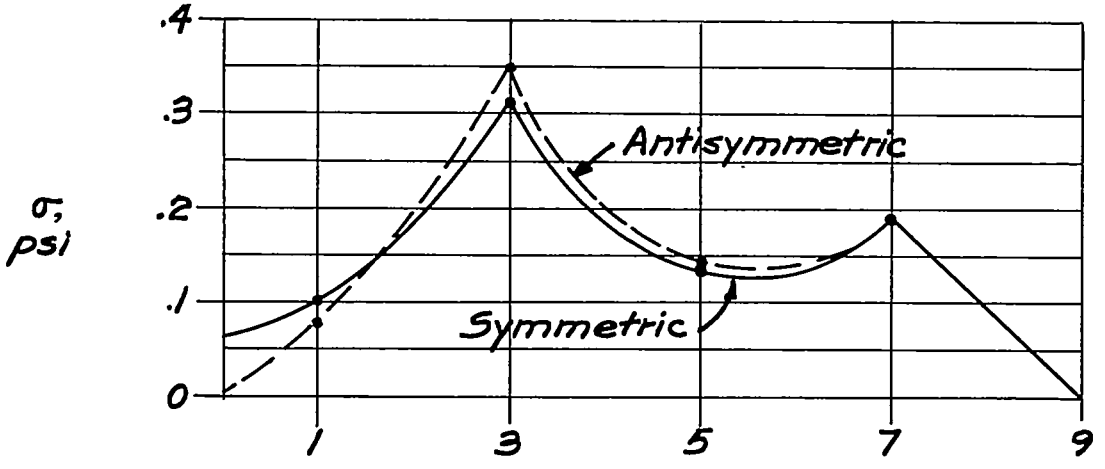

(b) Rectangular section.

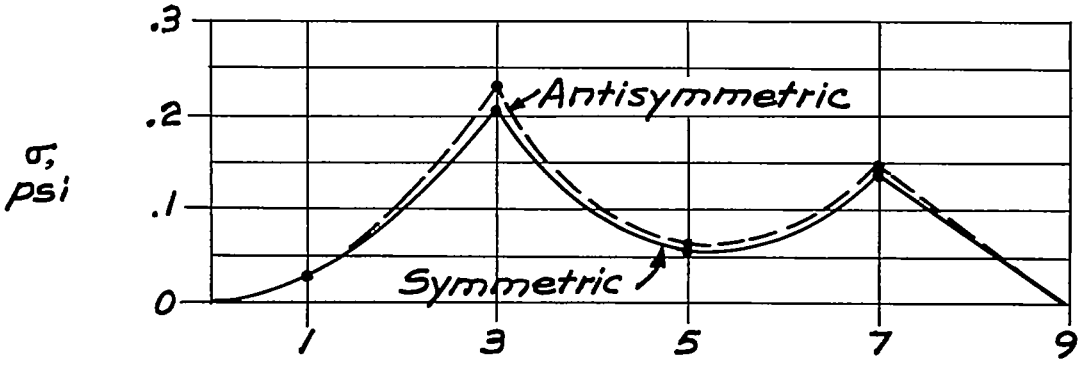

(c) Biconvex section.

Figure 41.- Spanwise normal stress along leading edge due to torsional load. Aspect ratio, 4.

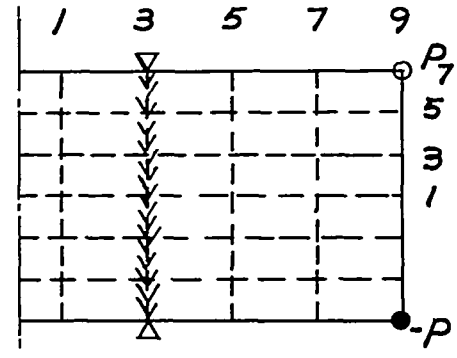

(a) Loading points. P = 1 pound.

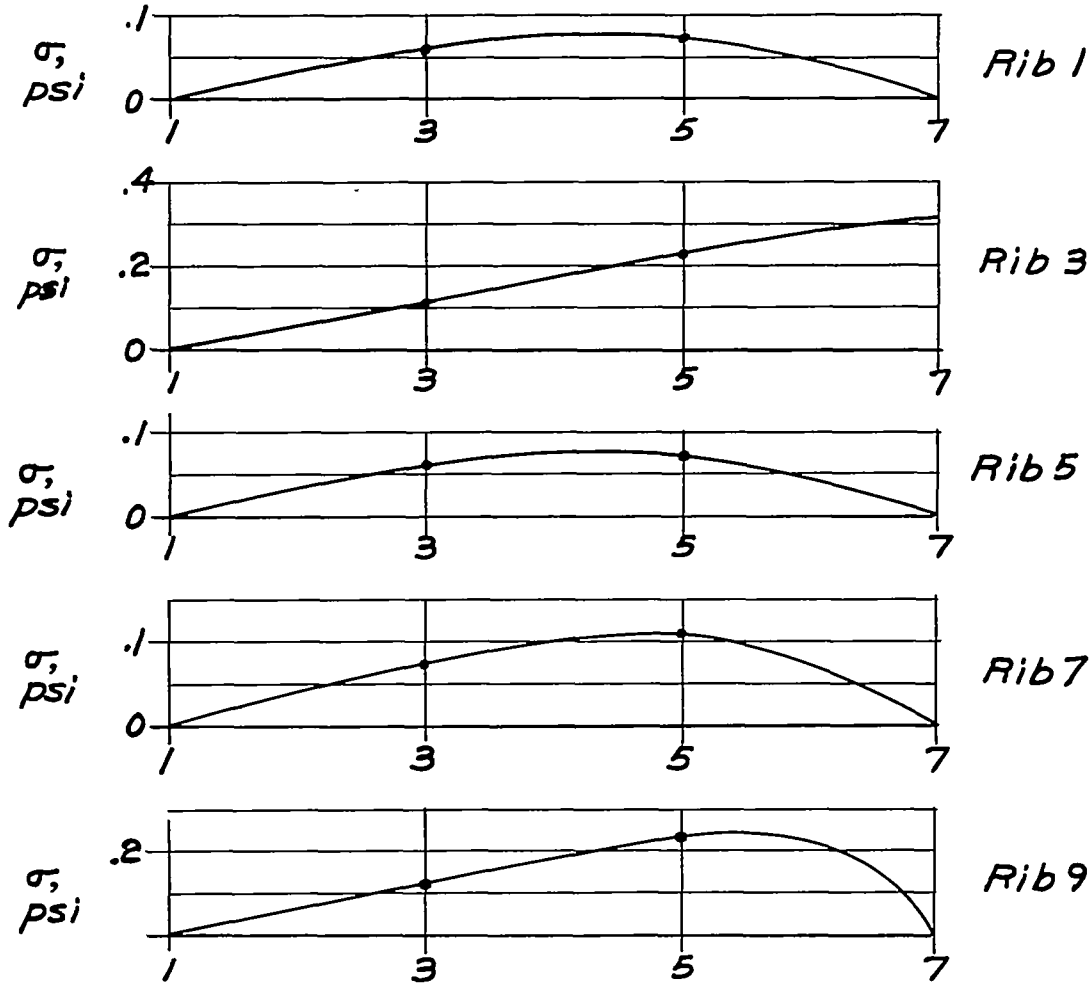

(b) Normal stress along ribs.

Figure 42.- Chordwise normal stress. Aspect ratio, 2. Symmetric torsion. Rectangular section.

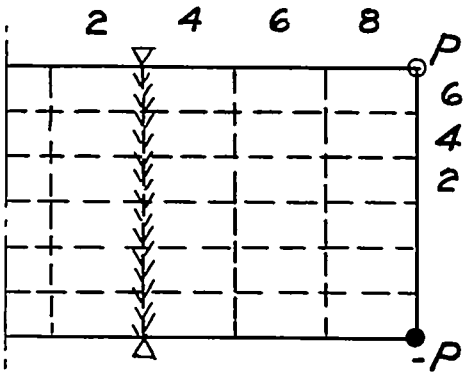

(a) Loading points. P = 1 pound.

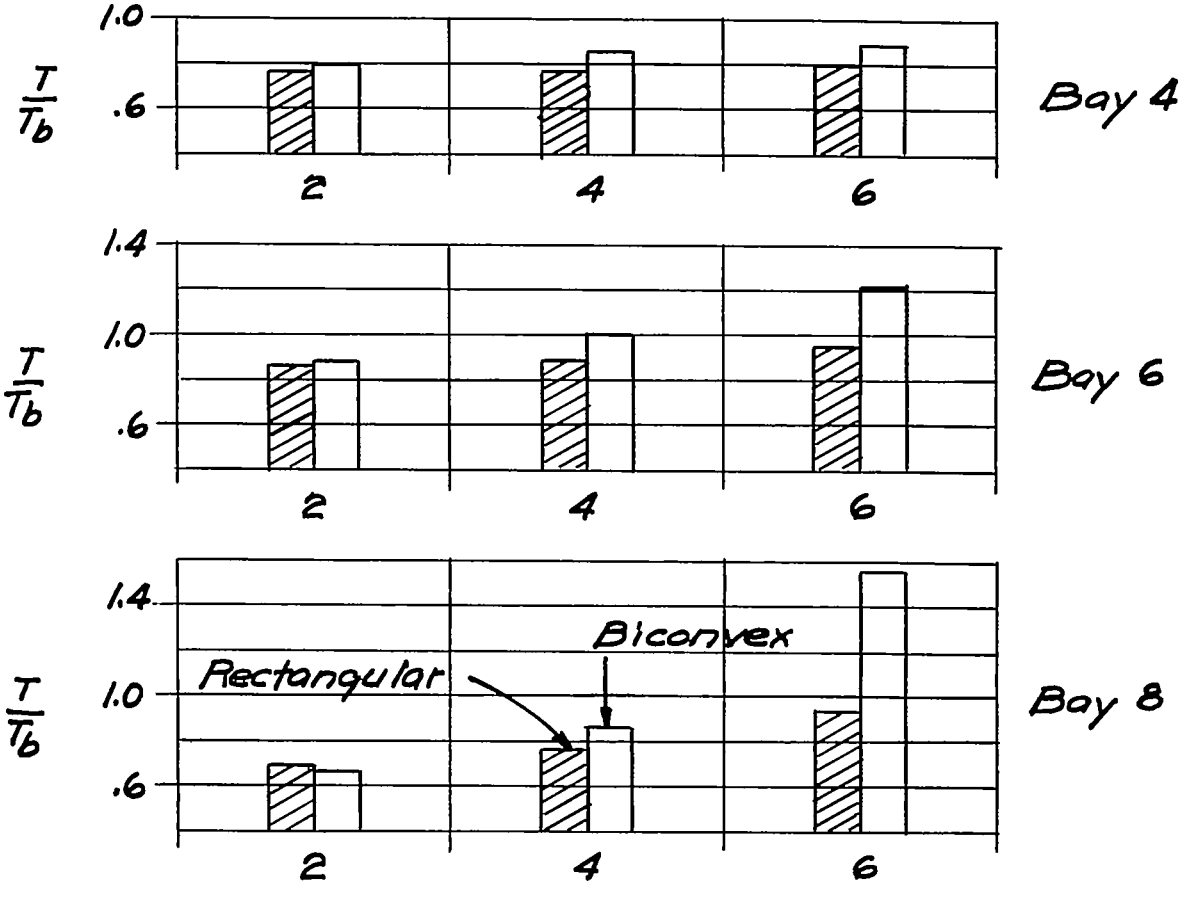

(b) Relative values of twisting moments.

Figure 43.- Twisting moments on chordwise cross-sections. Symmetric torsion. Aspect ratio, 2.

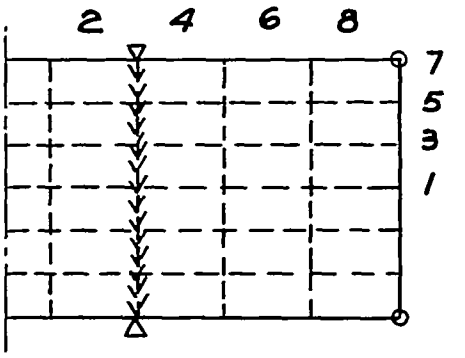

(a) Loading points.

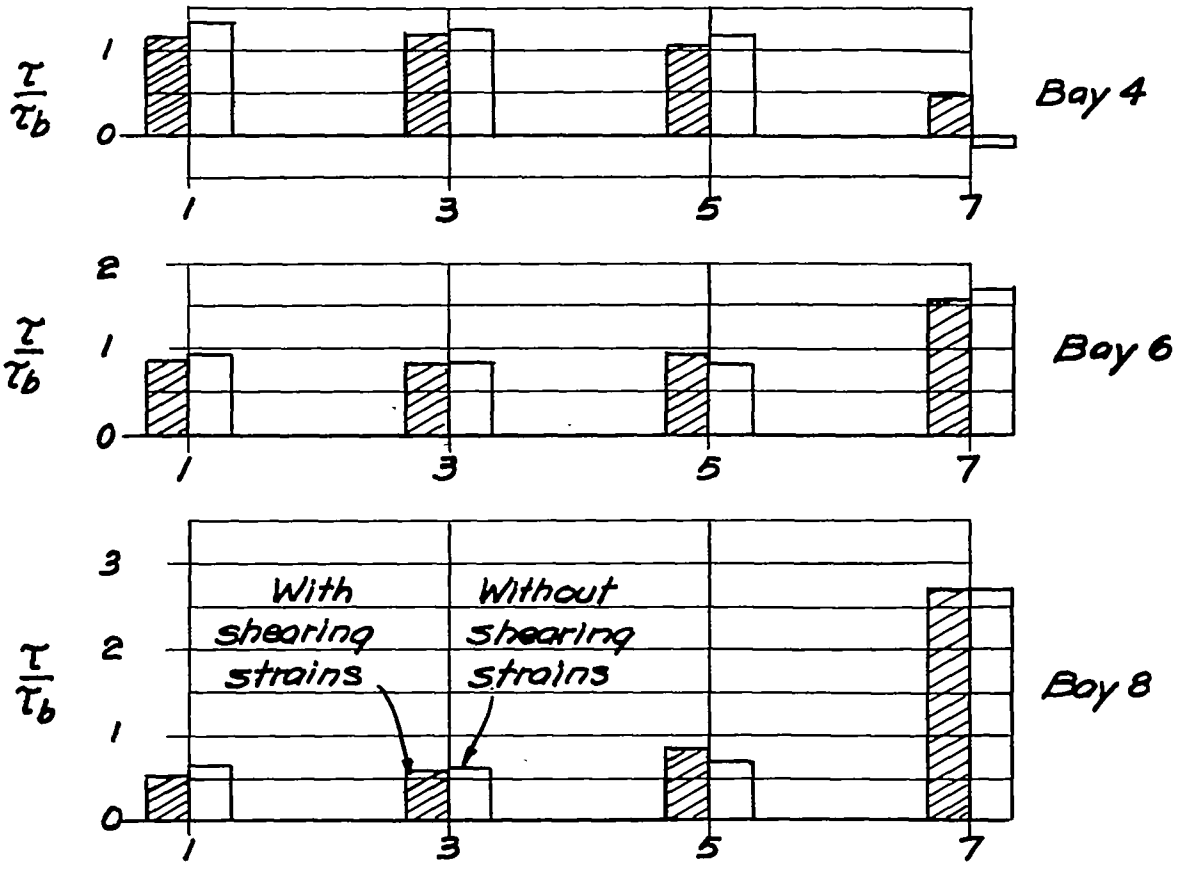

(b) Relative values of shearing stress.

Figure 44.- Effect of shearing strains upon distribution of shears in spars. Aspect ratio, 4. Symmetric bending. Rectangular section.

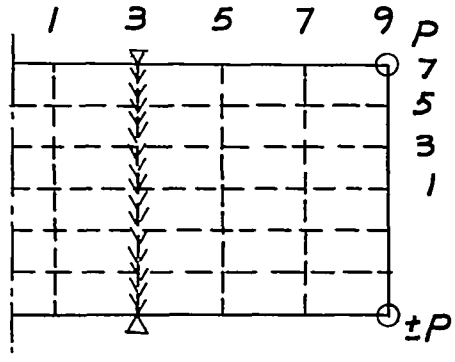

(a) Loading points. P = 1 pound.

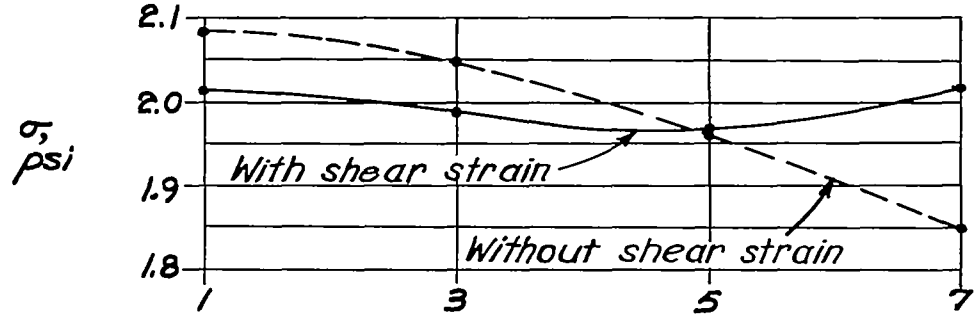

(b) Symmetric bending.

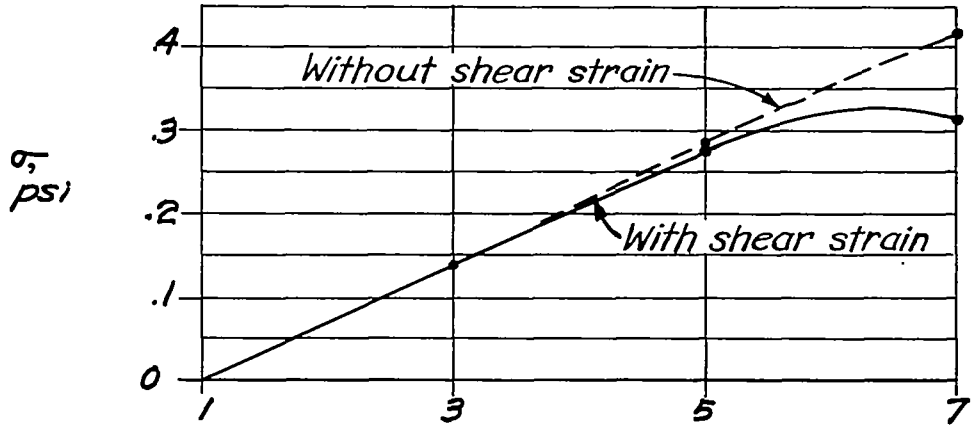

(c) Symmetric torsion.

Figure 45.- Effect of shearing strains upon spanwise normal stress over support. Rectangular section. Aspect ratio, 4.

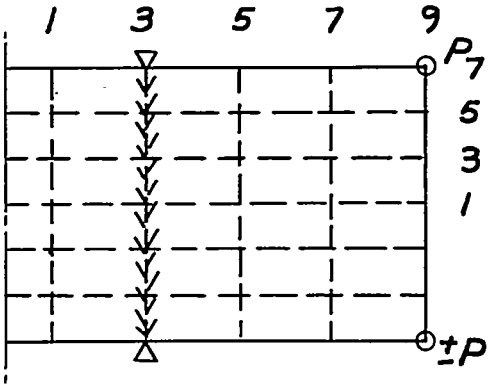

(a) Loading points. P = 1 pound.

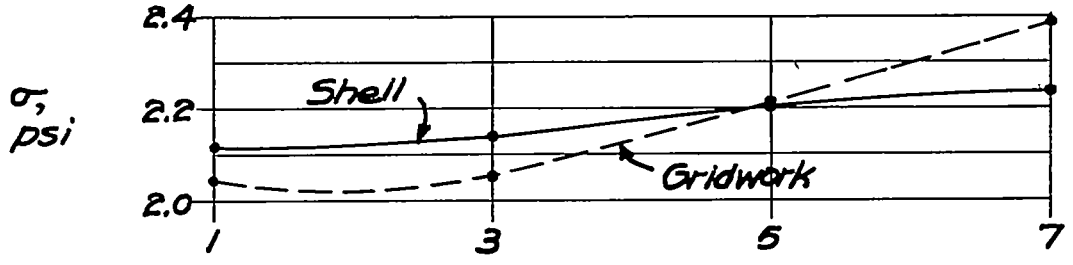

(b) Symmetric bending.

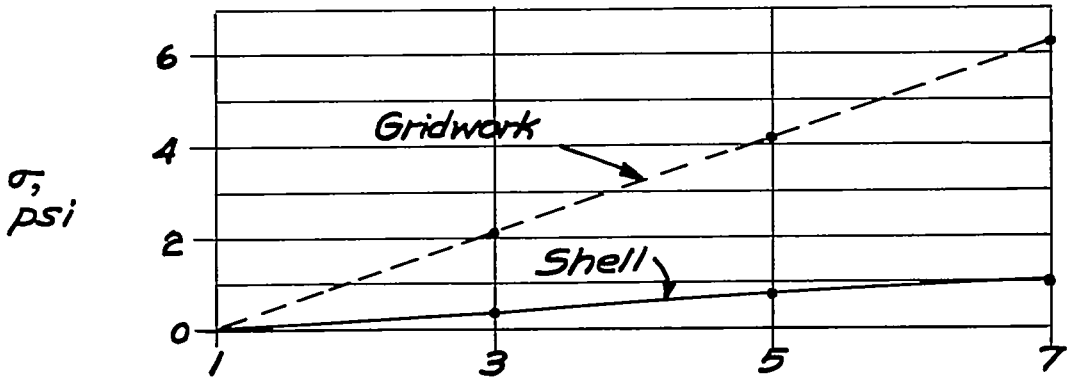

(c) Symmetric torsion.

Figure 46.- Spanwise normal stress over support in gridwork. Rectangular section. Aspect ratio, 2.

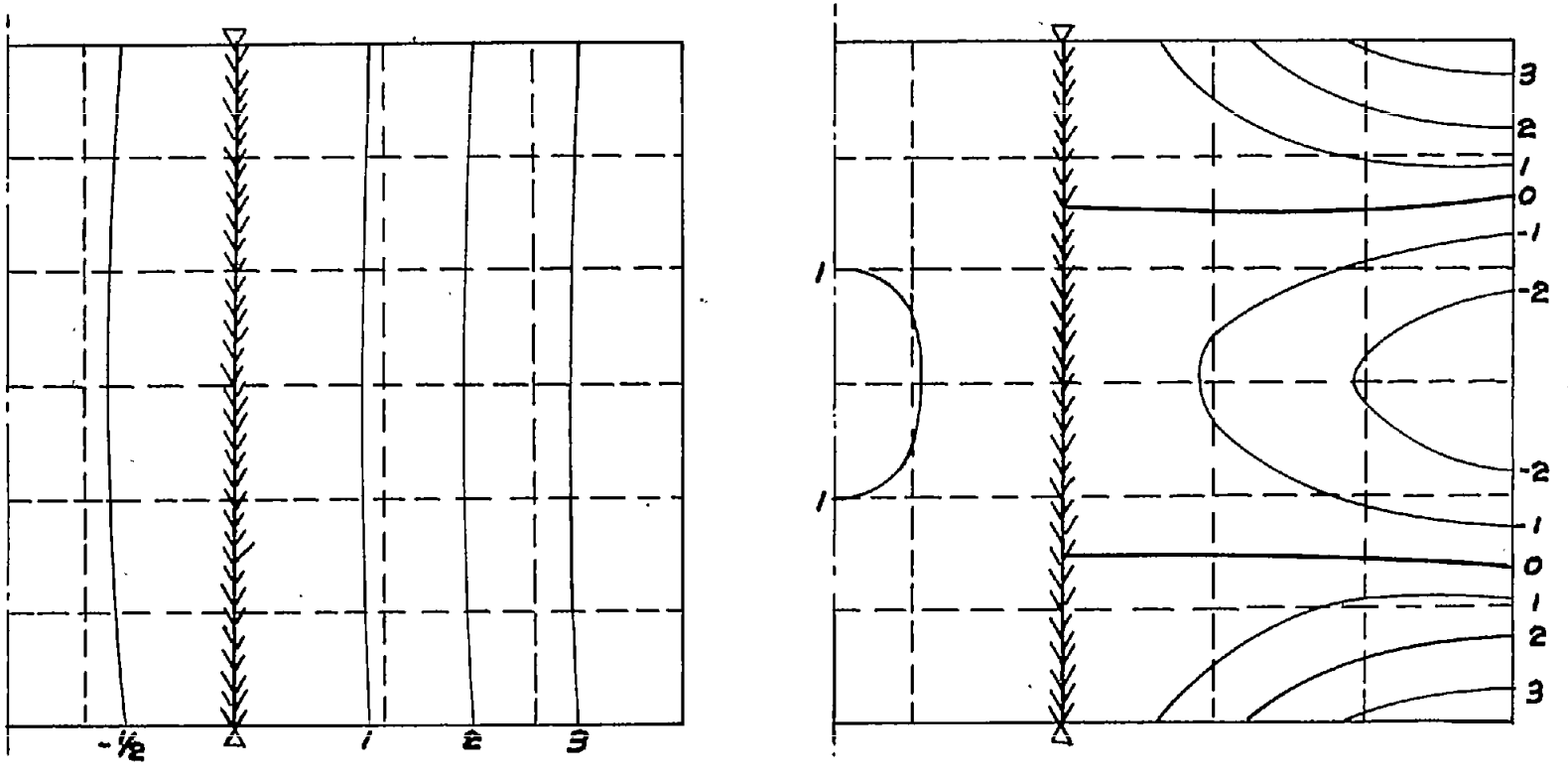

(a) First symmetric bending mode; f = 48.0 cps.

(b) Second symmetric bending mode; f = 261 cps.

Figure 47.- Vibration modes. Rectangular cross section. Aspect ratio, 2.

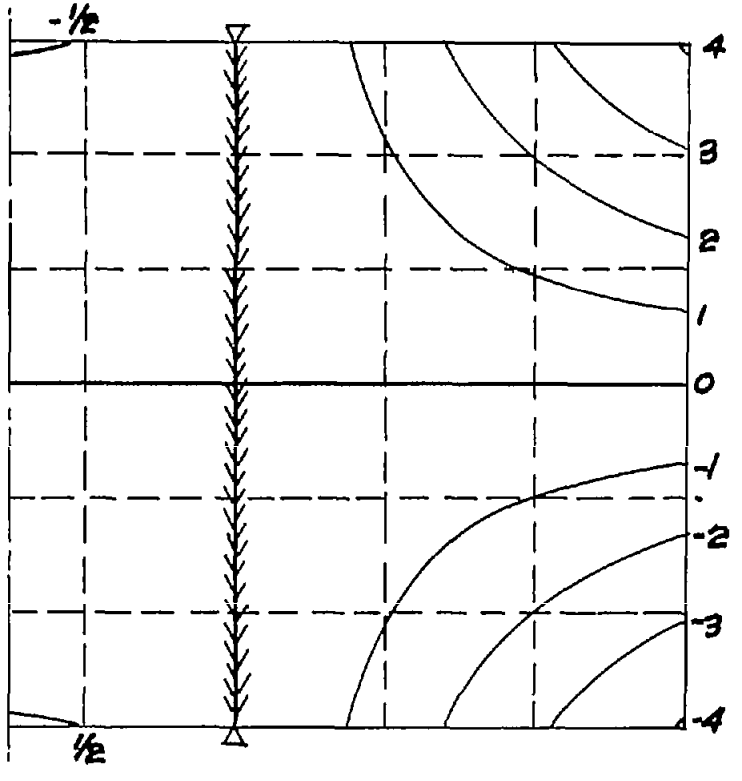

(c) First symmetric torsion mode; f = 110.5 cps.

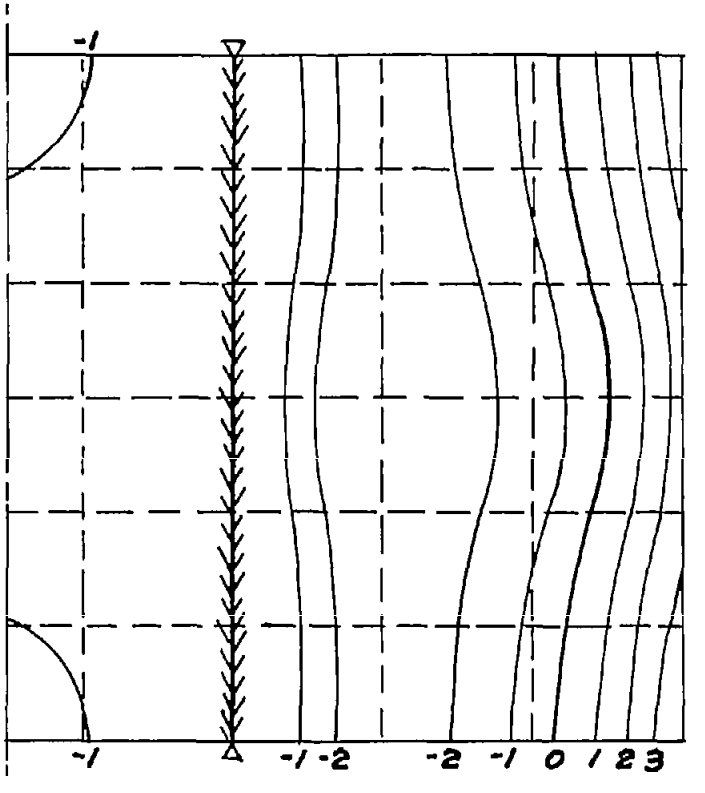

(d) Third symmetric bending mode; f = 339 cps.

Figure 47.- Concluded.

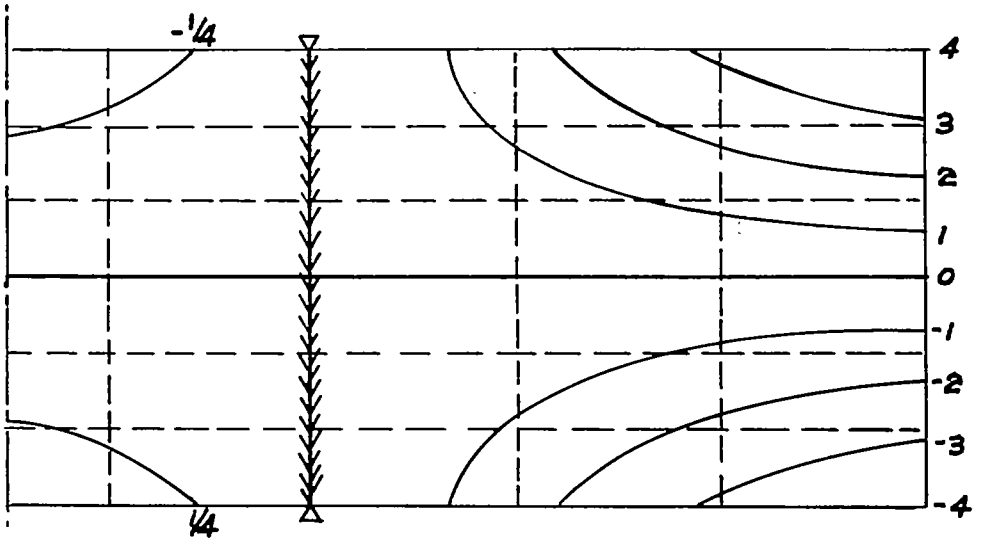

(a) First symmetric torsion mode; f = 94.7 cps.

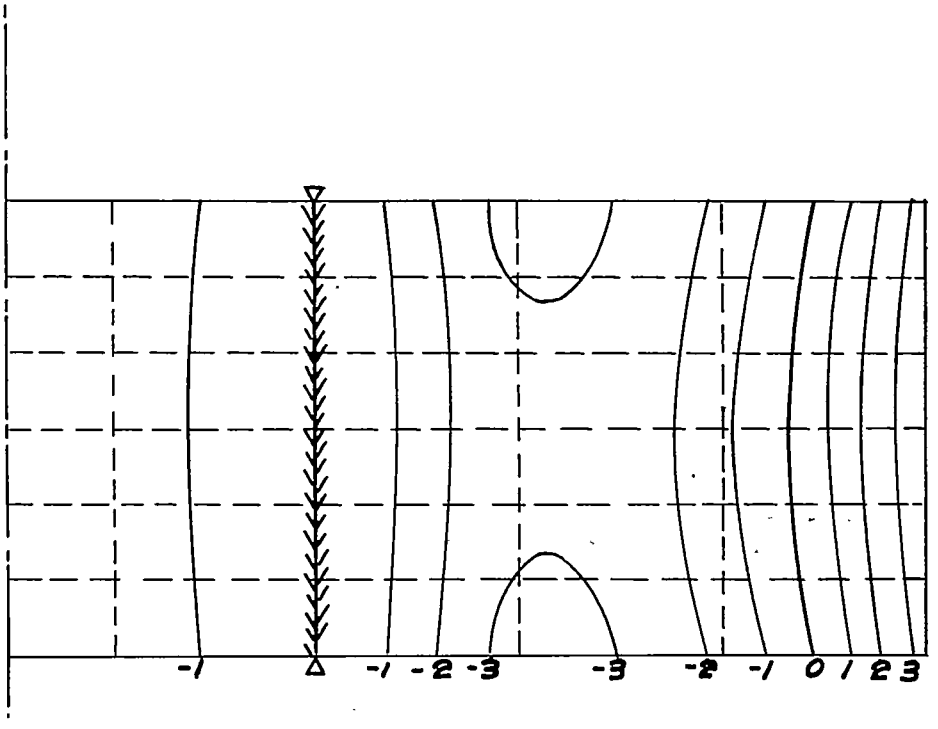

(b) Third symmetric bending mode; f = 183 cps.

Figure 48.- Vibration modes. Rectangular cross section. Aspect ratio, 4.

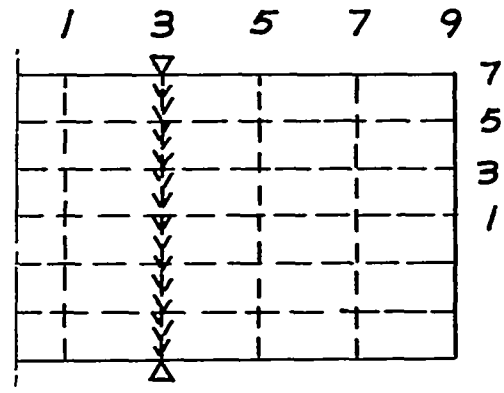

(a) Plan form.

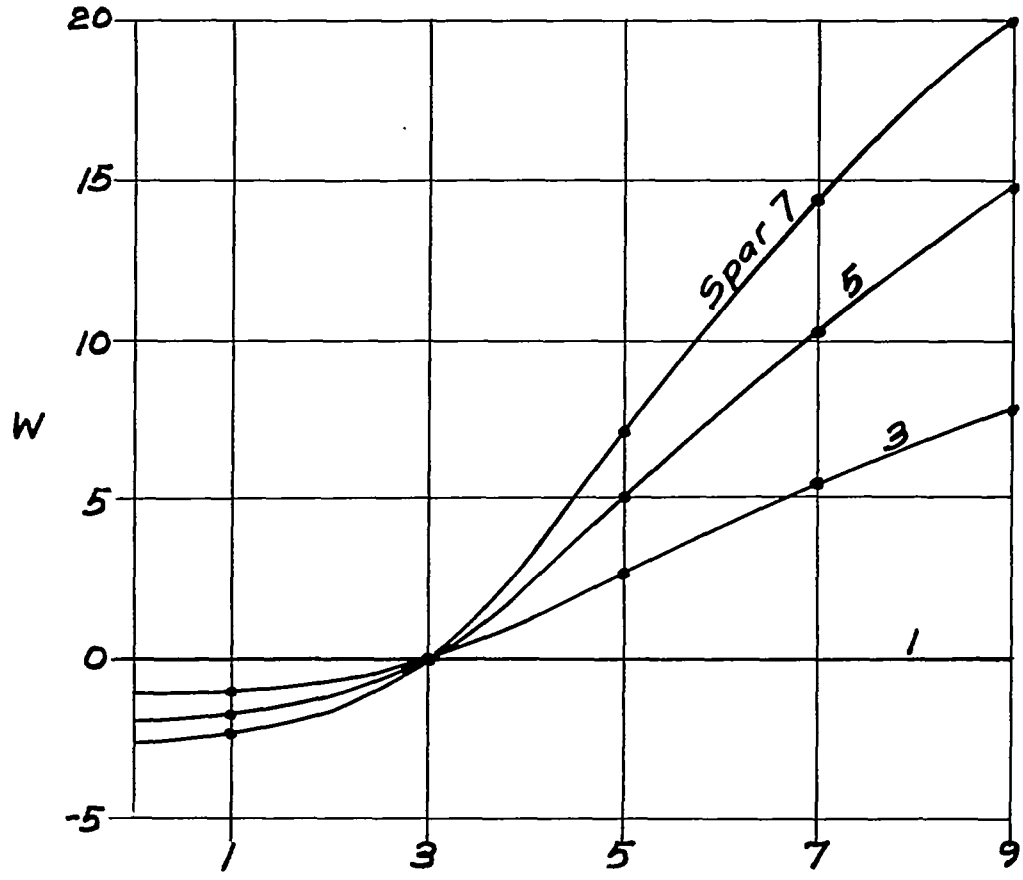

(b) Deflections.

Figure 49.- Deflection of spars in first symmetric torsion mode. Rectangular section. Aspect ratio, 2.

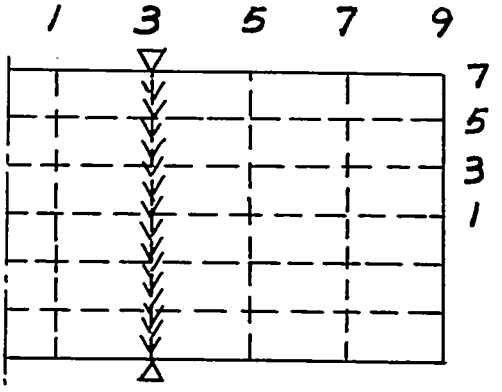

(a) Plan form.

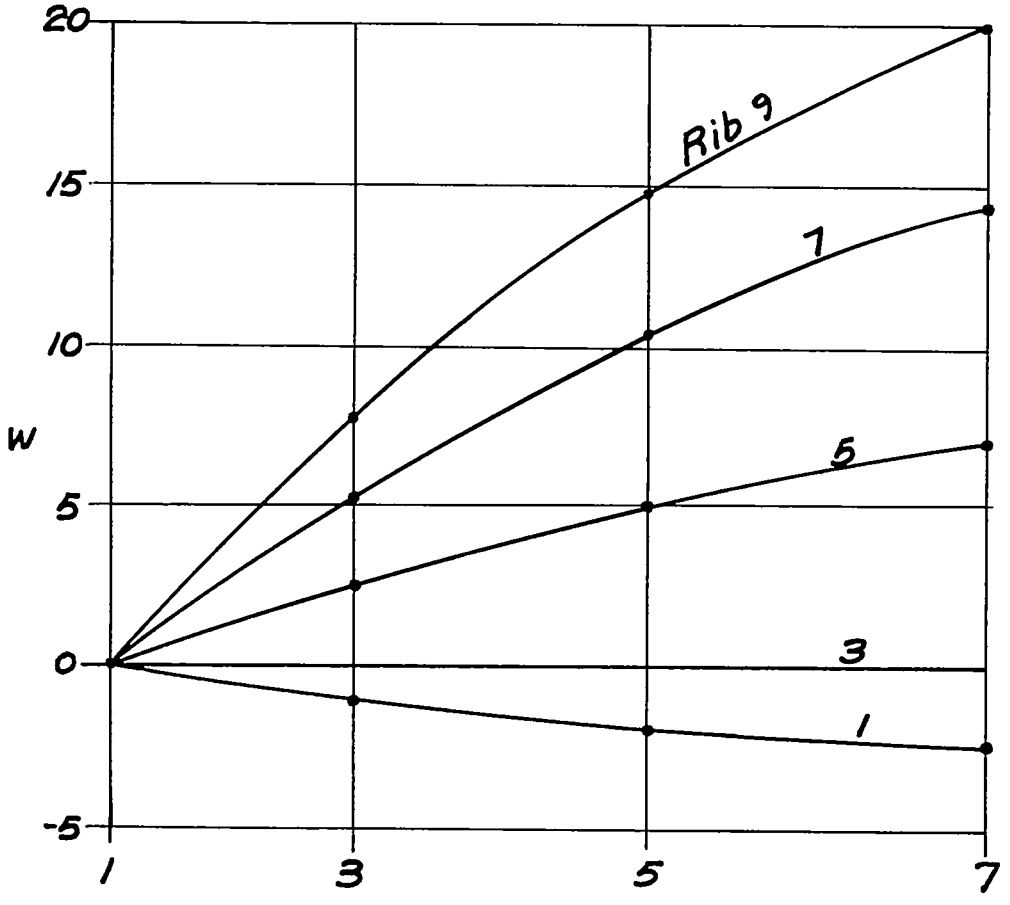

(b) Deflections.

Figure 50.- Deflection of ribs in first symmetric torsion mode. Rectangular section. Aspect ratio, 2.

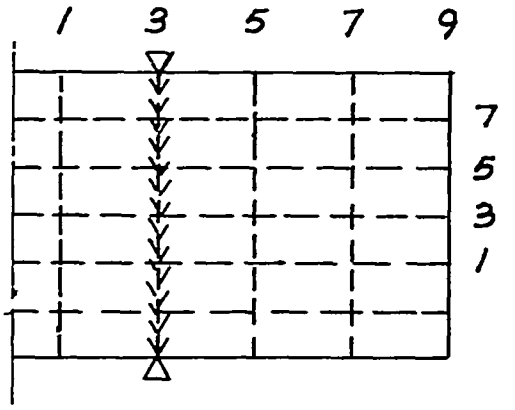

(b) Plan form.

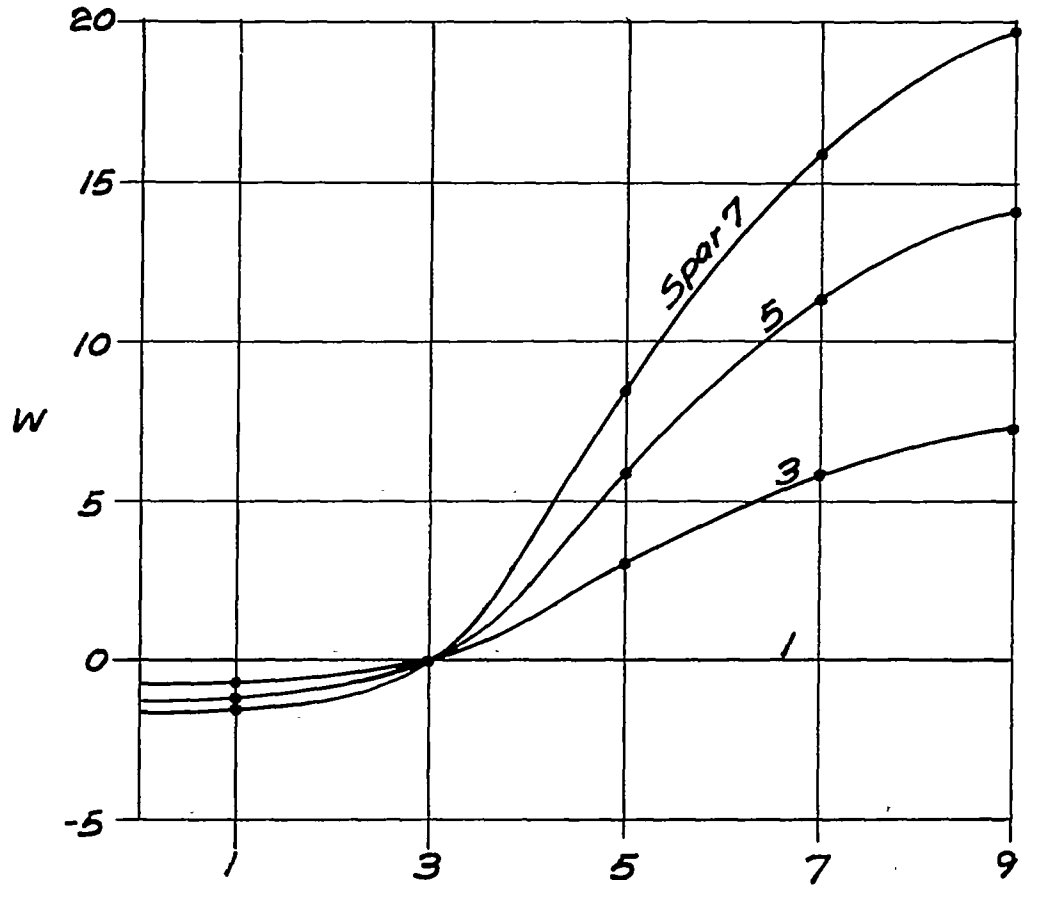

(b) Deflections.

Figure 51.- Deflections of spars in first symmetric torsion mode. Rectangular section. Aspect ratio, 4.

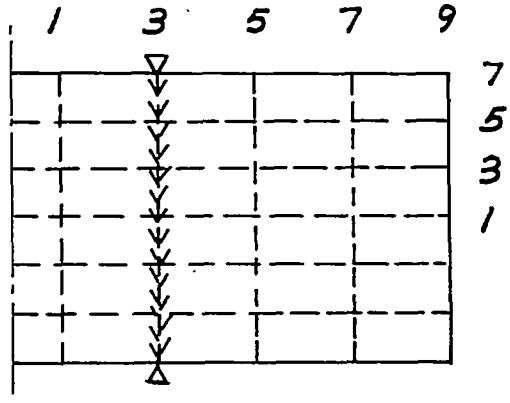

(a) Plan form.

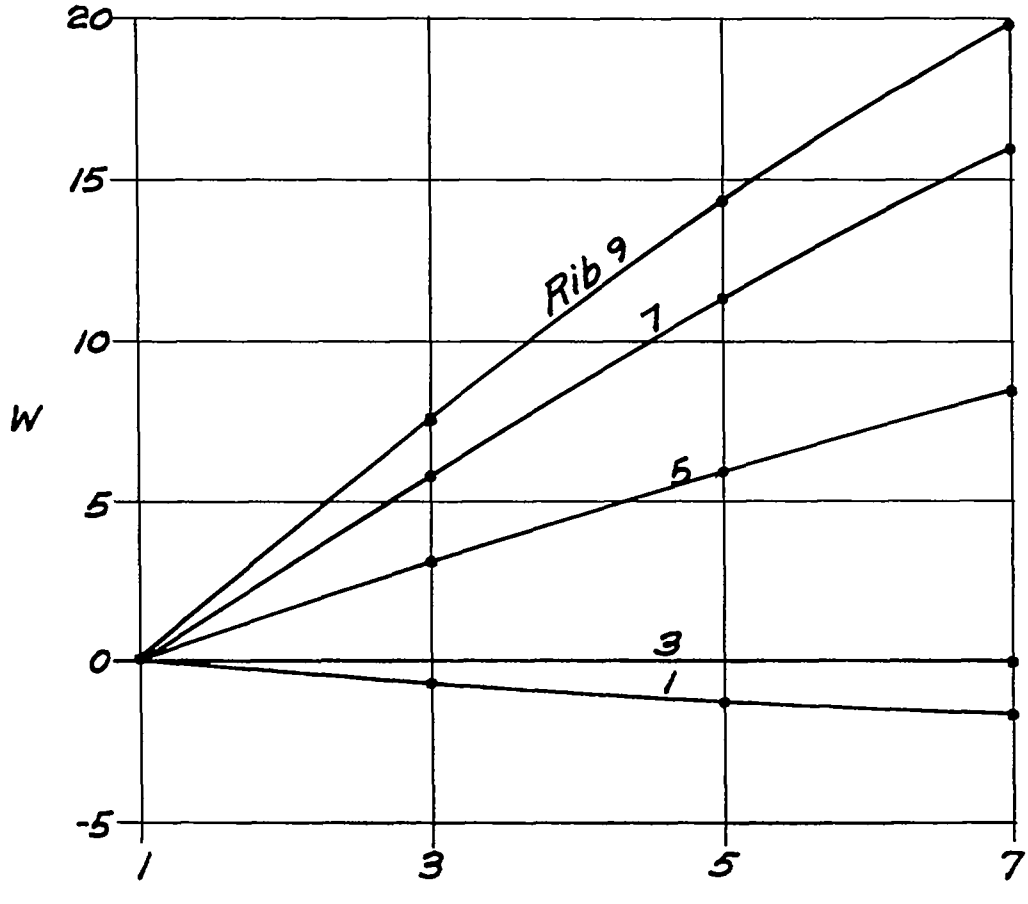

(b) Deflections.

Figure 52.- Deflection of ribs in first symmetric torsion mode. Rectangular section. Aspect ratio, 4.

NACA-Langley - 1-11-54 - 1000